Republic of Iraq
Ministry of Higher Education
and Scientific Research
University of Al-Qadisiyah

Application of Chemometric Models for Extraction and Determination of Some Acid Dyes

Thesis Submitted to the Council of the College of Science/ University of AL-Qadisiyah in Partial Fulfillment of the Requirements for the Master's Degree in Chemistry

By

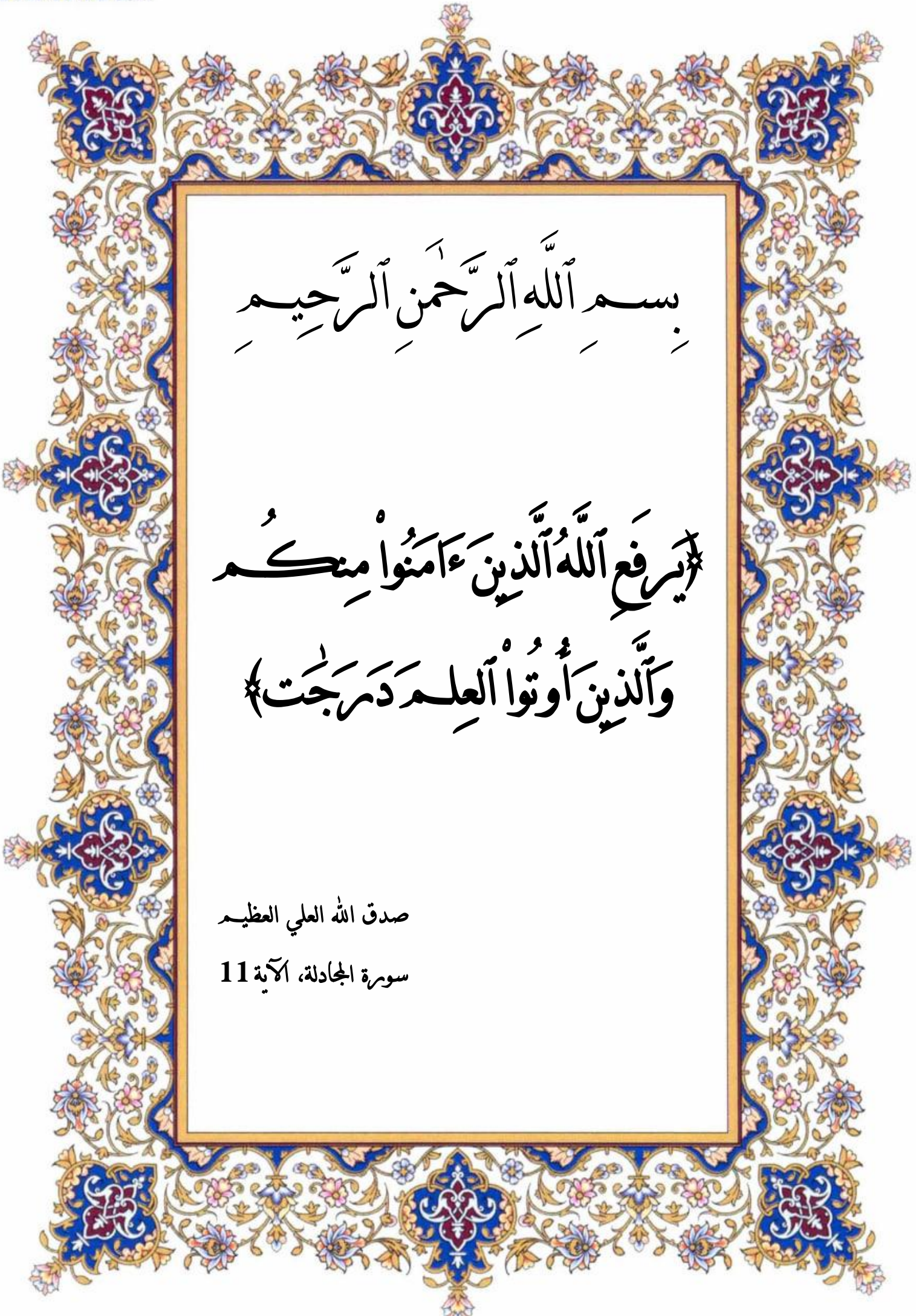
Raghad Abdul-Ridha Wasaf

Supervised by

Prof. Dr. Zainab Tariq Ibrahim

2026 A.C **1448 A.H**

ERSIANGRAPHIC.com



بسم الله الرحمن الرحيم

﴿يرفع الله الذين ءامنوا منكم
والذين أوتوا العلم درجات﴾

صدق الله العلي العظيم

سورة المجادلة، الآية 11

Supervisor Certification

Linguistic Certification

The Rectified Scientific Declaration

Signature

Name:

Scientific degree:

Address

Date: / / 2026

DEDICATION

In the name of Allah, the Most Gracious, the Most Merciful.

"My success comes only through Allah. In Him I trust, and unto Him I turn."

To the one whom Allah chose as a mercy to all creation, and whose biography He made a light that guides hearts and minds to our Noble Prophet Muhammad (blessings and peace be upon him and his pure family), I dedicate this work in love, loyalty, and inspiration from a legacy that remains immortal in human history.

To:

My Mother

and My Father

To the first story of my life and the purest prayers that accompanied my steps: what I write today did not begin on these pages, but rather with both of you—from a love that taught me, patience that embraced me, and prayers whose true worth I only realized upon reaching this milestone.

To the one who generously bestowed his time upon me and honored me with his kindness, in acknowledgment of his virtue and recognition of his right, as he was my best support and pillar:

"My Beloved Husband Abbas"

To my second family (Uncle Medhat, Aunt, Firas, osama).

In appreciation of their efforts, support, and assistance in completing this research, I extend my sincere thanks and gratitude.

To those who were the secret of my strength, the source of my determination, and the inspiration behind my success the joy of my life, my sons Ali and Benyamin: I dedicate the fruit of this success to you both.

To my brothers and sisters, through whom Allah strengthened my pillar and support in my journey to success.

To my friends:

To those who shared the path with me, and to those whose actions were truer than any words of thanks.

And to everyone who left an impact on my reaching this moment, even though a single word, a sincere prayer, or a genuine deed, I dedicate this achievement.

ACKNOWLEDGEMENTS

Praise be to Allah, who makes every effort bear fruit, gives every endeavor a purpose, and leaves a mark for every step taken in the pursuit of knowledge. To Him belongs all praise for guidance, and all thanks for the completion of this journey.

How beautiful it is to conclude hard work with gratitude and to meet kindness with virtue. From this standpoint, I extend my heartfelt thanks and deepest appreciation to **Dr. Zainab Tariq**, the supervisor of this thesis, for the solid scientific knowledge, sound guidance, and gracious oversight she provided, which had a prominent impact on the completion of this work.

I also express my profound appreciation to the Deanship of the College of Science and the Headship of the Department of Chemistry, represented by **Dr. Bassam Faroun**, for the support and cooperation they provided, which contributed to completing this academic path.

To everyone who contributed to this achievement through knowledge, advice, or a kind gesture, I hold a gratitude in my heart that words cannot fully express, and an appreciation that stands as a lasting testament to their beautiful impact. Praise be to Allah for the completion of the journey and the grace of reaching the destination.

Abstract

Abstract

This study developed a simple method to extract Acid Red 18 and Methyl Orange dyes from water and determine them by UV–Vis spectrophotometry. It couples switchable-solvent liquid microextraction (SHS-LLME) with magnetic solid-phase extraction (MSPE) on polyaniline magnetite (Fe_3O_4/PANI) nanoparticles.

Part One: Preparation and Characterization of Nanoparticles

Fe_3O_4/PANI composite (50:50 w/w) was prepared by mixing polyaniline and magnetite in acetone. It was characterised by a set of advanced analytical techniques:

- X-ray diffraction (XRD)
- Scanning electron microscopy (SEM)
- Transmission electron microscopy (TEM)
- Vibrating sample magnetometry (VSM)
- Fourier-transform infrared spectroscopy (FTIR)

These techniques gave detailed information on the structural, morphological and magnetic properties of the nanoparticles. They confirmed the polyaniline coating: the particle size rose from 11.7 to 21.0 nm, and the saturation magnetisation fell from 11.42 to 4.68 emu g^{-1}, but the material stayed magnetic.

Abstract

Part Two: Application of the SHS Technique

Developed a switchable-solvent microextraction method based on using N,N-Dimethylcyclohexylamine (DMCHA) to extract and spectrophotometrically determine Acid Red 18 and Methyl Orange dyes. By exploiting the amine's acid/base switching behavior,the procedure combined the efficiency of homogeneous extraction with simple phase separation without requiring a disperser solvent or centrifugation.

eight factors were studied one at a time: solution pH (2–9), extraction solvent type , DMCHA volume (1–3 mL), HCl volume (100–1000 µL), NaOH volume (100–1000 µL), bath temperature (30–50 °C), extraction time (1-10 s) and the type and concentration of added salt ($CaCl_2$, NaCl, and KCl, 1–10% w/v). The best conditions were pH 3, 2.5 mL of DMCHA, 400 µL each of HCl and NaOH, 40 °C, 10 s and 10 % $CaCl_2$ for Acid Red 18, and pH 3, 2.0 mL, 300 µL of HCl, 100 µL of NaOH, 40 °C, 8 s and 5 % $CaCl_2$ for Methyl Orange.

Part Three: Application of Statistical Chemometric Methods

Chemometric methods optimized the extraction systematically with fewer experiments and showed the interactions between the variables. A central composite design (31 runs per dye) covered pH and the volumes of solvent, HCl and NaOH. The modelling showed the key factors and tested the model fit: both quadratic models were significant ($P < 0.001$), pH was the most important factor, and the Methyl Orange model had no significant lack of fit ($P = 0.640$). The predicted optimum pH was 2 for both dyes.

Part Four: Magnetic Solid-Phase Extraction (MSPE)

Fe_3O_4/PANI composite was then used as a magnetic sorbent for the same dyes and was collected with a magnet. With methanol as the eluent, the best conditions were 0.5 g, 30 min adsorption and 20 min desorption for

Abstract

Acid Red 18, and 0.4 g, 20 min and 20 min for Methyl Orange. The extraction reached 93 % and 92 %, respectively.

Part Five: Application to Real Samples

The coupled method was linear over 10–100 mg L^{-1}. The LOD was 2.088 and 2.630 mg L^{-1}, and the LOQ was 6.961 and 8.769 mg L^{-1}, for Acid Red 18 and Methyl Orange. The method was applied to tap, river and wastewater samples to test its practical use in real matrices. Acid Red 18 was found only in wastewater (19.76 mg L^{-1}). Spiked samples gave recoveries of 96.0–100.3 %, with RSD below 5 %.

Overall, SHS-LLME coupled with MSPE on Fe_3O_4/PANI composite is a promising method for extracting and determining the studied dyes. It is easy to operate, separates quickly with a magnet, uses little solvent and can improve analytical performance, so it suits environmental samples.

List of Contents		
Seq.	**Title**	**Page**
Abstract		II
List of Contents		V
List of Tables		X
List of Figures		XIV
List of Abbreviations		XIX
CHAPTER ONE: INTRODUCTION		
1.1	Water Pollution by Synthetic Dyes	1
1.2	Azo Dyes	2
1.2.1	Acid Red 18 (Ponceau 4R)	4
1.2.2	Methyl Orange	5
1.3	Green Analytical Chemistry and the Role of Sample Preparation	6
1.4	Microextraction Techniques	7
1.4.1	Classification	8
1.5	Switchable-Hydrophilicity Solvents	9
1.5.1	Concept and origin	9
1.5.2	Physicochemical requirements for switchable behaviour	11
1.5.3	Switchable-hydrophilicity solvent liquid–liquid microextraction (SHS-LLME)	12
1.5.4	Factors affecting SHS-LLME	13
1.6	Solid-Phase Microextraction	15
1.7	Magnetic Solid-Phase Extraction	17
1.7.1	Iron oxide nanoparticles	18
1.7.2	Surface functionalisation	18
1.7.3	Coating materials	20
1.8	Polyaniline and PANI/Fe_3O_4 Nanocomposites	21
1.8.1	Polyaniline as a sorbent	21
1.8.2	Magnetic polyaniline composites for anionic azo dyes	23
1.9	Coupling SHS-LLME with Magnetic Solid-Phase Extraction	24
1.10	Chemometric Optimisation of the Extraction	26
1.11	Previous Studies	28
1.12	Aim of the Study	31

List of Contents		
Seq.	**Title**	**Page**
CHAPTER TWO: INSTRUMENTS AND MATERIALS		
2.1	Instruments and Apparatus	33
2.2	Chemicals and Reagents	33
2.3	Preparation of the Standard and Reagent Solutions	34
2.3.1	Stock standard solution of Acid Red 18	34
2.3.2	Stock standard solution of Methyl Orange	35
2.3.3	Hydrochloric acid, 6 M	35
2.3.4	Sodium hydroxide, 10 M	35
2.3.5	Solutions used to adjust the pH	35
2.3.6	Salt solutions	36
2.4	Preparation and Characterization of the Nanoparticles (PANI/Fe_3O_4)	36
2.4.1	X-ray diffraction	37
2.4.2	Fourier-transform infrared spectroscopy	38
2.4.3	Field-emission scanning electron microscopy	38
2.4.4	Transmission electron microscopy	38
2.4.5	Vibrating-sample magnetometry	38
2.4.6	Surface-area and porosity analysis	38
2.5	Spectrophotometric Determination of Acid Red 18 and Methyl Orange	39
2.6	SHS-LLME Extraction Procedure and the Factors Affecting It	39
2.6.1	Effect of the extraction solvent type	41
2.6.2	Effect of the extraction solvent volume	41
2.6.3	Effect of the acid volume	41
2.6.4	Effect of the temperature	42
2.6.5	Effect of the base volume	42
2.6.6	Effect of the salt type and concentration	42
2.6.7	Effect of the pH of the aqueous phase	42
2.6.8	Effect of the extraction time	42
2.7	Chemometric Optimisation by Response Surface Methodology	42
2.7.1	Selection of the variables and their levels	43
2.7.2	Design matrix	43

List of Contents		
Seq.	**Title**	**Page**
2.7.3	Model and statistical analysis	44
2.8	Calibration Curves of Acid Red 18 and Methyl Orange Using the SHS-LLME Method	44
2.9	General Procedure for the Extraction of the Dyes Using the SHS-LLME Method Coupled with the MSPE Method	44
2.10	Factors Affecting the Extraction by Using the MSPE Method	46
2.10.1	Effect of the amount of the magnetic sorbent	46
2.10.2	Effect of the adsorption time	47
2.10.3	Effect of the type of desorption solvent	47
2.10.4	Effect of the desorption time	47
2.11	Calibration Curves of the Dyes Using the SHS-LLME Method Coupled with the MSPE Method	47
2.12	Extraction Percentage	47
2.13	Application to Real Samples	48
CHAPTER THREE: RESULTS AND DISCUSSION		
3.1	Absorption Spectra of Acid Red 18 and Methyl Orange	49
3.2	Characterization of the Prepared Magnetic Nanomaterial	50
3.2.1	X-ray diffraction	50
3.2.2	Infrared spectroscopy	52
3.2.3	Electron microscopy	54
3.2.4	Magnetic properties	56
3.2.5	Surface area and porosity	57
3.3	Factors Affecting the Extraction of Acid Red 18 by the SHS-LLME Method	59
3.3.1	Effect of the pH of the aqueous phase	59
3.3.2	Effect of the extraction solvent type	60
3.3.3	Effect of the volume of the switchable solvent	62
3.3.4	Effect of the volume of hydrochloric acid	63
3.3.5	Effect of the volume of sodium hydroxide	64
3.3.6	Effect of temperature	65
3.3.7	Effect of extraction time	66

List of Contents		
Seq.	**Title**	**Page**
3.3.8	Effect of the type and concentration of added electrolyte	67
3.4	Factors Affecting the Extraction of Methyl Orange by the SHS-LLME Method	68
3.4.1	Effect of the pH of the aqueous phase	69
3.4.2	Effect of the extraction solvent type	70
3.4.3	Effect of the volume of the switchable solvent	71
3.4.4	Effect of the volume of hydrochloric acid	72
3.4.5	Effect of the volume of sodium hydroxide	73
3.4.6	Effect of temperature	74
3.4.7	Effect of the type and concentration of added electrolyte	74
3.4.8	Effect of extraction time	76
3.5	Chemometric Optimization by Central Composite Design	77
3.5.1	Design of the experiments	78
3.5.2	Acid Red 18	79
3.5.3	Methyl Orange	86
3.6	Calibration of the SHS-LLME Method	94
3.7	Factors Affecting the Extraction of Acid Red 18 by the MSPE Method	96
3.7.1	Effect of the mass of the magnetic sorbent	96
3.7.2	Effect of the adsorption time	98
3.7.3	Effect of the type of desorption solvent	99
3.7.4	Effect of the desorption time	100
3.8	Factors Affecting the Extraction of Methyl Orange by the MSPE Method	101
3.8.1	Effect of the mass of the magnetic sorbent	101
3.8.2	Effect of the adsorption time	102
3.8.3	Effect of the type of desorption solvent	103
3.8.4	Effect of the desorption time	104
3.9	Calibration Curves of the Dyes Using the SHS-LLME Method Coupled with the MSPE Method	106
3.10	Application to Real Samples	108

List of Contents		
Seq.	**Title**	**Page**
3.11	Conclusions	109
3.12	Recommendations	111
References		112

List of Tables		
No. Tab.	**The Title**	**Page**
CHAPTER ONE: INTRODUCTION		
1-1	Identity and physicochemical properties of the two dyes studied in this work.	3
1-2	Comparison of conventional extraction and microextraction techniques [23–26].	8
1-3	Advantages and limitations of solid-phase microextraction [44,45].	16
1-4	Structural types of magnetic iron oxide nanoparticle hybrids [55,56,58].	19
1-5	Organic and inorganic coatings for iron oxide nanoparticles [56,57].	20
1-6	Reported performance of polyaniline-based magnetic sorbents towards anionic azo dyes.	24
1-7	Summary of previous studies related to the extraction, preconcentration, and determination of synthetic dyes.	29
CHAPTER TWO: INSTRUMENTS AND MATERIALS		
2-1	Instruments used in this study, with model, manufacturer and place of use.	33
2-2	Chemicals and reagents used in this study.	34
2-3	Variables examined by the one-factor-at-a-time approach and the ranges studied.	41
2-4	Independent variables and the levels at which the two central composite designs were executed.	43
CHAPTER THREE: RESULTS AND DISCUSSION		
3-1	The principal infrared bands and their assignment.	53
3-2	Effect of the pH of the aqueous phase on the extraction percentage, (%E) of Acid Red 18 by the SHS-LLME method.	60
3-3	Effect of the extraction solvent type on the extraction percentage, (%E) of Acid Red 18 by the SHS-LLME method.	61

List of Tables		
No. Tab.	**The Title**	**Page**
3-4	Effect of the extraction solvent volume on the extraction percentage, (%E) of Acid Red 18 by the SHS-LLME method	62
3-5	Effect of the volume of hydrochloric acid on the extraction percentage, (%E) of Acid Red 18 by the SHS-LLME method	63
3-6	Effect of the volume of sodium hydroxide on the extraction percentage, (%E) of Acid Red 18 by the SHS-LLME method	64
3-7	Effect of temperature on the extraction percentage, (%E) of Acid Red 18 by the SHS-LLME method	65
3-8	Effect of extraction time on the extraction percentage, (%E) of Acid Red 18 by the SHS-LLME method	66
3-9	Effect of the type and concentration of added electrolyte on the extraction percentage, (%E) of Acid Red 18 by the SHS-LLME method	67
3-10	Univariate optimisation of the switchable-solvent microextraction of Acid Red 18.	68
3-11	Effect of the pH of the aqueous phase on the extraction percentage, (%E) of methyl orange by the SHS-LLME method	69
3-12	Effect of the extraction solvent type on the extraction percentage, (%E) of methyl orange by the SHS-LLME method.	70
3-13	Effect of the volume of the switchable solvent on the extraction percentage, (%E) of methyl orange by the SHS-LLME method.	71
3-14	Effect of the volume of hydrochloric acid on the extraction percentage, (%E) of methyl orange by the SHS-LLME method	72
3-15	Effect of the volume of sodium hydroxide on the extraction percentage, (%E) of methyl orange by the SHS-LLME method	73

List of Tables		
No. Tab.	**The Title**	**Page**
3-16	Effect of temperature on the extraction percentage, (%E) of methyl orange by the SHS-LLME method	74
3-17	Effect of the type and concentration of added electrolyte on the extraction percentage, (%E) of methyl orange by the SHS-LLME method	75
3-18	Effect of extraction time on the extraction percentage, (%E) of methyl orange by the SHS-LLME method	76
3-19	Univariate optimization of the switchable-solvent microextraction of methyl orange.	77
3-20	Structure of the two central composite designs, as executed.	78
3-21	Central composite design matrix with the experimental and model-predicted absorbance of Acid Red 18.	78
3-22	Analysis of variance for the quadratic model fitted to the Acid Red 18 response.	80
3-23	Optimum predicted for Acid Red 18 by the desirability function.	85
3-24	Central composite design matrix with the experimental and model-predicted absorbance of Methyl Orange	86
3-25	Analysis of variance for the quadratic model fitted to the Methyl Orange response.	87
3-26	Optimum predicted for Methyl Orange from the fitted model.	94
3-27	Calibration data and the figures of merit derived from them.	96
3-28	Effect of the mass of the magnetic sorbent on the extraction percentage, (%E) of Acid Red 18 by the MSPE method	97
3-29	Effect of the adsorption time on the extraction percentage, (%E) of Acid Red 18 by the MSPE method	99

List of Tables		
No. Tab.	**The Title**	**Page**
3-30	Effect of the type of desorption solvent on the extraction percentage, (%E) of Acid Red 18 by the MSPE method	100
3-31	Effect of the desorption time on the extraction percentage, (%E) of Acid Red 18 by the MSPE method	101
3-32	Univariate optimisation of the magnetic solid-phase extraction of Acid Red 18	101
3-33	Effect of the mass of the magnetic sorbent on the extraction percentage, (%E) of Methyl Orange by the MSPE method.	102
3-34	Effect of the adsorption time on the extraction percentage, (%E) of Methyl Orange by the MSPE method.	103
3-35	Effect of the type of desorption solvent on the extraction percentage, (%E) of Methyl Orange by the MSPE method	104
3-36	Effect of the desorption time on the extraction percentage, (%E) of Methyl Orange by the MSPE method	105
3-37	Univariate optimisation of the magnetic solid-phase extraction of Methyl Orange.	105
3-38	Calibration data and the figures of merit derived from them	107
3-39	Determination and recovery of Acid Red 18 in real water samples using the proposed method	108

List of Figures		
No. Fig.	**The Title**	**Page**
CHAPTER ONE: INTRODUCTION		
1-1	Sources, pathways and consequences of synthetic dye pollution in the aquatic environment.	2
1-2	Chemical structures of the two dyes studied in this work.	6
1-3	Classification of microextraction techniques according to the nature of the extracting phase.	9
1-4	Reversible switching of a hydrophilicity-switchable solvent between its hydrophilic (protonated) and hydrophobic (neutral) forms.	10
1-5	Step-by-step SHS-LLME procedure with N,N-dimethyl cyclohexyl amine	12
1-6	Variables that control the recovery of an SHS-LLME procedure and the reason each one matters.	13
1-7	Solid-phase microextraction: (a) direct-immersion and (b) headspace sampling modes, followed by (c) desorption into the analytical instrument.	16
1-8	Schematic representation of the magnetic solid-phase extraction procedure.	17
1-9	Typical morphologies of magnetic composite nanomaterials.	20
1-10	Routes for modifying the surface properties of iron oxide nanoparticles.	21
1-11	Oxidation states of polyaniline and the reversible protonic-acid doping of the emeraldine base to the conducting emeraldine salt.	22
1-12	Proposed retention mechanism of an anionic sulfonated azo dye on a PANI/Fe_3O_4 composite, and magnetic recovery of the loaded sorbent.	23
1-13	The coupled SHS-LLME/MSPE procedure	25
1-14	(a) Geometry of a three-factor central composite design, and (b) a fitted second-order response surface with its contour projection.	27
CHAPTER TWO: INSTRUMENTS AND MATERIALS		

List of Figures		
No. Fig.	**The Title**	**Page**
2-1	Preparation of the PANI/Fe_3O_4 (50:50 w/w) composite by solvent-assisted physical mixing.	37
2-2	The SHS-LLME procedure used for the extraction of Acid Red 18 and Methyl Orange.	40
2-3	The MSPE stage applied to the extract obtained from the SHS-LLME stage.	46
CHAPTER THREE: RESULTS AND DISCUSSION		
3-1	Ultraviolet–visible absorption spectra of the two dyes. (a) Acid Red 18, (b) Methyl orange	50
3-2	X-ray diffraction patterns of the a) pure Fe_3O_4 (magnetite) b) Fe_3O_4/polyaniline composite	52
3-3	Infrared spectra recorded as potassium bromide discs. (a) pure Fe_3O_4 (magnetite) (b) Fe_3O_4/polyaniline composite.	53
3-4	Scanning electron micrographs of pure Fe_3O_4 (magnetite) (a, b) and of Fe_3O_4/polyaniline composite (c, d), recorded at 20.0 kV with a secondary-electron detector.	54
3-5	Transmission electron micrographs of (a) pure Fe_3O_4 (magnetite) and (b) Fe_3O_4/polyaniline composite.	55
3-6	Magnetisation curves of the pure Fe_3O_4 (magnetite) and Fe_3O_4/polyaniline composite measured between ± 10 kOe.	56
3-7	Nitrogen physisorption at 77 K for the pure Fe_3O_4 (magnetite) and the Fe_3O_4/polyaniline composite: (a) adsorption–desorption isotherms, (b) BET plots, (c) pore-size distributions and (d) cumulative pore volume.	58
3-8	Effect of the pH of the aqueous phase on the extraction of Acid Red 18 by the SHS-LLME method.	60
3-9	Effect of the extraction solvent type on the extraction of Acid Red 18 by the SHS-LLME method.	61
3-10	Effect of the volume of the switchable solvent on the extraction of Acid Red 18 by the SHS-LLME method.	62

List of Figures		
No. Fig.	**The Title**	**Page**
3-11	Effect of the volume of hydrochloric acid on the extraction of Acid Red 18 by the SHS-LLME method.	63
3-12	Effect of the volume of sodium hydroxide on the extraction of Acid Red 18 by the SHS-LLME method.	64
3-13	Effect of temperature on the extraction of Acid Red 18 by the SHS-LLME method.	65
3-14	Effect of extraction time on the extraction of Acid Red 18 by the SHS-LLME method.	66
3-15	Effect of the type and concentration of added electrolyte on the extraction of Acid Red 18 by the SHS-LLME method.	67
3-16	Effect of the pH of the aqueous phase on the extraction of methyl orange by the SHS-LLME method.	69
3-17	Effect of the extraction solvent type on the extraction of methyl orange by the SHS-LLME method.	70
3-18	Effect of the volume of the switchable solvent on the extraction of methyl orange by the SHS-LLME method.	71
3-19	Effect of the volume of hydrochloric acid on the extraction of methyl orange by the SHS-LLME method.	72
3-20	Effect of the volume of sodium hydroxide on the extraction of methyl orange by the SHS-LLME method.	73
3-21	Effect of temperature on the extraction of methyl orange by the SHS-LLME method.	74
3-22	Effect of the type and concentration of added electrolyte on the extraction of methyl orange by the SHS-LLME method.	75
3-23	Effect of extraction time on the extraction of methyl orange by the SHS-LLME method.	76
3-24	Pareto chart of the standardised effects on the absorbance of the extracted Acid Red 18.	81

List of Figures		
No. Fig.	**The Title**	**Page**
3-25	Main-effects plots for the Acid Red 18 model: fitted absorbance against each factor with the other three held at the centre of the design (pH 5.5, 2 mL of solvent, 550 µL of HCl and 550 µL of NaOH).	82
3-26	Interaction plots for the Acid Red 18 model: (left) solvent volume at two levels of pH, (centre) HCl volume at two levels of pH, and (right) HCl volume at two solvent volumes. The remaining factors are held at the centre of the design.	83
3-27	Three-dimensional response surfaces for absorbance as a function of (left) pH and solvent volume, (centre) pH and HCl volume, and (right) pH and NaOH volume.	84
3-28	Contours of the quadratic model fitted to the Acid Red 18 response: (left) pH–solvent plane, (centre) pH–acid plane and (right) pH-base plane.	84
3-29	Predicted against measured absorbance for the thirty-one runs of the Acid Red 18 design	85
3-30	Response-optimization (desirability) plot for Acid Red 18	85
3-31	Pareto chart of the standardised effects on the absorbance of the extracted Methyl Orange.	89
3-32	Main-effects plots for the Methyl Orange model.	90
3-33	Interaction plots for the Methyl Orange model: (left) solvent volume, (centre) HCl volume and (right) NaOH volume.	90
3-34	Three-dimensional response surfaces for Methyl Orange absorbance as a function of (left) pH and solvent volume, (centre) pH and HCl volume, and (right) pH and NaOH volume	91
3-35	Contours of the quadratic model fitted to the Methyl Orange response.	92
3-36	Predicted against measured absorbance for the thirty-one runs of the Methyl Orange design	93

List of Figures		
No. Fig.	**The Title**	**Page**
3-37	Response-optimization (desirability) plot for Methyl Orange	93
3-38	Calibration of the spectrophotometric determination. Linear range, 10–100 mg L^{-1}, (a) Acid Red 18, (b) Methyl Orange	95
3-39	Effect of the mass of the magnetic sorbent on the extraction of Acid Red 18 by the MSPE method	97
3-40	Effect of the adsorption time on the extraction of Acid Red 18 by the MSPE method.	98
3-41	Effect of the type of desorption solvent on the extraction of Acid Red 18 by the MSPE method	99
3-42	Effect of the desorption time on the extraction of Acid Red 18 by the MSPE method	100
3-43	Effect of the mass of the magnetic sorbent on the extraction of Methyl Orange by the MSPE method.	102
3-44	Effect of the adsorption time on the extraction of Methyl Orange by the MSPE method	103
3-45	Effect of the type of desorption solvent on the extraction of Methyl Orange by the MSPE method	104
3-46	Effect of the desorption time on the extraction of Methyl Orange by the MSPE method.	105
3-47	Calibration of the spectrophotometric determination of Acid Red 18 and Methyl Orange dyes	107

List of Abbreviations	
Abbreviation	**Name**
Abs	Absorbance
Adj MS	Adjusted mean square
Adj SS	Adjusted sum of squares
AGREE	Analytical GREEnness metric
ANOVA	Analysis of variance
AR 18	Acid Red 18
BET	Brunauer–Emmett–Teller (surface-area method)
CAS	Chemical Abstracts Service
CCD	Central composite design
C.I.	Colour Index
COF	Covalent organic framework
DAD	Diode-array detector
DBAE	2-(Dibutylamino)ethanol
DES	Deep eutectic solvent
DES-VA-DLLME	Deep eutectic solvent-based vortex-assisted dispersive liquid–liquid microextraction
DF	Degrees of freedom
DLLME	Dispersive liquid–liquid microextraction
DMCHA	N,N-Dimethylcyclohexylamine
D-MSPME	Dispersive magnetic solid-phase microextraction
DNA	Deoxyribonucleic acid
DPA	Dipropylamine
D-μ-SPE	Dispersive micro-solid-phase extraction
%E	Extraction percentage
EF	Enrichment factor
EFSA	European Food Safety Authority
EME	Electromembrane extraction
EnF	Enhancement factor
FTIR	Fourier-transform infrared spectroscopy
GO	Graphene oxide
HF-LPME	Hollow-fibre liquid-phase microextraction
HPLC	High-performance liquid chromatography
LLE	Liquid–liquid extraction
LOD	Limit of detection

List of Abbreviations	
Abbreviation	**Name**
LOQ	Limit of quantification
LSPR	Localised surface plasmon resonance
MEPS	Microextraction by packed sorbent
MNPs	Magnetic nanoparticles
MO	Methyl Orange
MSPE	Magnetic solid-phase extraction
MWCNT	Multi-walled carbon nanotube
ND	Not detected
NR	Not reported
P4R	Ponceau 4R
PANI	Polyaniline
PANI/Fe_3O_4	Polyaniline-coated magnetite nanocomposite
PDA	Polydopamine
PEG	Poly(ethylene glycol)
PEI	Polyethyleneimine
PF	Preconcentration factor
pH	Negative logarithm of the hydrogen-ion activity
pK_a	Negative logarithm of the acid dissociation constant
pK_{aH}	pK_a of the conjugate acid (protonated amine)
PLA	Poly(lactic acid)
PMMA	Poly(methyl methacrylate)
PT-SPE	Pipette-tip solid-phase extraction
R^2	Coefficient of determination
r_p	Pore radius
RSD	Relative standard deviation
RSM	Response surface methodology
s(b)	Standard deviation of the intercept
S_{BET}	BET specific surface area
SBSE	Stir-bar sorptive extraction
SDME	Single-drop microextraction
SEM	Scanning electron microscopy
SERS	Surface-enhanced Raman scattering
SHS	Switchable-hydrophilicity solvent

List of Abbreviations	
Abbreviation	**Name**
SHS-LLME	Switchable-hydrophilicity solvent-based liquid–liquid microextraction
SPE	Solid-phase extraction
SPME	Solid-phase microextraction
SS-LME	Switchable-solvent liquid microextraction
SS-LPME	Switchable-solvent liquid-phase microextraction
SY	Sunset Yellow
s(y/x)	Residual standard deviation of the regression
TEA	Triethylamine
TEM	Transmission electron microscopy
UA-D-μ-SPE	Ultrasound-assisted dispersive micro-solid-phase extraction
UFLC	Ultra-fast liquid chromatography
UV	Ultraviolet
UV–Vis	Ultraviolet–visible
V_p	Pore volume
VSM	Vibrating-sample magnetometry
w/v	Weight per volume
w/w	Weight per weight
XRD	X-ray diffraction
λ_{max}	Wavelength of maximum absorption

CHAPTER 1 INTRODUCTION

1.1 Water Pollution by Synthetic Dyes

Water is the resource on which every form of life depends, and the pressure placed on it by industrial expansion has grown faster than the capacity to treat what industry returns to it. Among industrial sectors, textile manufacturing is one of the heaviest users of water and one of the largest producers of coloured effluent. Global production of synthetic dyes is currently estimated at around 7×10^5 tonnes per year, and between 15 and 50 % of the azo dye applied in a dyeing operation never binds to the fibre and is discharged with the spent liquor [1]. The resulting effluent is coloured, chemically complex, and frequently released with little or no treatment [2,3].

The consequences for the receiving water body are both physical and biochemical. Colour reduces light penetration, which suppresses photosynthesis by aquatic plants and algae; the dissolved oxygen concentration falls as a result, and the microbial communities that would normally mineralise organic waste can no longer function efficiently [2,4]. Textile effluent also raises the biochemical and chemical oxygen demand of the receiving water and often carries heavy metals such as chromium, lead, mercury and arsenic that originate from the dyestuffs and from the auxiliaries used in dyeing [2,3].

The health argument is equally direct. Many synthetic dyes and their breakdown products are absorbed, metabolised and biotransformed by cytochrome P450 enzymes into electrophilic intermediates and aromatic amines capable of forming adducts with DNA and proteins [4]. Reported effects of chronic exposure include dermatitis, allergic conjunctivitis and occupational asthma among workers, and mutagenic and carcinogenic outcomes attributable to the aromatic amines released when the dye molecule is reduced [1,2,5]. Because dyes are designed to resist light, washing and

microbial attack, they are persistent: they are now detected routinely in surface water, sediment and even in wild fish, which is precisely why reliable analytical methods for their determination at low concentrations are needed [3,6].

The route from the dyehouse to the exposed population, and the successive effects along it, are summarised in Figure 1-1.

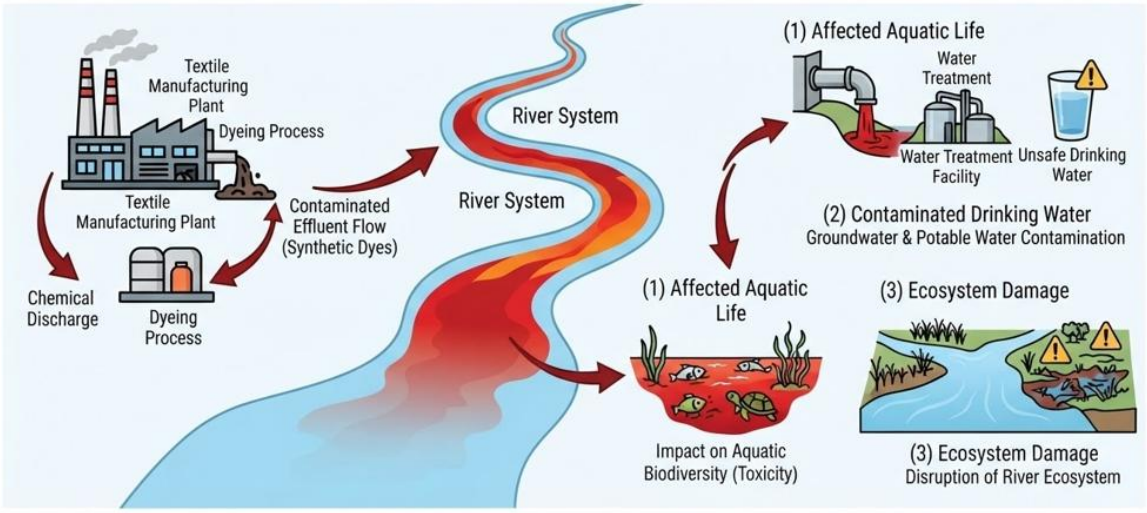


Figure 1-1: Sources, pathways and consequences of synthetic dye pollution in the aquatic environment.

1.2 Azo Dyes

Azo dyes are characterised by one or more azo linkages (–N=N–) connecting aromatic systems, and they account for roughly 60–70 % of all synthetic colourants produced. Their dominance follows from the chemistry: the diazotisation–coupling sequence used to make them is simple, cheap and tolerant of a very wide range of coupling components, so a colourist can obtain almost any shade with a high molar absorptivity and good fastness [5,7]. They are used across textiles, paper, leather, cosmetics, pharmaceuticals and food.

The same azo linkage that gives these compounds their colour is also the source of their toxicological concern. Under the reducing conditions found in

the intestinal tract, in anaerobic sediment and in the presence of azoreductase-producing bacteria, the –N=N– bond is cleaved to give aromatic amines, several of which are established or suspected carcinogens [5,7]. Adverse effects therefore arise not so much from the intact dye as from what it becomes after reduction, which is why regulatory limits are set on the parent colourant and why residues must be monitored in both environmental and food matrices [8]. The two dyes examined in this work, Acid Red 18 and Methyl Orange, were chosen because between them they cover the two contexts in which azo dyes matter most: Acid Red 18 is a permitted food colourant subject to a statutory acceptable daily intake, while Methyl Orange is a bulk textile dye and a common laboratory indicator that is discharged in industrial wastewater. Both are anionic sulfonated monoazo compounds, so both are highly water-soluble and difficult to remove from an aqueous matrix by conventional partitioning. Their principal identifiers and properties are collected in Table 1-1 and their structures are shown in Figure 1-2.

Table 1-1: Identity and physicochemical properties of the two dyes studied in this work.

Property	Acid Red 18	Methyl Orange
Common synonyms	Ponceau 4R, Cochineal Red A, New Coccine, E 124	Orange III, Helianthine, C.I. Acid Orange 52
Colour Index number	C.I. 16255	C.I. 13025
CAS registry number	2611-82-7	547-58-0
Molecular formula	$C_{20}H_{11}N_2Na_3O_{10}S_3$	$C_{14}H_{14}N_3NaO_3S$
Molar mass (g mol^{-1})	604.47	327.33
Chromophore class	Monoazo, naphthalene-based	Monoazo, aminoazobenzene-based
Sulfonate groups per molecule	Three ($–SO_3^-$)	One ($–SO_3^-$)
Ionic character in water	Anionic over the whole practical pH range	Anionic above pH ≈ 4
pK_a	Not applicable (fully ionised sulfonates)	3.46 [9,10]
λ_{max} in water (this work)	506.5 nm	485.5 nm

Property	Acid Red 18	Methyl Orange
Principal field of use	Food and beverage colourant	Textile dyeing; acid–base indicator

1.2.1 Acid Red 18 (Ponceau 4R)

Acid Red 18, marketed as Ponceau 4R and coded E 124 in the European additive list, is a strawberry-red monoazo colourant used mainly in soft drinks, confectionery, jellies, desserts and some pharmaceutical preparations [11]. Its three sulfonate groups make it freely soluble in water and stable to light and to moderate changes in pH, which is exactly what a beverage manufacturer wants and exactly what makes it persistent once discharged.

The compound has been re-evaluated more than once. The EFSA Panel on Food Additives reduced the acceptable daily intake from the earlier value of 0–4 mg kg^{-1} body weight per day to 0.7 mg kg^{-1} body weight per day [12], and a subsequent refined exposure assessment examined intake across European population groups against that revised figure [13]. Reported effects associated with excessive intake include hypersensitivity reactions, urticaria and, in susceptible children, behavioural effects; recent in vitro work has also reported chromosome aberrations, sister-chromatid exchange and increased comet tail length in human lymphocytes at higher concentrations [14]. A further concern is that the dye is not stable indefinitely in the product: photodegradation of Ponceau 4R in a real beverage matrix yields sulfonated aromatic amine and amide products that test positive in the Ames assay [15]. Survey data indicate that roughly one in nine processed food items contains at least one azo colourant, Ponceau 4R among them [16].

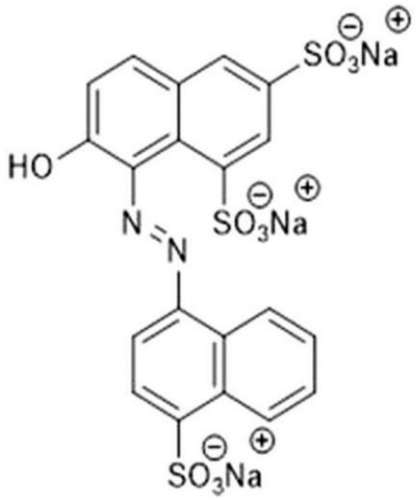
For the analytical chemist the relevant point is that Ponceau 4R exists in aqueous solution as an azo–hydrazone tautomeric pair whose position is sensitive to solvent polarity and hydrogen bonding, so both the wavelength and the intensity of its absorption band depend on the medium in which it is

measured [17]. This is one reason the absorbance of an extract must always be read against a blank carried through the identical procedure.

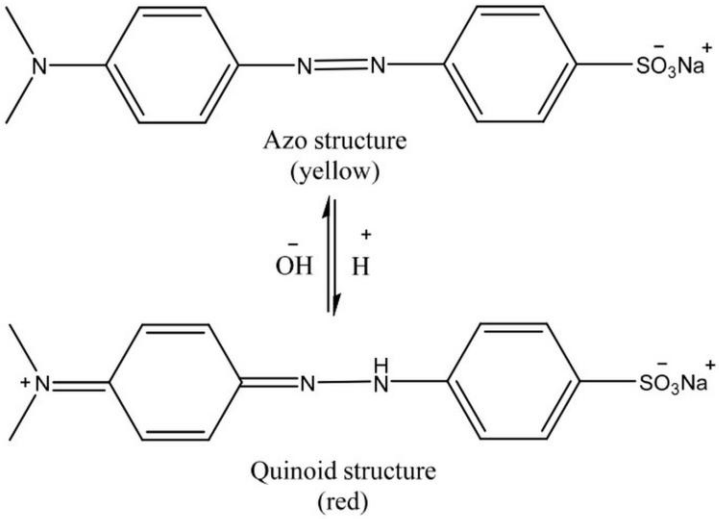
1.2.2 Methyl Orange

Methyl Orange is a water-soluble monoazo sulfonate used extensively in textile dyeing and, in the laboratory, as an acid–base indicator. It reaches the environment mainly through textile effluent, and its persistence and toxicity have both been documented: it has been described as a carcinogenic sulfonated azo dye [18], and sub-lethal exposure of the freshwater amphipod Gammarus pulex produces measurable oxidative-stress and detoxification responses, including altered superoxide dismutase, catalase and glutathione peroxidase activity and raised malondialdehyde [19].

Its most important property for the present work is its acid–base behaviour. Methyl Orange has a single ionisable centre with pK_a = 3.46 [9,10]. Below that value the molecule is protonated at the azo nitrogen and rearranges to the red quinoid (azonium) form; above it, the yellow azo form predominates, and the sulfonate group keeps the species anionic [9,10]. Because the two tautomers absorb at different wavelengths, the pH of the measured solution must be fixed if the absorbance is to be reproducible, and because the protonated form is markedly less hydrophilic than the deprotonated one, pH also controls how readily the dye transfers into an organic phase. The equilibrium is shown in Figure 1-2(b). Because of it the analytical maximum of Methyl Orange is not a fixed number: the value of 485.5 nm entered in Table 1-1 and used throughout Chapters Two and Three is that of the medium in which the extracts were actually read, and lies between the maxima of the pure azo (464 nm) and azonium (508 nm) forms (Section 3.1).



(a) Acid Red 18 (Ponceau 4R)



(b) Methyl Orange: the azo (yellow) and quinoid (red) forms

Figure 1-2: Chemical structures of the two dyes studied in this work.

1.3 Green Analytical Chemistry and the Role of Sample Preparation

Analytical chemistry has spent the past two decades reassessing its own environmental cost. The twelve principles of green analytical chemistry set out by Gałuszka and co-workers place the emphasis on eliminating or minimising reagents and solvents, reducing energy consumption, avoiding derivatisation, and protecting the operator [20]. Quantitative tools such as the

AGREE metric now allow a proposed procedure to be scored against those principles rather than merely described as green [21].

Sample preparation is where most of that environmental cost sits. A raw sample, whether taken from a river or from a soft drink, is rarely fit for direct measurement: it contains interfering species, its ionic background varies, and the analyte is often present below the concentration that the detector can handle. Extraction addresses all three problems at once by separating the analyte from the matrix, removing competing species and raising the concentration to a measurable level. The classical approach relies on partitioning between two immiscible phases, and the extent of transfer is governed by the distribution ratio of the analyte between them [22].

1.4 Microextraction Techniques

Microextraction is the general term for a family of procedures in which the extracting phase is reduced to the microlitre or milligram scale relative to the sample. These procedures are usually non-exhaustive: only a fraction of the analyte is transferred, but the fraction is reproducible and the phase ratio is so favourable that the concentration in the extracting phase is far higher than in the original sample [23,24]. Sensitivity and selectivity are gained, solvent consumption and extraction time fall, and the resulting methods score well on greenness metrics. The main differences between conventional extraction and microextraction are summarised in Table 1-2.

Table 1-2: Comparison of conventional extraction and microextraction techniques [23–26].

Aspect	Microextraction techniques	Conventional extraction techniques
Extracting-phase volume	Microlitres (µL) to a few millilitres	Tens to hundreds of millilitres
Time and cost	Fast, low cost, minimal sample handling	Time-consuming, expensive, labour-intensive
Sensitivity and selectivity	High enrichment; suitable for trace analysis	Moderate; limited preconcentration
Automation	Readily automated and coupled on-line	Difficult to automate
Environmental impact	Low solvent consumption; consistent with green analytical chemistry	Large solvent waste stream
Representative methods	SDME, HF-LPME, EME, DLLME, SHS-LLME, SPME, SBSE, MEPS, MSPE	LLE, Soxhlet extraction, conventional SPE

1.4.1 Classification

Microextraction methods divide naturally into two families according to the physical state of the extracting phase [24,25]. In liquid-based methods the extractant is a small volume of solvent: single-drop microextraction (SDME), in which the analyte is extracted into a microlitre droplet suspended from a syringe needle [27]; hollow-fibre liquid-phase microextraction (HF-LPME), in which the solvent is immobilised in the pores and lumen of a porous polypropylene fibre [28]; electromembrane extraction (EME), in which an electrical potential drives ionised analytes across a supported liquid membrane [29]; dispersive liquid–liquid microextraction (DLLME), in which a ternary solvent system produces a cloudy dispersion of fine extractant droplets and hence an enormous interfacial area [30]; and switchable-hydrophilicity solvent-based liquid–liquid microextraction (SHS-LLME), the technique used in this work.

In solid-based methods the extracting phase is a sorbent held on or dispersed as a solid support: solid-phase microextraction (SPME), stir-bar sorptive extraction (SBSE), microextraction by packed sorbent (MEPS) and magnetic solid-phase extraction (MSPE) [26]. The classification is shown in Figure 1-3.

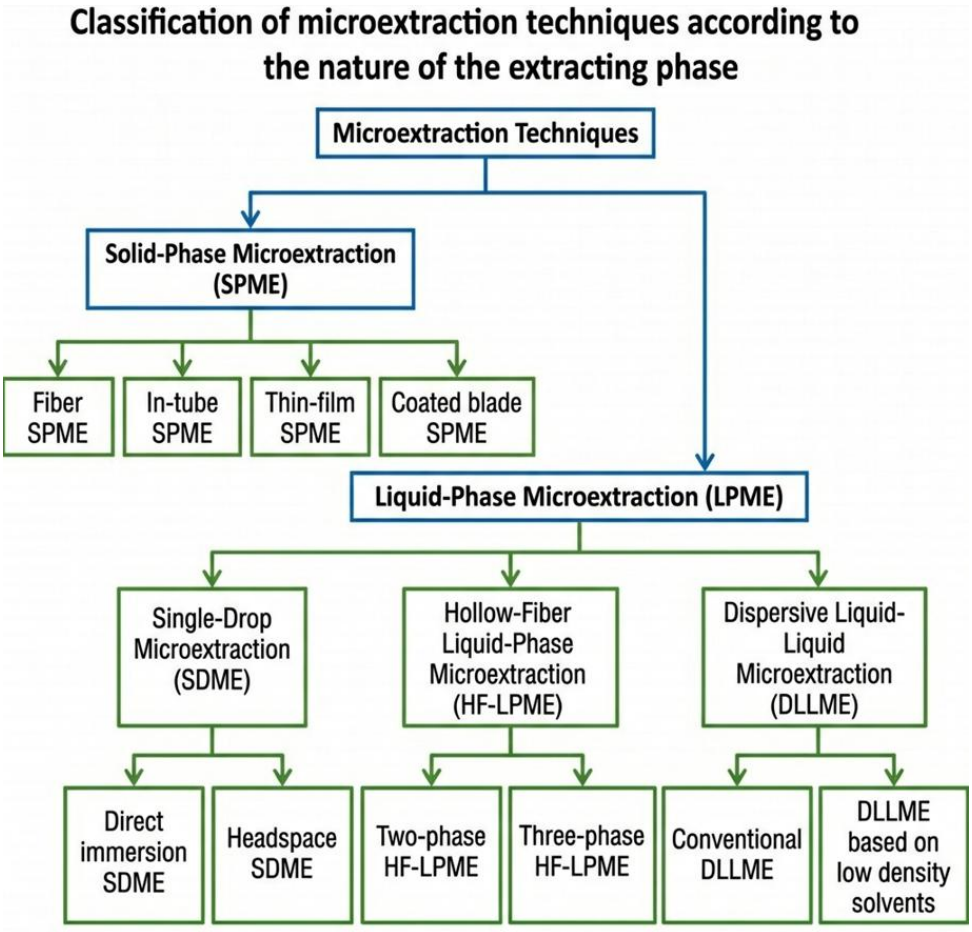


Figure 1-3: Classification of microextraction techniques according to the nature of the extracting phase.

1.5 Switchable-Hydrophilicity Solvents

1.5.1 Concept and origin

The idea of a solvent whose polarity can be reversed on demand was introduced by Jessop and co-workers in 2005, who showed that a mixture of an alcohol and an amidine is converted to an ionic liquid on exposure to carbon dioxide and reverts to the non-ionic form when the CO_2 is removed

under nitrogen or argon [31]. The term switchable-hydrophilicity solvent (SHS) was defined five years later for a solvent that is hydrophobic and water-immiscible under air but becomes fully water-miscible under one bar of CO_2, the first example being N,N,N′-tributylpentanamidine [32]. The concept was then extended to inexpensive, commercially available tertiary amines, which is the class used in analytical microextraction today [33].

The switching chemistry is an acid–base equilibrium. In contact with carbonated water, or with an added mineral acid, a tertiary amine is protonated to the corresponding ammonium salt, which is water-soluble; addition of a base, or removal of CO_2, regenerates the neutral amine, which separates as a distinct organic phase. For a tertiary amine the equilibrium is:

$$R_3N + H_2O + CO_2 \rightleftharpoons R_3NH^+ + HCO_3^- \qquad (1\text{-}1)$$

and for a secondary amine, where carbamate formation competes:

$$2\ R_2NH + CO_2 \rightleftharpoons R_2NH_2^+ + R_2NCOO^- \qquad (1\text{-}2)$$

In analytical practice the CO_2/N_2 cycle is usually replaced by the simpler and faster addition of hydrochloric acid to dissolve the amine and sodium hydroxide to regenerate it, which is the route adopted in this work. The two states of the solvent are illustrated in Figure 1-4.

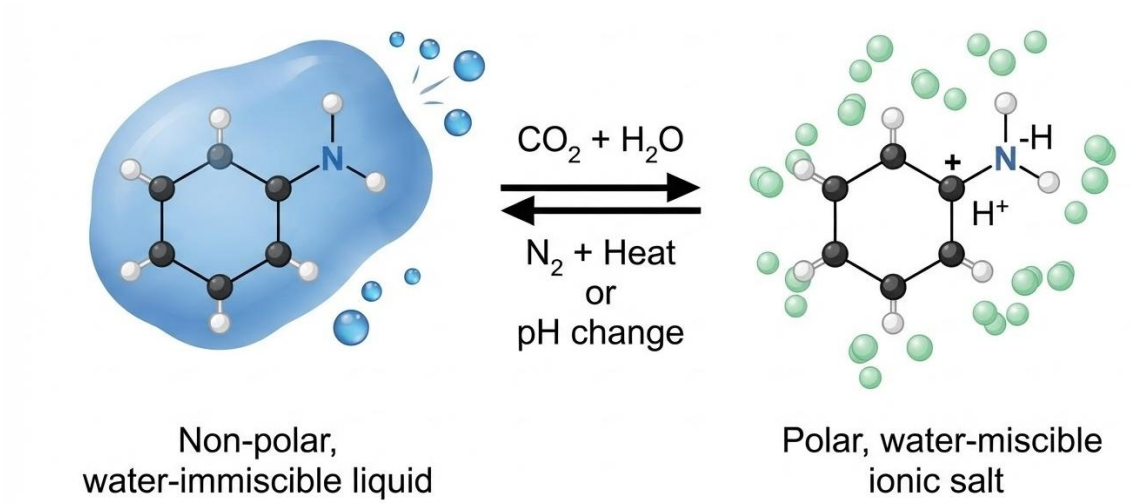


Figure 1-4: Reversible switching of a hydrophilicity-switchable solvent between its hydrophilic (protonated) and hydrophobic (neutral) forms.

1.5.2 Physicochemical requirements for switchable behaviour

Not every amine will act as an SHS. Two numerical windows have to be satisfied simultaneously, and both bounds of each window exist for a specific physical reason [34,35].

The first is a hydrophilicity window. The amine must have a partition coefficient in the range $1.0 < \log K_{ow} < 2.5$ [35]. Below this range the neutral amine is already miscible with water, so there is no biphasic 'off' state to switch from; above it the protonated bicarbonate salt remains too hydrophobic to dissolve in the aqueous phase, so the switch never occurs [34].

The second is a basicity window, $9.5 < pK_{aH} < 11$ [35]. The lower bound exists because carbonated water is only weakly acidic: an amine that is **not basic enough** will not be protonated to an appreciable extent and will therefore fail to become water-miscible. Vanderveen and co-workers state the point directly: if an amine has insufficient basicity it will not react with carbonated water enough for a switch from a biphasic to a monophasic mixture [34]. The upper bound exists for the opposite reason: an amine that is too basic guanidines, with pK_{aH} near 13.6, are the standard example binds CO_2 so strongly that it cannot be stripped by sparging or mild heating, and the reverse switch fails [34].

Two qualifications should be noted. First, the window can be shifted: raising the CO_2 pressure or the water-to-amine volume ratio allows some amines lying outside it to function as SHSs [35]. Second, these are necessary but not sufficient conditions amines that satisfy both criteria and nevertheless fail to switch have been reported [34]. N,N-Dimethylcyclohexylamine (DMCHA), the solvent selected in this work, lies within both windows and is among the most widely used tertiary-amine SHSs in analytical practice [33,36].

1.5.3 Switchable-hydrophilicity solvent liquid–liquid microextraction (SHS-LLME)

The first analytical use of an SHS as a microextraction solvent was reported by Lasarte-Aragonés and co-workers, who dissolved DMCHA in an aqueous sample under CO_2 and then recovered it as a separate organic phase by adding sodium hydroxide, with no centrifugation required [37]. The sequence has since become standard: the protonated amine is fully miscible with the sample, so extraction takes place under homogeneous conditions with no interfacial mass-transfer resistance; addition of base then regenerates the neutral amine as fine droplets that carry the analyte with them and coalesce into a small, analyte-enriched phase [36]. The approach has proved effective for dyes in particular. It has been applied to Sudan dyes in solid foods with HPLC–UV detection [38], to Sudan I in spices with spectrophotometric detection [39], to Sudan I–IV in food and water samples by HPLC–DAD in a total analysis time of about four and a half minutes [40], and to tartrazine with chemometric optimisation [41]. The attraction for dye analysis is that the extraction, the preconcentration and the phase separation are all achieved with a few hundred microlitres of a single, recoverable amine. The complete sequence, as applied in this work, is illustrated in Figure 1-5.

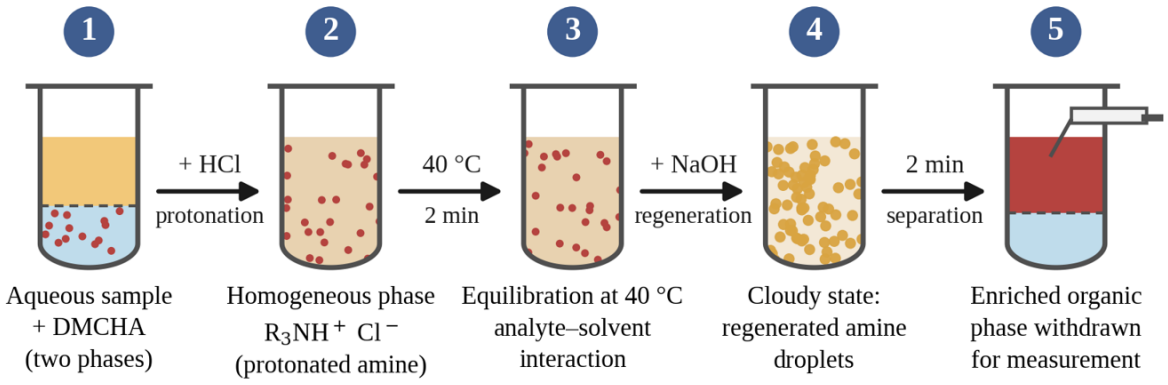


Figure 1-5: Step-by-step SHS-LLME procedure with N,N-dimethyl cyclohexyl amine

1.5.4 Factors affecting SHS-LLME

Seven operating variables govern the recovery obtained in an SHS-LLME procedure (Figure 1-6), and each of them was examined experimentally in this work.

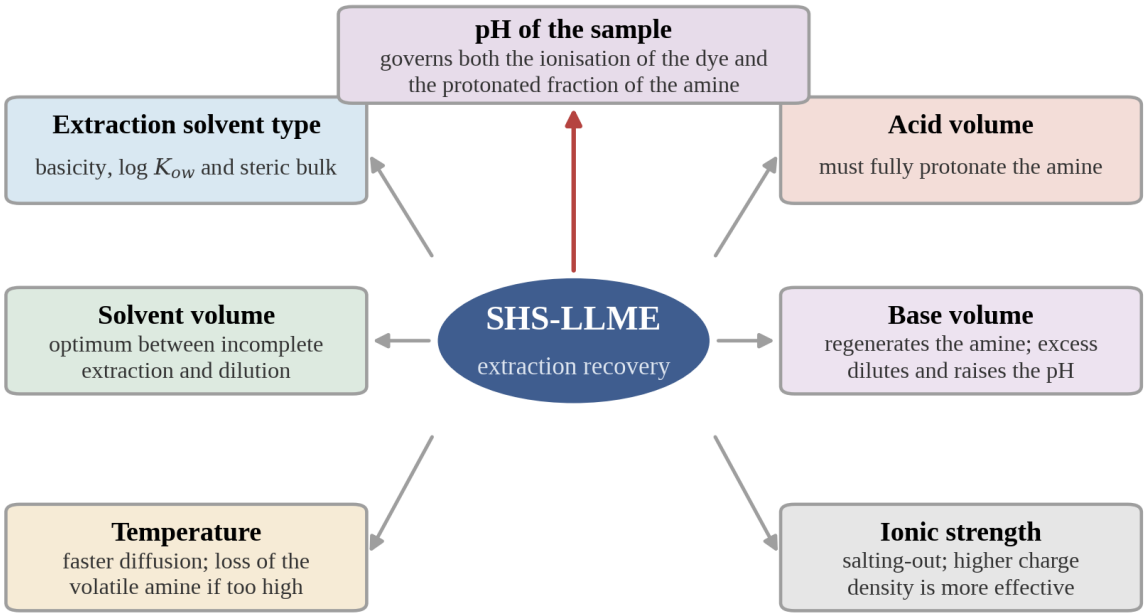


Figure 1-6: Variables that control the recovery of an SHS-LLME procedure and the reason each one matters.

1.5.4.1 Type of extraction solvent

The identity of the amine determines both the efficiency of the switch and the affinity of the regenerated organic phase for the analyte. Amines differ in basicity, in log K_{ow} and in steric bulk, and the balance between these determines which analytes partition well [34,36]. Selecting the solvent is therefore the first optimisation step, not a matter of convenience.

1.5.4.2 Volume of extraction solvent

The response to solvent volume passes through a maximum. Too little solvent gives incomplete extraction and poor phase separation, and the precision deteriorates; beyond the optimum, the extracted analyte is distributed through

a larger organic volume and the measured concentration and hence the absorbance falls through simple dilution [36].

1.5.4.3 Temperature

A moderate rise in temperature lowers the viscosity of the medium, raises diffusion coefficients and speeds the approach to equilibrium, so that the extraction is completed in less time. Excessive heating is counterproductive: it promotes evaporative loss of the volatile amine and may destabilise the analyte [36].

1.5.4.4 Volume of acid

Acid is the trigger for the forward switch. Enough must be added to protonate the amine completely and produce a single homogeneous phase; below that point the extraction is incomplete. Once protonation is complete, further acid contributes nothing to the switch but does increase the ionic strength and the total aqueous volume, which can reduce the measured response [36].

1.5.4.5 Volume of base

Base drives the reverse switch, deprotonating the ammonium salt and regenerating the hydrophobic amine as a separate phase. The amount required is stoichiometrically related to the acid already present. An excess dilutes the system and raises the pH of the aqueous phase, which for an ionisable analyte such as Methyl Orange shifts the equilibrium towards the more hydrophilic anionic form and lowers recovery [36].

1.5.4.6 Ionic strength

Adding an inorganic salt raises the ionic strength of the aqueous phase. Salt ions compete with the analyte and with the solvent for water molecules, so the solubility of the dye in the aqueous phase falls and its transfer to the organic phase is favoured the salting-out effect [42]. The magnitude of the

effect depends on the charge density of the cation, so divalent salts such as calcium chloride are generally more effective than sodium or potassium chloride at the same mass concentration. Above a certain concentration the benefit is offset by increased viscosity, which slows mass transfer between the phases [42].

1.5.4.7 pH of the sample

For an ionisable analyte, pH is normally the dominant variable, and it acts on both partners in the extraction at once. It fixes the fraction of the amine present in the protonated, water-miscible form, and it fixes the ionisation state of the dye. Sulfonated azo dyes remain anionic across the practical pH range, so their transfer into a neutral organic phase depends on ion association with the protonated amine: the more acidic the medium, the larger the fraction of amine available in the cationic form and the more effective the ion pairing [36,43]. For Methyl Orange there is an additional contribution, since below its pK_a of 3.46 the neutral quinoid form itself has a higher affinity for the organic phase [9,10].

1.6 Solid-Phase Microextraction

Solid-phase microextraction was introduced by Arthur and Pawliszyn in 1990 [44]. The analyte partitions between the sample matrix and a thin stationary-phase coating, typically 1–2 cm of polymer or sorbent applied to a fused-silica fibre. Extraction is carried out either by immersing the fibre directly in the sample or by exposing it to the headspace above it, and the analytes are then desorbed thermally in a gas-chromatographic injector or eluted with a small volume of solvent for HPLC or capillary electrophoresis [45].

The procedure therefore has two steps. In extraction, the analytes are adsorbed or absorbed onto the coating according to their affinity for it, which gives selective preconcentration. In desorption, the loaded fibre is transferred

to the instrument and the analytes are released. The advantages and limitations of the technique are summarised in Table 1-3. Related sorbent-based methods include stir-bar sorptive extraction, which uses a much larger volume of poly(dimethylsiloxane) on a magnetic stir bar and therefore recovers low-log K_{ow} analytes better than SPME [46], and microextraction by packed sorbent, in which a few milligrams of sorbent are packed directly into a syringe barrel for on-line operation [47].

Both sampling modes and the desorption step are shown in Figure 1-7.

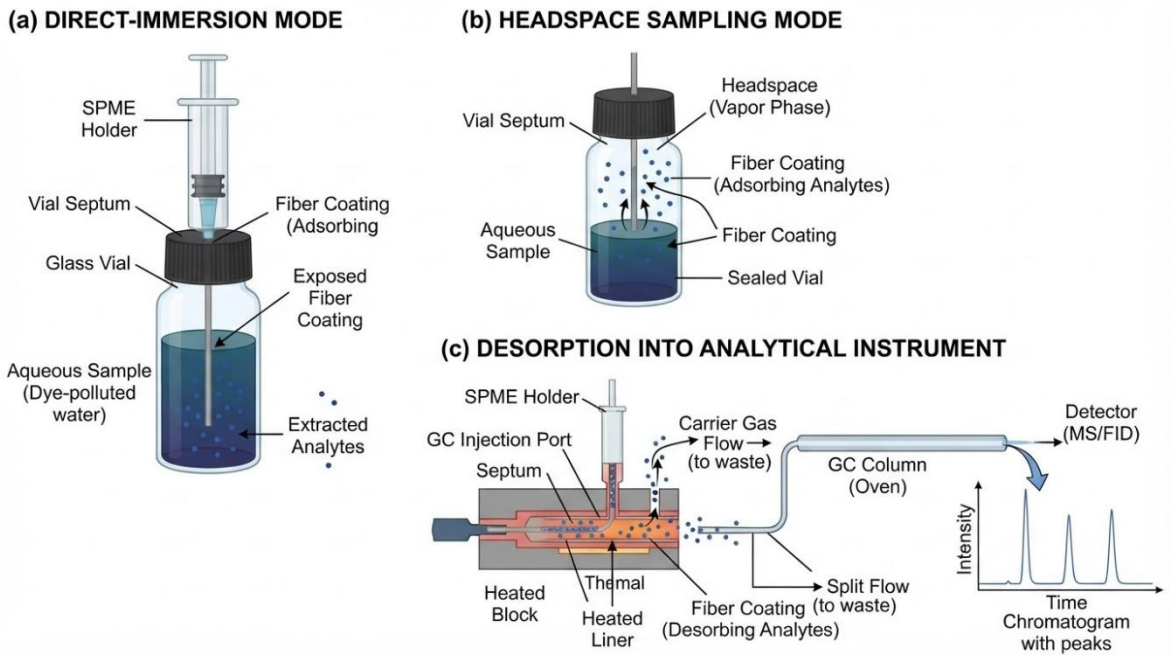


Figure 1-7: Solid-phase microextraction: (a) direct-immersion and (b) headspace sampling modes, followed by (c) desorption into the analytical instrument.

Table 1-3: Advantages and limitations of solid-phase microextraction [44,45].

Advantages	Limitations
Solvent-free or near-solvent-free, minimising chemical waste	Coating deteriorates with repeated use, so extraction efficiency falls and fibres need periodic replacement
Integrates sampling, extraction and sample introduction in a single step	Selectivity depends entirely on the availability of a suitable coating chemistry
Rapid sample preparation compared with conventional methods	Limited sorbent capacity, so the linear range can be narrow for concentrated samples

Advantages	Limitations
Miniaturised format suitable for portable and high-throughput use	Less effective for proteins and other high-molecular-weight species; carryover between runs must be controlled

1.7 Magnetic Solid-Phase Extraction

Magnetic solid-phase extraction was described by Šafaříková and Šafařík in 1999 as a way of avoiding the packed cartridge altogether [48]. Instead of passing the sample through a column, a magnetic or magnetisable sorbent is dispersed directly into the sample or suspension. Because the particles are distributed throughout the bulk liquid, the diffusion path is short and the whole of the available surface is accessible, so adsorption equilibrium is reached quickly. Once the analytes have been retained, an external magnet usually a neodymium–iron–boron block is held against the vessel wall to collect the sorbent, and the supernatant is decanted. Filtration and centrifugation are eliminated, which removes two of the steps at which analyte is most often lost [49,50]. The retained analytes are then eluted with a small volume of a suitable solvent, and the sorbent can generally be regenerated and reused. The sequence is shown in Figure 1-8.

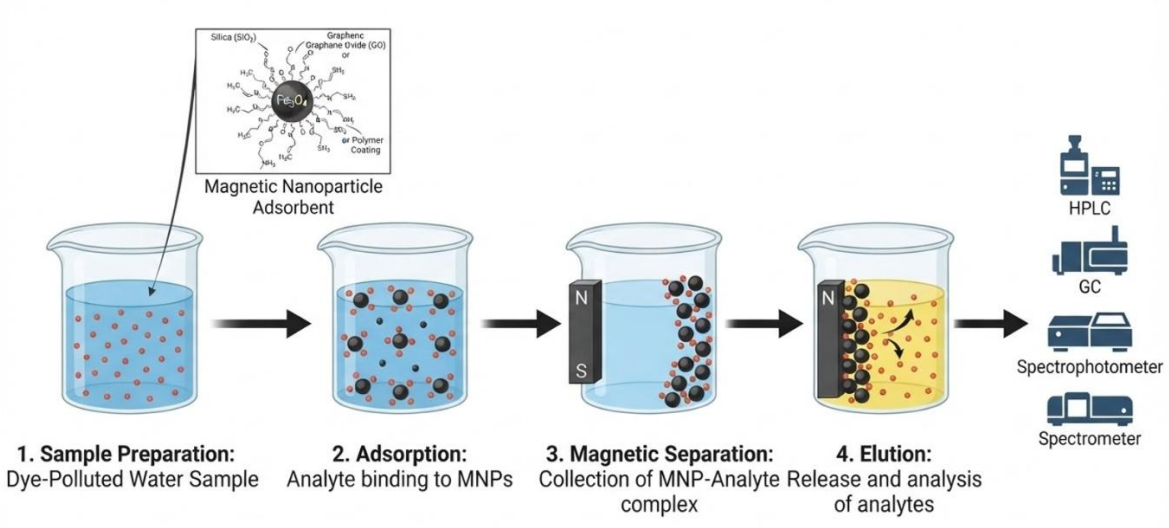


Figure 1-8: Schematic representation of the magnetic solid-phase extraction procedure.

MSPE has been applied to a wide range of analyte classes, and a recent review is devoted specifically to the extraction and preconcentration of anionic azo dyes on modified magnetic nanoparticles, where the nature of the surface

modifier, the pH, the zeta potential and the specific surface area are identified as the variables that control recovery [51]. Applications to dyes in food and water matrices have been reviewed separately [50].

1.7.1 Iron oxide nanoparticles

Nanoparticles are materials with at least one characteristic dimension between 1 and 100 nm. Their defining feature is a very high surface-area-to-volume ratio, which multiplies the number of accessible surface sites and thereby raises the rate and capacity of interfacial processes such as adsorption [52,53]. Three iron oxide phases are magnetically relevant: hematite (α-Fe_2O_3), maghemite (γ-Fe_2O_3) and magnetite (Fe_3O_4) [54]. Magnetite is the phase of choice for extraction work because it combines a high saturation magnetisation with superparamagnetic behaviour at small particle size it responds strongly to an applied field but retains no appreciable remanence once the field is removed, so the particles redisperse instead of aggregating irreversibly [52,53]. Its surface, terminated by hydroxyl groups, is also readily modified, which is what allows selectivity to be engineered into the sorbent.

1.7.2 Surface functionalisation

Bare magnetite nanoparticles have a high surface energy and a strong tendency to aggregate in order to reduce it. They are also chemically active and oxidise on exposure to air, gradually losing both dispersibility and magnetisation [55,56]. A protective coating is therefore not optional. Functionalisation serves several purposes at once: it prevents aggregation, it

protects the core against oxidation and acid dissolution, it improves dispersibility in aqueous media, and it introduces the functional groups on which selective retention of the analyte depends [56,57].

Four architectures are commonly distinguished, shown in Figure 1-9 and compared in Table 1-4 [55,58].

Table 1-4: Structural types of magnetic iron oxide nanoparticle hybrids [55,56,58].

Structure	Description	Typical shell materials	Principal advantage
Core–shell	An iron oxide core encapsulated within an organic or inorganic shell	Silica, poly(ethylene glycol), gold	Colloidal stability plus surface functional groups for further modification
Shell–core–shell	The magnetic core is placed between two non-magnetic functional layers	Polymer, silica, fluorescent materials	Prevents aggregation and sedimentation and adds a second surface function
Matrix-dispersed	Magnetic particles dispersed within a continuous matrix	Polymeric or amorphous carriers	Prevents formation of bulk ferromagnetic domains; suitable for composite sorbents
Janus	Asymmetric particles carrying magnetic and functional material on opposite faces	Au–Fe_3O_4, Pt–Fe_3O_4, γ-Fe_2O_3–SiO_2	Dual functionality on a single particle; anisotropic surface chemistry

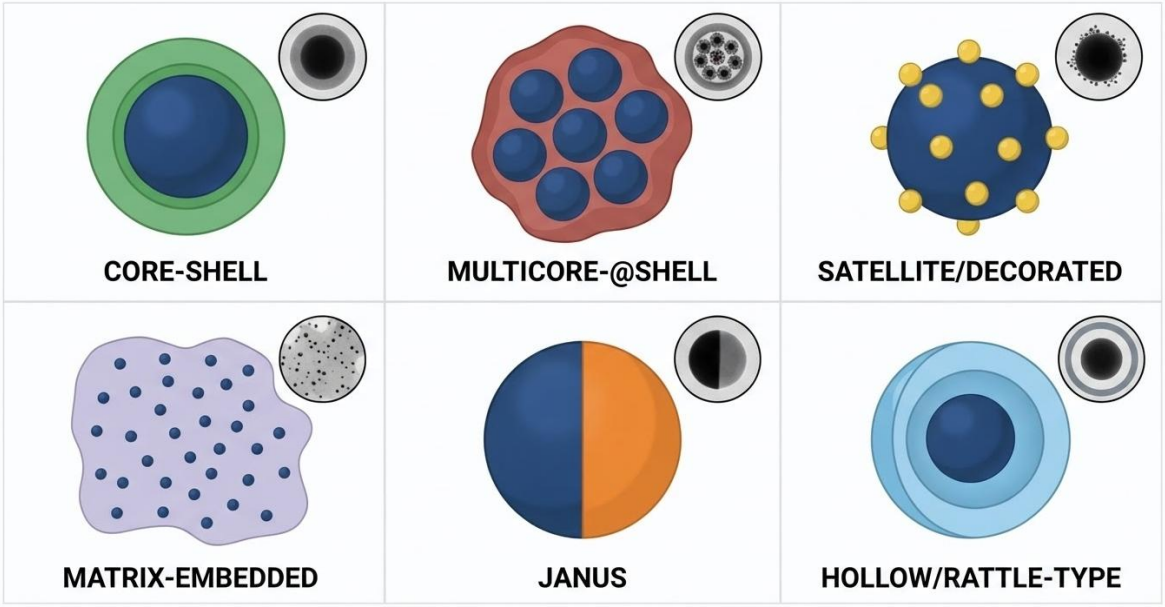


Figure 1-9: Typical morphologies of magnetic composite nanomaterials.

The magnetic iron oxide particles are shown in blue and the non-magnetic functional entities and matrix materials in other colours.

1.7.3 Coating materials

Coatings are broadly either organic or inorganic, and the two families offer different trade-offs, as set out in Table 1-5. The available modification routes are summarised in Figure 1-10.

Table 1-5: Organic and inorganic coatings for iron oxide nanoparticles [56,57].

Coating type	Representative examples	Key properties	Notes and limitations
Organic (polymers and surfactants)	Dextran, starch, PEG, PLA, PEI, alginate, PMMA, polyaniline	Biocompatible, hydrophilic, prevent aggregation; surface readily functionalised (–OH, –COOH, $–NH_2$)	Can affect pharmacokinetics and biodistribution; thermal stability lower than inorganic shells
Inorganic – silica	SiO_2 (Fe_3O_4@SiO_2)	Improves colloidal and chemical stability; surface rich in silanol groups	Requires surface activation before conjugation

Coating type	Representative examples	Key properties	Notes and limitations
Inorganic – carbon	Carbon shell (Fe_3O_4@C)	High thermal and chemical stability; conductive and oxidation-resistant	Multi-step synthesis: core, polymer coat, then thermal treatment
Inorganic – metal	Gold, silver, copper	Optical properties (LSPR, SERS); magneto-optical hybrid behaviour	Lattice mismatch; stabilisers or encapsulation usually needed

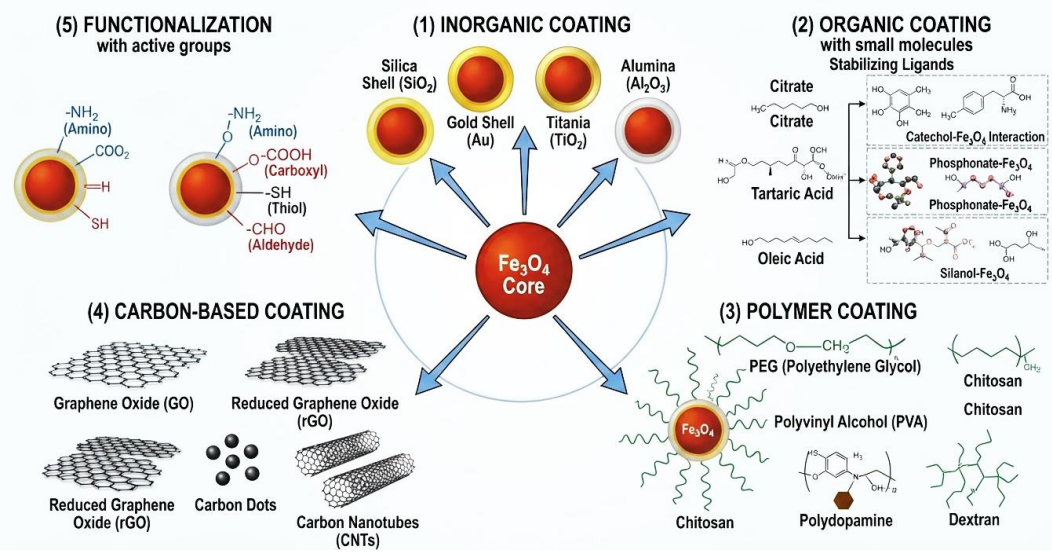


Figure 1-10: Routes for modifying the surface properties of iron oxide nanoparticles.

1.8 Polyaniline and PANI/Fe_3O_4 Nanocomposites

1.8.1 Polyaniline as a sorbent

Polyaniline is the conducting polymer most often used as an adsorbent, and the reason lies in its nitrogen chemistry. The emeraldine base form is converted to the conducting emeraldine salt by protonic acid doping, and the resulting material is an environmentally stable nitrogen base salt rather than a carbonium ion species; its conductivity depends on two variables, the degree of oxidation and the degree of protonation [59]. In that salt, most of the positive charge resides on the nitrogen atoms [60]. Those protonated amine (–NH^+–) and imine (=NH^+–) centres, charge-balanced by mobile counter-anions, are the sites at which an incoming anion can exchange.

The oxidation states of the polymer and the doping equilibrium that generates these sites are shown in Figure 1-11.

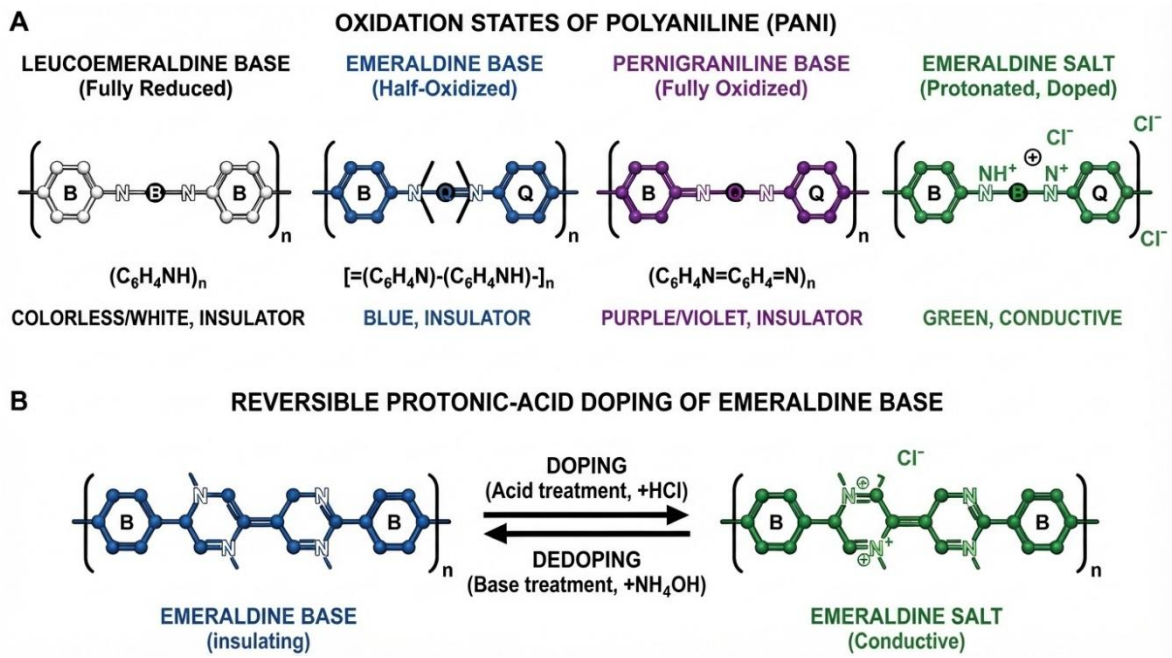


Figure 1-11: Oxidation states of polyaniline and the reversible protonic-acid doping of the emeraldine base to the conducting emeraldine salt.

For an anionic sulfonated dye this produces a direct electrostatic interaction between the dye sulfonate groups and the protonated nitrogen sites of the polymer. Density-functional calculations on the polyaniline–Methyl Orange system support electrostatic interaction as the mechanism mainly responsible for adsorption [61], and comparable amine-functionalised magnetic sorbents show the same behaviour, the $–NH_3^+$ groups binding the $–SO_3^-$ groups of the dye [62]. Electrostatics does not act alone: the nitrogen atoms can form hydrogen bonds, the aromatic backbone allows π–π interactions with the aromatic dye, and van der Waals forces contribute as well [43,63,64].

The interaction is strongly pH-dependent, because polyaniline itself converts between its conducting salt and non-conducting base forms in the region of pH 4–6 [43]. Uptake of sulfonated azo dyes is therefore highest in acidic to mildly acidic media, where the nitrogen sites are protonated while the dye is fully ionised, and falls in alkaline solution because hydroxide ions compete

with the dye anion for the protonated sites [62]. This same pH dependence is what makes an alkaline or alcoholic eluent effective in the desorption step. Polyaniline is stable in both strongly acidic and strongly alkaline media, which is one reason it has been adopted as a solid-phase extraction sorbent rather than only as a bulk adsorbent [64]. Reported adsorption capacities for polyaniline-based materials against a range of dyes have been compiled in dedicated reviews [63,65,66].

The interactions involved, together with the magnetic recovery step that follows adsorption, are summarised in Figure 1-12.

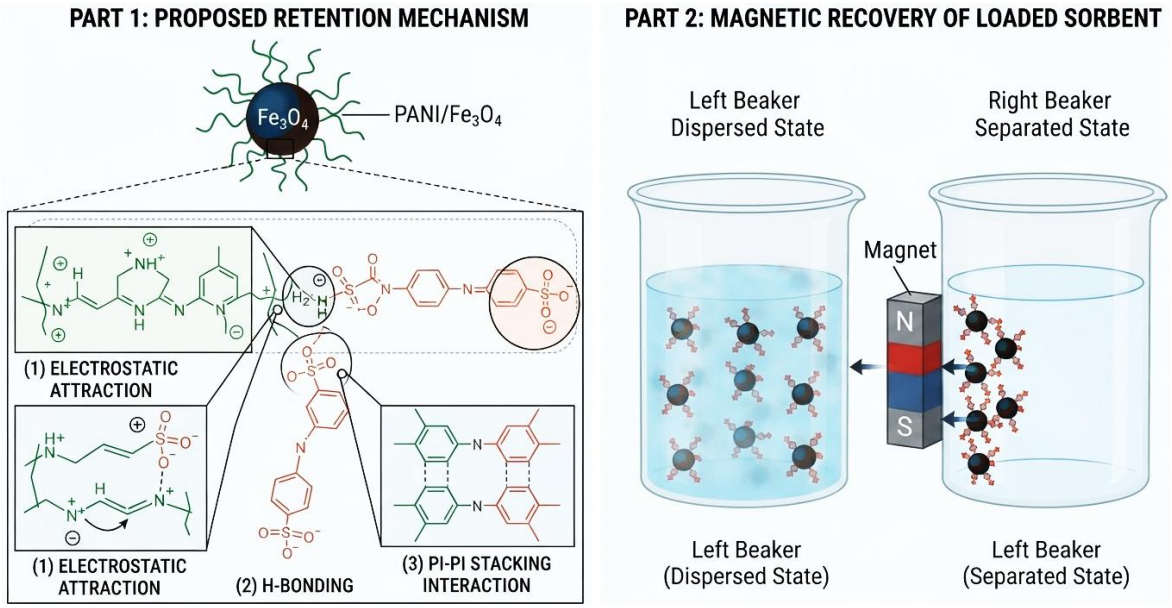


Figure 1-12: Proposed retention mechanism of an anionic sulfonated azo dye on a PANI/Fe_3O_4 composite, and magnetic recovery of the loaded sorbent.

1.8.2 Magnetic polyaniline composites for anionic azo dyes

Combining polyaniline with magnetite gives a material that has the binding chemistry of the polymer and the separability of the oxide. The magnetite provides the response to an external field that allows the sorbent to be recovered in seconds, while the polymer layer supplies the functional groups and, incidentally, protects the oxide core from dissolution [67]. Coating also

reduces aggregation of the magnetite particles and keeps a larger fraction of the surface accessible.

Materials of this type have performed well against exactly the analytes of interest here. Reported capacities for Methyl Orange range from 156 mg g^{-1} on a polyaniline/Fe_3O_4–hydrotalcite composite [68] through 231 mg g^{-1} on Fe_3O_4@PANI [69] and 446 mg g^{-1} on a hierarchical MWCNT/Fe_3O_4/PANI composite [67] to 585 mg g^{-1} on a hierarchical GO/Fe_3O_4/PANI composite [70]. For Acid Red 18, a superparamagnetic $CoFe_2O_4$/polyaniline nanocomposite gave a Langmuir capacity of 172 mg g^{-1} under ultrasonic assistance [71]. In most cases the uptake was pH-dependent and the material could be regenerated over several cycles. A summary is given in Table 1-6.

Table 1-6: Reported performance of polyaniline-based magnetic sorbents towards anionic azo dyes.

Sorbent	Target dye	Capacity (mg g^{-1})	Reference
Fe_3O_4@PANI	Methyl Orange	231	[69]
Fe_3O_4@PANI	Reactive Orange 16	234	[69]
GO / Fe_3O_4 / PANI	Methyl Orange	585	[70]
MWCNT / Fe_3O_4 / PANI	Methyl Orange	446	[67]
MWCNT / Fe_3O_4 / PANI	Congo Red	417	[67]
PANI / Fe_3O_4–hydrotalcite	Methyl Orange	156	[68]
$CoFe_2O_4$ / polyaniline	Acid Red 18	172	[71]

1.9 Coupling SHS-LLME with Magnetic Solid-Phase Extraction

The two techniques described above operate by different mechanisms, and combining them in sequence exploits that difference. In the first stage, SHS-LLME transfers the dye out of the bulk aqueous sample by ion association with the protonated amine and delivers it into a small, solvent-rich phase. In the second stage, MSPE retains the dye from that phase on the surface of the PANI/Fe_3O_4 composite by electrostatic interaction with the protonated

nitrogen sites, after which the sorbent is collected magnetically and the analyte released into a small volume of eluent.

Liquid-phase partitioning followed by solid-phase adsorption gives two orthogonal separation mechanisms, so matrix components that survive the first stage are unlikely to survive the second. Phase separation is simplified, since

the magnet replaces filtration and centrifugation, and the total organic solvent consumption remains small. Precedent for the combination is established: Hassan and co-workers coupled SHS-LLME to magnetic-nanoparticle dispersive solid-phase microextraction with spectrophotometric detection for erythrosine in food [72], and a closely related SHS-LLME/MSPE procedure has been reported for Sunset Yellow on modified Fe_3O_4 [73]. Magnetic sorbents have also been used on their own for Ponceau 4R and related colourants in candies and beverages [74,75], and green miniaturised extraction has been applied to the same group of red dyes in food [76]. The complete two-stage procedure is set out in Figure 1-13.

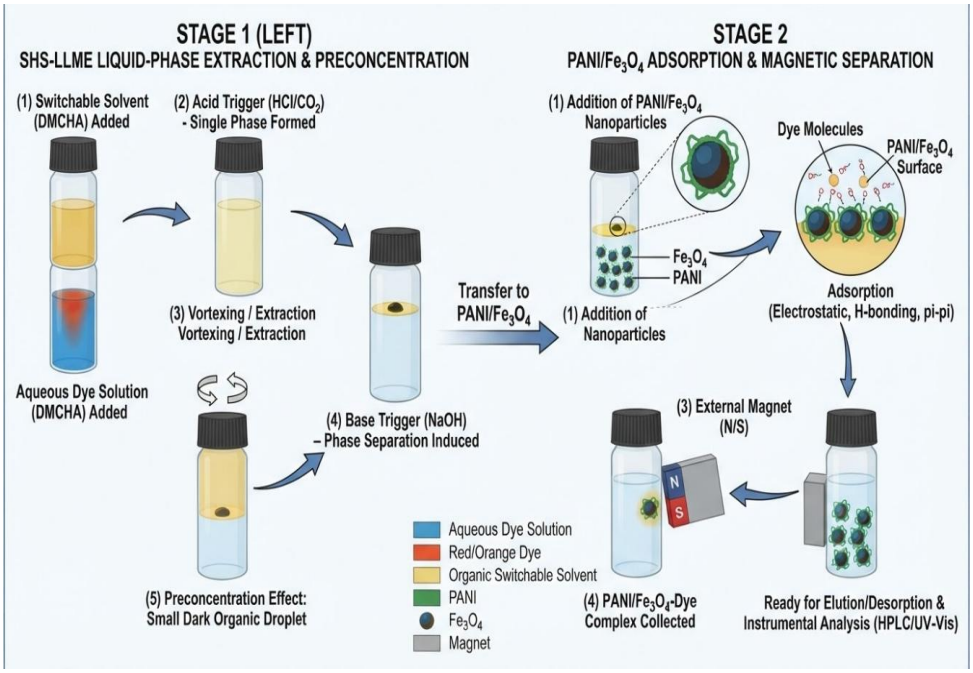


Figure 1-13: The coupled SHS-LLME/MSPE procedure

1.10 Chemometric Optimisation of the Extraction

An extraction procedure governed by four or more interacting variables cannot be optimised reliably by changing one factor at a time. The one-factor-at-a-time approach explores only a narrow path through the experimental domain, it cannot detect interactions between variables, and the optimum it reports is conditional on the arbitrary values at which the other factors were held [77,78]. Where interactions are present and in a system where pH governs both the ionisation of the dye and the protonation of the solvent, they certainly are the true optimum can lie well away from anything the univariate study visits [79].

Experimental design addresses this by varying all factors simultaneously according to a planned pattern, so that main effects and interactions can be estimated independently from a modest number of runs [78,80]. Screening designs such as the Plackett–Burman design identify which of many candidate variables actually matter [81], after which a response-surface design is used to model the region around the optimum.

Response surface methodology, introduced by Box and Wilson [82], fits a second-order polynomial to the measured response as a function of the coded factor levels:

$$y = \beta_0 + \Sigma \beta_i x_i + \Sigma \beta_{ii} x_i^2 + \Sigma \beta_{ij} x_i x_j + \varepsilon \qquad (1\text{-}3)$$

where y is the response, x_i the coded factors, β_0 the constant term, β_i the linear coefficients, β_{ii} the quadratic coefficients, β_{ij} the interaction coefficients and ε the residual [77]. The two designs most used for this purpose are the central composite design and the Box–Behnken design [83,84]. A central composite design for k factors comprises a two-level factorial portion of 2^k runs, an axial or star portion of 2k runs at a distance α from the centre, and a number of replicated centre points that provide an estimate of pure error; setting α =

$(2^k)^{1/4}$ makes the design rotatable, whereas setting $\alpha = 1$ gives the face-centred variant, in which no factor is examined outside its factorial range [77,85].

The fitted model is assessed by analysis of variance. Significance of the regression is judged from the model F-value and the associated probability, the proportion of variance explained from R^2 and its adjusted and predicted forms, and the adequacy of the functional form from the lack-of-fit test, in which the residual variance is compared against the pure error obtained from the replicated centre points; a significant lack of fit indicates that the second-order polynomial does not adequately describe the curvature of the data and must be addressed rather than ignored [86]. Multicollinearity among the model terms is monitored through the variance inflation factor.

The geometry of the design and the shape of the surface it produces are illustrated in Figure 1-14.

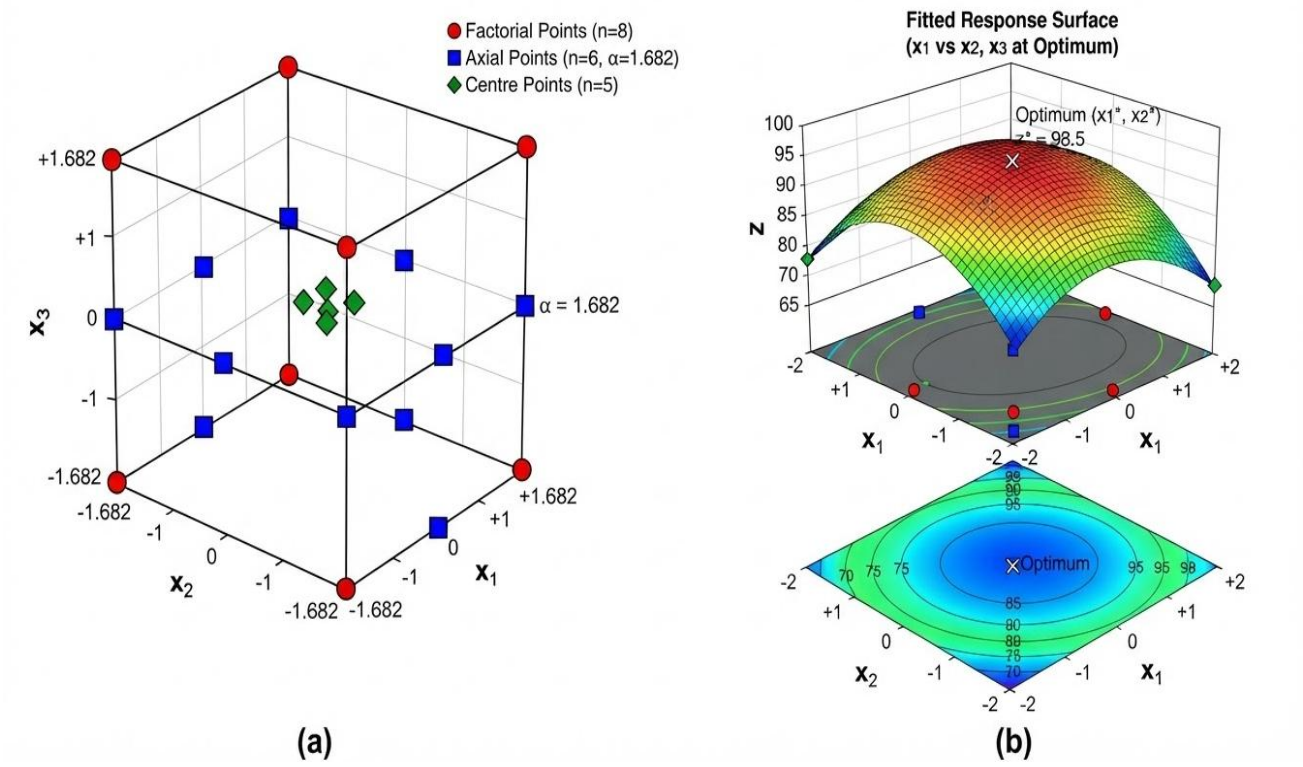


Figure 1-14: (a) Geometry of a three-factor central composite design, and (b) a fitted second-order response surface with its contour projection.

Once an adequate model is available, the operating point is located with the desirability function of Derringer and Suich, which converts the response into a dimensionless desirability on a scale from zero to one and maximises it over the experimental domain [87,88]. Where the optimum is found at a boundary of the design space, the true optimum lies outside the region studied and this should be stated explicitly. The approach has been applied widely to microextraction procedures, including for the preconcentration of azo dyes [41,89–91].

1.11 Previous Studies

Numerous investigations have addressed the extraction, preconcentration and determination of synthetic dyes using sorbent-based and solvent-based microextraction techniques. Table 1-7 collects twenty representative studies published between 2013 and 2025, giving for each of them the extraction technique, the sorbent or extraction solvent employed, the analytes, the detection system and the reported figures of merit (linear range, limit of detection, precision, enrichment or preconcentration factor and recovery), together with the matrix analysed. Entries marked NR indicate values that the original publication does not report or that could not be retrieved from the accessible record. Taken together, the table shows that magnetic sorbents based on conducting polymers and switchable-hydrophilicity solvents have each been applied successfully to azo dyes, but that the two have rarely been combined, and that Acid Red 18 and Methyl Orange have received markedly less attention than the food colourants Sunset Yellow and Tartrazine.

Table 1-7: Summary of previous studies related to the extraction, preconcentration, and determination of synthetic dyes.

Author(s) (Year)	Technique	Sorbent / extraction solvent	Analyte(s)	Detection	Linear range	LOD	RSD (%)	EF / PF	Recovery (%)	Matrix	Ref.
Bagheri et al. (2013)	D-μ-SPE	Fe_3O_4@poly(aniline-naphthylamine)	Rhodamine B	Spectro-fluorimetry	0.35–5.00 μg L^{-1}	0.10 μg L^{-1}	4.2	NR	92 (abs.); 94–99 (rel.)	Cosmetics, detergents	[92]
Shariati-Rad et al. (2014)	MSPE (CCD)	SiO_2@Fe_3O_4	Methyl Orange	UV–Vis (505 nm)	10.0–120.0 ng mL^{-1}	3.7 ng mL^{-1}	1.8–3.9	PF 45	97.8–114.2	River water, wastewater	[93]
Xu et al. (2015)	MSPE	Fe_3O_4@PANI	Sudan I–IV	UFLC–UV	NR	0.041–0.151 ng mL^{-1}	1.3–5.4 (intra); 2.6–7.3 (inter)	NR	92.4–106.9	Environmental water	[94]
Ghasemi & Kaykhaii (2016)	Micro-cloud point extraction	Triton X-114	Orange G, Methyl Orange, Acid Red 18	UV–Vis	2.0–10.0; 0.2–1.0; 2–12 mg L^{-1}	1.6; 0.6; 111.0 μg L^{-1}	< 13.1	NR	NR	Water	[95]
Jangju et al. (2017)	D-μ-MSPE	Zein-modified Fe_3O_4	Carmoisine, Ponceau 4R, Sunset Yellow, Allura Red	HPLC–DAD (500 nm)	1–1000 ng mL^{-1}	0.3–0.9 ng mL^{-1}	< 5.8	EF 224–441	100–103	Beverages, snack, candy	[75]
Pochivalov et al. (2018)	Surfactant-mediated SHS microextraction	Sodium hexanoate / hexanoic acid	Sudan I–III	HPLC–UV	NR	0.028–0.19 mg kg^{-1}	NR	NR	NR	Salted salmon, spices	[38]
Chen et al. (2019)	MSPE	PEI-functionalised Fe_3O_4	Amaranth, Ponceau 4R, Sunset	HPLC	NR	NR	NR	NR	NR	Candy, jelly, carbonat	[74]

Author(s) (Year)	Technique	Sorbent / extraction solvent	Analyte(s)	Detection	Linear range	LOD	RSD (%)	EF / PF	Recovery (%)	Matrix	Ref.
			Yellow, Allura Red							ed drink	
Faraji (2019)	DES-VA-DLLME	Thymol / benzyltriethylammonium chloride DES	Amaranth, Ponceau 4R (Acid Red 18), Allura Red, Azorubine, Erythrosine	HPLC	0.5–500 μg L^{-1}	0.01 – 0.08 μg L^{-1}	< 6	EF 95–100	90–97 (abs.); 94.2–100.8 (rel.)	Beverage, jelly, chocolate	[76]
Hashemi et al. (2019)	PT-SPE (Box–Behnken)	$NiFe_2O_4$-decorated exfoliated graphite	Methyl Orange, Acid Red 18	UV–Vis	5–250 μg L^{-1}	0.9 (MO); 1.0 (AR 18) μg L^{-1}	NR	NR	NR	Seawater	[96]
Hassan et al. (2021)	SHS-LLME + D-MSPME	Octylamine; Fe_3O_4@XAD-16	Erythrosine	UV–Vis (520 nm)	86.3–1000 ng mL^{-1}	< 25.9 ng mL^{-1}	< 4.1 (intra); < 7.2 (inter)	NR	94.6–103.9	Food	[72]
Hassan et al. (2021)	SHS-LLME + D-MSPME	DMCHA; Fe_3O_4@XAD-16	Quercetin	UV–Vis	NR	9.0–11.9 ng mL^{-1}	< 3.2 (intra); < 8.9 (inter)	NR	92.1–107.4	Apple, pepper, onion	[97]
Miri et al. (2021)	UA-D-μ-SPE	Fe_3O_4@PDA@PANI	Tartrazine, Sunset Yellow	Derivative UV–Vis	NR	0.2–0.5 ng mL^{-1}	NR	NR	NR	Food	[98]
Al-Nidawi et al. (2024)	SHS-LLME	Octylamine	Sudan I	UV–Vis (445 nm)	NR	0.009–0.021 μg mL^{-1}	< 8.6	EF 5.3–12.9	92.5–104.4	Spices	[39]
Guan et al. (2024)	MSPE	NH_2-COF (TpPa-NH_2)@Fe_3O_4	Anionic azo dyes	HPLC–UV	5–500 μg L^{-1}	2.3–3.4 μg L^{-1}	< 4.6	NR	87.5–96.9	Carbonated beve	[99]

Author(s) (Year)	Technique	Sorbent / extraction solvent	Analyte(s)	Detection	Linear range	LOD	RSD (%)	EF / PF	Recovery (%)	Matrix	Ref.
										rages	
Mohammadi et al. (2024)	D-μ-SPE (CCD)	MgO/$MgFe_2O_4$/GO	Sunset Yellow, Tartrazine	UV–Vis	0.5–2.50 mg L^{-1}	0.14–0.16 mg L^{-1}	< 3.5	EF 20.7–36.7; PF 20	93.0–107.0	Water, soft drinks	[100]
Tariq & Alwan (2024)	SHS-LLME (CCD/RSM)	N-methyldipropylamine	Tartrazine	UV–Vis (430 nm)	0.5–10 μg mL^{-1}	0.23 μg mL^{-1}	1.71	EF 63; PF 33.3	NR	Aqueous standards	[41]
Tariq & Hassan (2024)	SHS-LLME + MSPE	Switchable solvent; magnetic sorbent	Sunset Yellow	UV–Vis (482 nm)	10–100 mg L^{-1}	5.20 mg L^{-1}	NR	PF 100	NR	Aqueous standards	[73]
Abbas et al. (2025)	MSPE	GO/Co_3O_4/Fe_3O_4 MNPs	Acid Yellow 23	UV–Vis	0.2–5 mg L^{-1}	0.0104 mg L^{-1}	NR	PF 25; EnF 6	NR	Syrup drinks	[101]
Ahmed et al. (2025)	SS-LPME	N,N-dimethylbenzylamine carbonate	Sudan I–IV	HPLC–DAD	NR	NR	NR	PF 50	NR	Food, water	[40]
Didukh-Shadrina et al. (2025)	SPE	Al_2O_3–polyhexamethylene guanidine	Sunset Yellow, Ponceau 4R (Acid Red 18)	Diffuse reflectance	0.02–10.0; 0.02–11.0 mg L^{-1}	5 (SY); 7 (P4R) μg L^{-1}	≤ 9	NR	NR	Soft drinks, jelly	[102]

1.12 Aim of the Study

The present work sets out to develop, optimise and validate a green, rapid and inexpensive procedure for the determination of Acid Red 18 and Methyl Orange dyes at low concentrations, based on switchable-hydrophilicity solvent liquid–liquid microextraction coupled with magnetic solid-phase extraction on a polyaniline/Fe_3O_4 composite, with ultraviolet–visible spectrophotometric detection. The specific objectives are:

1.To develop an SHS-LLME procedure for both dyes and to examine, one factor at a time, the effect of the type and volume of the extraction solvent, the temperature, the volumes of acid and base, the ionic strength ,extraction time and the pH.

2.To optimise the significant variables simultaneously by a central composite design within response surface methodology, to assess the adequacy of the fitted models by analysis of variance, and to confirm the predicted optimum experimentally

3. To establish the maximum absorption wavelengths of the two dyes and to construct calibration graphs for each of them.

4.. To prepare a PANI/Fe_3O_4 (50/50 w/w) magnetic composite and to characterise it by X-ray diffraction, Fourier-transform infrared spectroscopy, field-emission scanning and transmission electron microscopy, vibrating-sample magnetometry and nitrogen adsorption analysis.

5. To couple the SHS-LLME step to a magnetic solid-phase extraction step on the PANI/Fe_3O_4 composite, and to examine the effect of the sorbent mass, the adsorption time, the identity of the eluent and the desorption time.

6. To evaluate the analytical figures of merit of the developed method linear range, limit of detection, limit of quantification, extraction recovery and precision for both dyes.

7. To apply the validated method to real water samples and to assess accuracy by standard addition, and to compare the performance of the proposed procedure with previously reported methods for the same analytes.

CHAPTER 2 INSTRUMENTS AND MATERIALS

2.1 Instruments and Apparatus

The instruments used for the physical, spectroscopic and analytical measurements reported in this work are listed in Table 2-1.

Table 2-1: Instruments used in this study, with model, manufacturer and place of use.

No.	Instrument	Model	Manufacturer and country	Place of use
1	UV–Visible spectrophotometer, double beam	UV-1650	Shimadzu, Japan	University of Al-Qadisiyah, Iraq
2	UV–Visible spectrophotometer, single beam	RS1200	FARLAB, Korea	University of Al-Qadisiyah, Iraq
3	Fourier-transform infrared spectrophotometer	FTIR-8400S	Shimadzu, Japan	University of Al-Qadisiyah, Iraq
4	X-ray diffractometer	XRD-6000	Shimadzu, Japan	Iran
5	Field-emission scanning electron microscope	—	—	Iran
6	Transmission electron microscope	A12AB	Leo, Germany	Iran
7	Vibrating-sample magnetometer	MDKB	Magnetic Daghigh Kavir, Iran	Iran
8	Surface-area and porosity analyser (BET)	—	—	Iran
9	Ultrasonic bath	LUC-410	Labtech, Korea	University of Al-Qadisiyah, Iraq
10	Centrifuge	EBA-20	Hettich, Germany	University of Al-Qadisiyah, Iraq
11	Analytical balance	EP214C	OHAUS, Switzerland	University of Al-Qadisiyah, Iraq
12	pH meter	350 pH Meter	JENWAY, England	University of Al-Qadisiyah, Iraq
13	Thermostatic water bath	—	—	University of Al-Qadisiyah, Iraq

2.2 Chemicals and Reagents

All chemicals were of analytical-reagent grade and were used as received without further purification. Deionised water was used throughout for the

preparation of all aqueous solutions. The materials used are listed in Table 2-2.

Table 2-2: Chemicals and reagents used in this study.

No.	Name	Molecular formula	M (g mol^-1^)	Supplier	Purity (%)
1	N,N-Dimethylcyclohexylamine (DMCHA)	$C_8H_{17}N$	127.23	Macklin	99
2	Triethylamine (TEA)	$C_6H_{15}N$	101.19	—	—
3	2-(Dibutylamino)ethanol (DBAE)	$C_{10}H_{23}NO$	173.30	—	—
4	Hydrochloric acid	HCl	36.46	Thomas Baker	37
5	Sodium hydroxide	NaOH	40.00	Fluka	99
6	Ethanol	C_2H_5OH	46.07	Merck, Germany	99.9
7	Methanol	CH_3OH	32.04	—	—
8	Acetonitrile	CH_3CN	41.05	—	—
9	Acetone	C_3H_6O	58.08	Merck, Germany	97
10	Sodium chloride	NaCl	58.44	Fluka	99
11	Potassium chloride	KCl	74.55	—	—
12	Calcium chloride	$CaCl_2$	110.98	Merck, Germany	98
13	Ammonium acetate	CH_3COONH_4	77.08	Merck, Germany	98
14	Acetic acid, glacial	CH_3COOH	60.05	—	—
15	Polyaniline (emeraldine base)	$(C_6H_5N)_n$	—	Sigma-Aldrich, USA	—
16	Iron(II,III) oxide (magnetite)	Fe_3O_4	231.53	Sigma-Aldrich, USA	97
17	Acid Red 18 (Ponceau 4R)	$C_{20}H_{11}N_2Na_3O_{10}S_3$	604.47	Sigma-Aldrich, USA	98
18	Methyl Orange	$C_{14}H_{14}N_3NaO_3S$	327.33	Sigma-Aldrich, USA	98

2.3 Preparation of the Standard and Reagent Solutions

2.3.1 Stock standard solution of Acid Red 18

A stock standard solution of Acid Red 18 at 1000 mg L^{-1} was prepared by dissolving 0.1000 g of the dye in deionised water in a 100 mL volumetric

flask and making up to the mark. The solution was stored in an amber glass bottle at 4 °C and protected from light, since Ponceau 4R is known to photodegrade in aqueous media.

2.3.2 Stock standard solution of Methyl Orange

A stock standard solution of Methyl Orange at 1000 mg L^{-1} was prepared in the same way, by dissolving 0.1000 g of the dye in deionised water in a 100 mL volumetric flask and making up to the mark. The solution was stored under the same conditions.

2.3.3 Hydrochloric acid, 6 M

A 6 M hydrochloric acid solution was prepared by transferring 12.5 mL of concentrated hydrochloric acid (37 % w/w, ≈ 12.1 M) into a 25 mL volumetric flask containing a small volume of deionised water, and making up to the mark with deionised water after the solution had cooled to room temperature. The acid was always added to the water and never the reverse.

2.3.4 Sodium hydroxide, 10 M

A 10 M sodium hydroxide solution was prepared by dissolving 10.0 g of sodium hydroxide pellets in a small volume of deionised water in a beaker, allowing the solution to cool, transferring it quantitatively to a 25 mL volumetric flask and making up to the mark.

2.3.5 Solutions used to adjust the pH

An acetate medium of 0.01 M was prepared by dissolving 0.7708 g of ammonium acetate in deionised water and making up to one litre, the pH being brought to 7.0 with dilute acetic acid or ammonia. Portions of this solution were then adjusted to the individual values required for the pH study

(pH 2 to 9) by the dropwise addition of 0.1 M hydrochloric acid for the acidic values and 0.1 M sodium hydroxide for the alkaline ones.

2.3.6 Salt solutions

Solutions of sodium chloride, potassium chloride and calcium chloride at 10 % (w/v) were prepared by dissolving 10.0 g of the corresponding salt in deionised water and making up to 100 mL in a volumetric flask. Lower concentrations used in the ionic-strength study were obtained by dilution of these solutions.

2.4 Preparation and Characterization of the Nanoparticles (PANI/Fe_3O_4)

Both components of the sorbent were obtained commercially and were not synthesised in this work. The composite was prepared by physically combining them in a volatile solvent, as follows. Equal masses of polyaniline and Fe_3O_4 were weighed to give a 50 : 50 (w/w) ratio and transferred to a clean, dry beaker. Acetone was then added dropwise from a dropper while the mixture was agitated manually, until a uniform slurry was obtained in which the polyaniline was distributed over the surface of the magnetite particles. The beaker was left in a fume hood at room temperature until the acetone had completely evaporated, leaving a dry, free-flowing PANI/Fe_3O_4 powder. The material was stored in a closed container and used without further treatment. The sequence is shown in Figure 2-1.

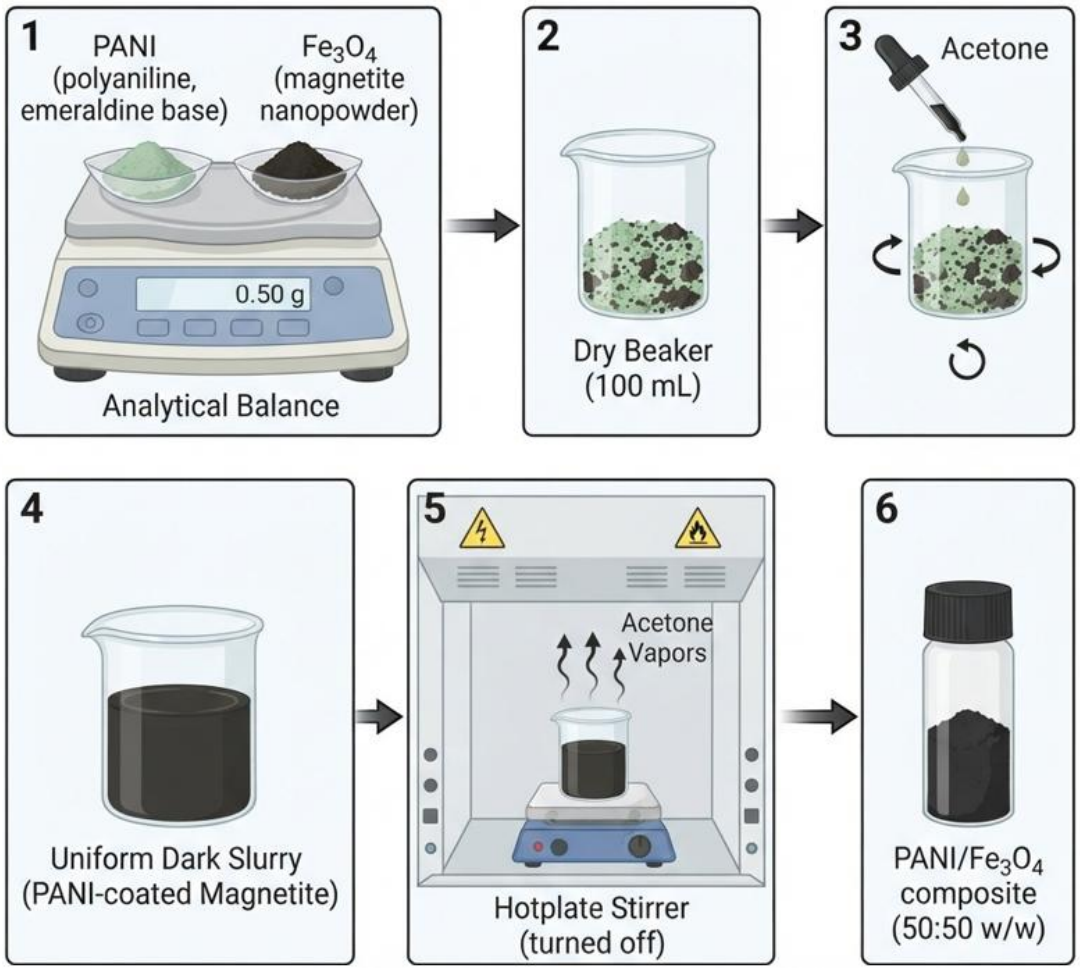


Figure 2-1: Preparation of the PANI/Fe_3O_4 (50:50 w/w) composite by solvent-assisted physical mixing.

Acetone was chosen because it wets both solids, disperses the polyaniline without dissolving it, and evaporates completely at room temperature, so that no residual solvent is carried into the extraction step.

The prepared composite, together with the two starting materials, was characterised by the techniques described below in order to confirm that polyaniline had been deposited on the magnetite and that the magnetic and structural properties of the core had been retained.

2.4.1 X-ray diffraction

Diffraction patterns were recorded with monochromatic Cu Kα radiation (λ = 1.5406 Å) using a nickel filter, in order to identify the crystalline phases

present and to establish whether the crystal structure of the magnetite survived the coating step.

2.4.2 Fourier-transform infrared spectroscopy

Infrared spectra were recorded over the range 400–4000 cm^{-1} using potassium bromide pellets, for Fe_3O_4 and the composite.

2.4.3 Field-emission scanning electron microscopy

Field-emission scanning electron micrographs were recorded at several magnifications to examine the surface morphology, the particle size and the degree of agglomeration of the material before and after coating.

2.4.4 Transmission electron microscopy

Transmission electron micrographs were recorded to observe the particles directly at the nanometre scale, so that the core size, the shape of the particles and the distribution of the polyaniline around them could be assessed. Samples were dispersed ultrasonically in ethanol and deposited on a carbon-coated copper grid before examination.

2.4.5 Vibrating-sample magnetometry

Magnetisation curves were recorded at room temperature over the available field range in order to determine the saturation magnetisation, the remanence and the coercivity of Fe_3O_4 and of the composite, and hence to confirm that the coated material retained sufficient magnetic response for it to be collected with a hand-held magnet [103].

2.4.6 Surface-area and porosity analysis

Nitrogen adsorption–desorption isotherms were recorded at 77 K. The specific surface area was calculated by the Brunauer–Emmett–Teller method over the appropriate relative-pressure range [104,105] and the pore volume and average pore diameter by the Barrett–Joyner–Halenda method applied to

the desorption branch [106]. The measurement was made on both the uncoated magnetite and the composite so that the effect of the polyaniline layer on the accessible surface could be assessed.

2.5 Spectrophotometric Determination of Acid Red 18 and Methyl Orange

The absorption spectrum of each dye was recorded at a concentration of 80 mg L^{-1} in a 1.00 cm quartz cell, against a blank of deionised water treated in the same way, Acid Red 18 was scanned over 200–1000 nm and Methyl Orange over 200–800 nm. The wavelength of maximum absorption was taken as the analytical wavelength for all subsequent measurements. Acid Red 18 gave its maximum at 506.5 nm and Methyl Orange at 485.5 nm.

2.6 SHS-LLME Extraction Procedure and the Factors Affecting It

The extraction was carried out in a 10 mL graduated glass tube. A 2 mL portion of the aqueous dye solution was placed in the tube and 2 mL of N,N-dimethylcyclohexylamine was added, giving two distinct phases. Hydrochloric acid (6 M) was then introduced and the tube was shaken by hand for about 10 s; protonation of the amine converted it to its water-miscible ammonium form and a single homogeneous phase was obtained. The tube was held in a thermostatic water bath at 40 °C for 2 min to allow the dye and the solvent to interact under homogeneous conditions. Sodium hydroxide (10 M) was then added, which deprotonated the amine and turned the medium cloudy as the regenerated hydrophobic solvent separated as fine droplets carrying the dye with them. After about 2 min the droplets had coalesced and the two phases were completely separated. The upper, analyte-rich organic layer was withdrawn with a syringe, diluted with 2 mL of ethanol to give a

volume sufficient for the cell, and its absorbance was measured at the corresponding λ_{max} against a blank carried through the identical procedure.

The procedure is shown schematically in Figure 2-2.

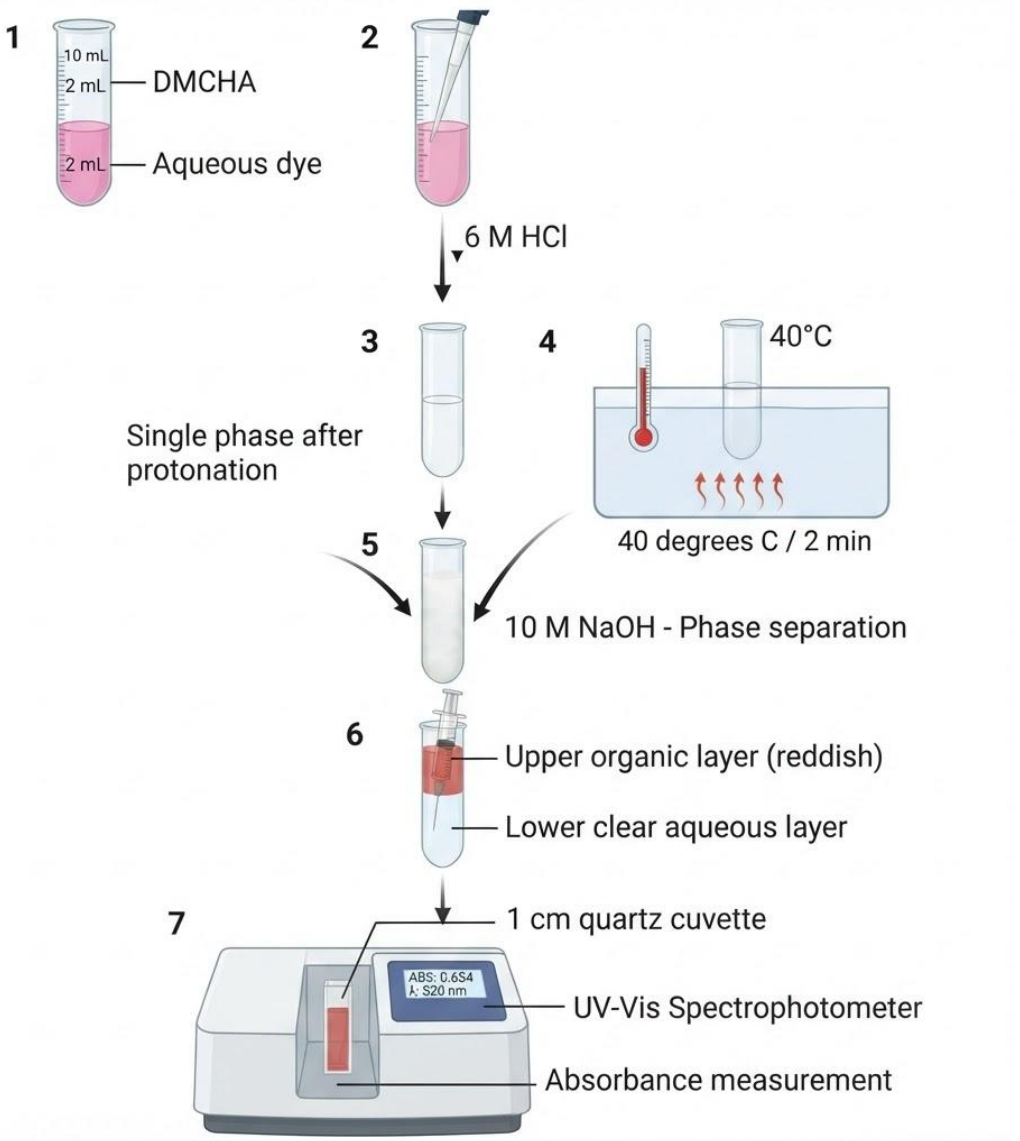


Figure 2-2: The SHS-LLME procedure used for the extraction of Acid Red 18 and Methyl Orange.

Each variable was examined in turn by applying the general procedure of Section 2.6 to a 40 mg L^{-1} solution of each dye while holding all the other variables constant, the absorbance of the diluted extract being taken as the response. Every determination was carried out in triplicate. The variables and the ranges covered are collected in Table 2-3.

Table 2-3: Variables examined by the one-factor-at-a-time approach and the ranges studied.

Variable	Range or levels studied
Type of extraction solvent	DMCHA, TEA, DBAE
Volume of extraction solvent	1.0 – 3.0 mL
Volume of hydrochloric acid (6 M)	100 – 1000 µL
Equilibration temperature	30 – 50 °C
Volume of sodium hydroxide (10 M)	100 – 1000 µL
Salt type and concentration	NaCl, KCl, $CaCl_2$; 1 – 10 % (w/v)
pH of the aqueous phase	1 – 8 (Acid Red 18); 2 – 9 (Methyl Orange)
Extraction (equilibration) time	1 – 10 s
Mass of PANI/Fe_3O_4	0.1 – 0.5 g
Adsorption time	5 – 30 min
Type of elution solvent	methanol, ethanol, acetonitrile, acetone
Desorption time	5 – 30 min (Acid Red 18); 5 – 35 min (Methyl Orange)

2.6.1 Effect of the extraction solvent type

Three switchable-hydrophilicity solvents were compared under otherwise identical conditions: N,N-dimethylcyclohexylamine (DMCHA), triethylamine (TEA) and 2-(dibutylamino)ethanol (DBAE). The solvent giving the highest absorbance was adopted for all subsequent work.

2.6.2 Effect of the extraction solvent volume

The volume of the selected solvent was varied from 1.0 to 3.0 mL, all other conditions being held constant. The volume giving the highest absorbance was adopted for all subsequent work.

2.6.3 Effect of the acid volume

The volume of 6 M hydrochloric acid was varied from 100 to 1000 µL. The volume giving the highest absorbance was adopted for all subsequent work.

2.6.4 Effect of the temperature

The temperature of the water bath was varied from 30 to 50 °C.The temperature giving the highest absorbance was adopted for all subsequent work.

2.6.5 Effect of the base volume

The volume of 10 M sodium hydroxide was varied from 100 to 1000 µL. The volume giving the highest absorbance was adopted for all subsequent work.

2.6.6 Effect of the salt type and concentration

Sodium chloride, potassium chloride and calcium chloride were each examined at 10 % (w/v), lower concentrations down to 1 % (w/v) being available by dilution as described in Section 2.3.6.

2.6.7 Effect of the pH of the aqueous phase

The pH of the sample was varied over the range 1 to 9 using the solutions described in Section 2.3.5, from pH 1 to 8 for Acid Red 18 and from pH 2 to 9 for Methyl Orange, all other conditions being held at their previously established values.

2.6.8 Effect of the extraction time

The time for which the tube was held in the thermostatic water bath after the switch to a single phase was varied from 1 to 10 s, in order to establish the interval needed for the dye and the regenerated solvent to reach equilibrium.

2.7 Chemometric Optimisation by Response Surface Methodology

Optimising a procedure governed by several interacting variables one factor at a time explores only a narrow path through the experimental domain and

cannot reveal interactions between the variables [77,78]. The variables identified as significant in the screening stage were therefore optimised simultaneously using a central composite design within a response-surface framework, the calculations being carried out with **Minitab** statistical software.

2.7.1 Selection of the variables and their levels

Four variables were carried forward into the design: the pH of the aqueous phase, the volume of the extraction solvent, the volume of hydrochloric acid and the volume of sodium hydroxide. The levels at which each design was actually executed are given in Table 2-4

Table 2-4: Independent variables and the levels at which the two central composite designs were executed.

Variable	Symbol	Unit	Levels used Acid Red 18	Levels used Methyl Orange
pH of the aqueous phase	A	—	2, 5.5, 9	2, 5.5, 9
Volume of extraction solvent	B	mL	0, 1, 2, 3, 4	1, 2, 3, 4
Volume of hydrochloric acid	C	µL	100, 550, 1000	100, 350, 550, 1000, 1450
Volume of sodium hydroxide	D	µL	100, 350, 550, 1000, 1450	100, 350, 550, 1000, 1450

2.7.2 Design matrix

Each design comprised 31 experiments arranged in a single block. A four-factor central composite design calls for 16 factorial points, 8 axial points and a set of replicated centre points, and neither design as executed carries the complete axial set: the Acid Red 18 design comprises 16 factorial, 7 axial and 8 centre runs, and the Methyl Orange design 16 factorial, 6 axial and 9 centre runs.

2.7.3 Model and statistical analysis

The experimental data were fitted to a full second-order polynomial of the form

$$y = \beta_0 + \Sigma \beta_i x_i + \Sigma \beta_{ii} x_i^2 + \Sigma \beta_{ij} x_i x_j + \varepsilon \quad (2\text{-}1)$$

in which y is the response, x_i the coded factors, β_0 the constant term, β_i, β_{ii} and β_{ij} the linear, quadratic and interaction coefficients respectively, and ε the residual [77,82]. The significance of the regression and of the individual terms was judged by analysis of variance, the proportion of the variance explained by the coefficient of determination and its adjusted and predicted forms, and the adequacy of the second-order form by the lack-of-fit test carried out against the pure error from the replicated centre points [85].

2.8 Calibration Curves of Acid Red 18 and Methyl Orange Using the SHS-LLME Method

The calibration curves for the studied dyes were constructed after Chemometric Optimisation by Response Surface Methodology and applying the general procedure of Section 2.6 to a series of standard solutions covering 10–100 mg L^{-1}. The absorbance of the diluted extract was plotted against the concentration in the original aqueous sample, and the slope, intercept and coefficient of determination were obtained by least-squares regression. Each point represents the mean of three independent extractions.

2.9 General Procedure for the Extraction of the Dyes Using the SHS-LLME Method Coupled with the MSPE Method

A 2 mL portion of the dye solution was placed in a 10 mL volumetric flask and the optimum volumes of extraction solvent and acid, established in Section 2.7 were added. The mixture was shaken by hand for 10 s to give a

single phase and then held in the water bath at the optimum temperature for the optimum time. The optimum volume of base was added and the phases were allowed to separate.

A weighed amount of the PANI/Fe_3O_4 composite was then added. The contents of the flask were transferred to a test tube and placed in an ultrasonic bath for 10 min so that the sorbent remained dispersed throughout the medium and the dye could be retained on its surface. The loaded sorbent was collected against the wall of the tube with a hand-held neodymium magnet, the supernatant was decanted, and the sorbent was washed twice with deionised water. Ethanol (2 mL) was then added as the elution solvent and the tube was returned to the ultrasonic bath for a further 5 min. The sorbent was again collected with the magnet and the absorbance of the clear eluate was measured at the corresponding λ_{max} against a blank prepared in the same way. The complete sequence is shown in Figure 2-3.

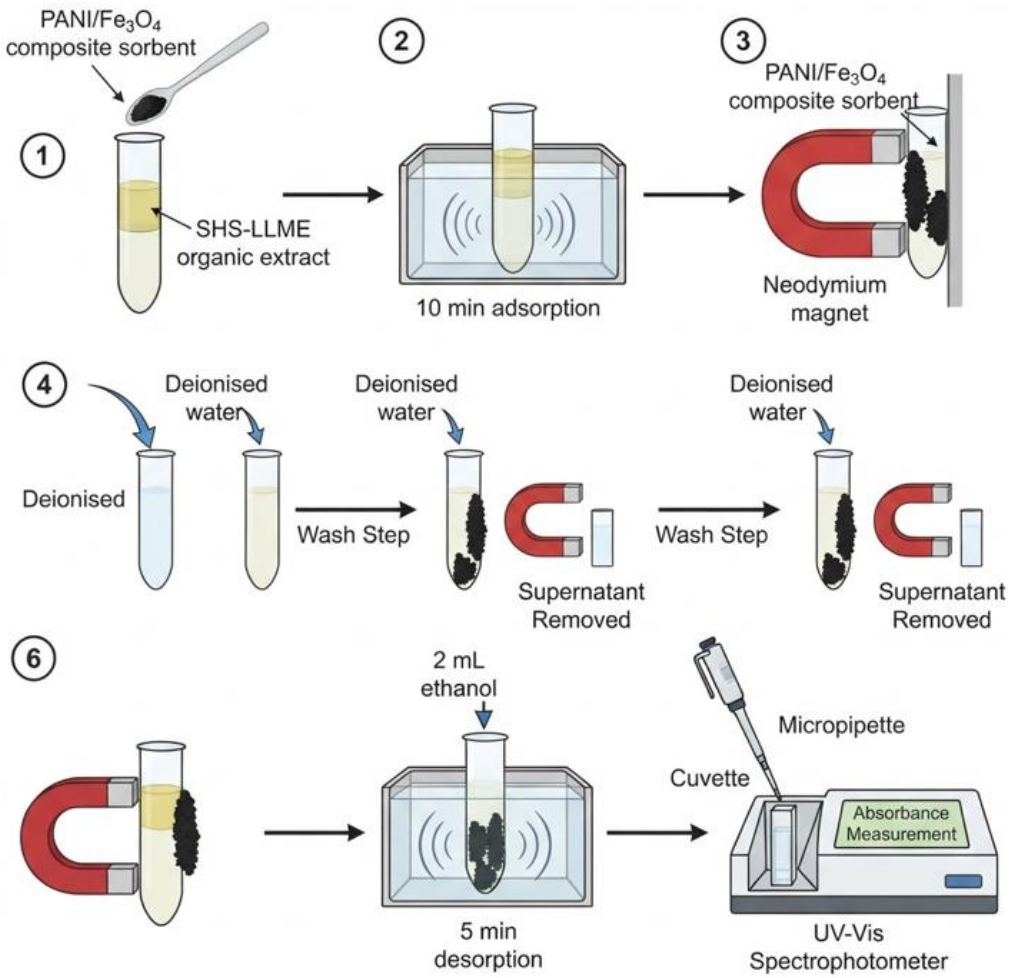


Figure 2-3: The MSPE stage applied to the extract obtained from the SHS-LLME stage.

2.10 Factors Affecting the Extraction by Using the MSPE Method

Each variable of the second stage was examined by applying the procedure of Section 2.9 while holding the remaining variables constant, the absorbance of the eluate being taken as the response. Determinations were carried out in triplicate.

2.10.1 Effect of the amount of the magnetic sorbent

The mass of the composite was varied from 0.1 to 0.5 g. The mass giving the highest absorbance was adopted for all subsequent work.

2.10.2 Effect of the adsorption time

The time for which the mixture was held in the ultrasonic bath after the addition of the sorbent was varied from 5 to 30 min, in order to establish the interval needed to reach adsorption equilibrium.

2.10.3 Effect of the type of desorption solvent

Methanol, ethanol, acetonitrile and acetone were compared as elution solvents, all other conditions being held constant. The solvent must be able to disrupt the electrostatic and hydrogen-bonding interactions holding the dye on the polyaniline surface, which makes its polarity and hydrogen-bonding capacity the relevant properties [62,64].

2.10.4 Effect of the desorption time

The time in the ultrasonic bath during the elution step was varied from 5 to 30 min for Acid Red 18 and from 5 to 35 min for Methyl Orange, in order to establish the interval required for complete release of the retained dye.

2.11 Calibration Curves of the Dyes Using the SHS-LLME Method Coupled with the MSPE Method

Once every variable of Sections 2.7 and 2.10 had been fixed at its optimum value, calibration graphs were constructed for both dyes by applying the coupled procedure of Section 2.9 to a series of standard solutions covering 10–100 mg L^{-1}.

2.12 Extraction Percentage

The extraction percentage, %E, was calculated using the following formula:

$$\%\boldsymbol{E} = (\boldsymbol{C_{org}} \times \boldsymbol{V_{org}} \ / \ \boldsymbol{C_{aq}} \times \boldsymbol{V_{aq}}) \times \mathbf{100} \qquad (\mathbf{2-2})$$

Where :

C_{org}: Concentration of the dye in the organic phase after separation.

V_{org} : Volume of the organic phase

C_{aq}: Concentration of the residual dye in the aqueous phase.

V_{aq}: Volume of the aqueous phase.

2.13 Application to Real Samples

The validated procedure was applied to real water samples collected from two sources: tap water taken from the laboratory supply after the line had been allowed to run, and Diwaniyah River water. The samples were collected in pre-cleaned glass bottles, rinsed three times with the water to be sampled before filling, and transported to the laboratory without headspace [107].

On arrival the samples were filtered through a 0.45 µm membrane filter to remove suspended matter [108] and stored in the dark at 4 °C until analysis, which was carried out within the shortest practicable interval. The pH of each sample was adjusted to the optimum value before extraction, and the coupled procedure of Section 2.9 was then applied under the optimised conditions.

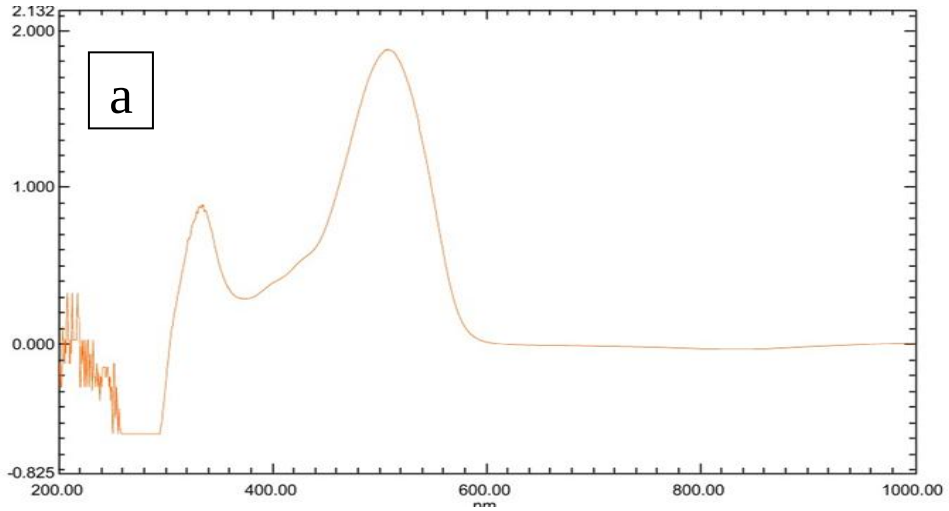
The accuracy of the procedure in the presence of a real matrix was assessed by the standard-addition method. Known amounts of each dye were added to real water samples at three concentration levels, the coupled procedure was applied to the spiked samples, and the percentage recovery was calculated for each level. Unspiked portions of the same samples were carried through the procedure in parallel so that any dye already present could be accounted .

3.1 Absorption Spectra of Acid Red 18 and Methyl Orange

The absorption spectra of Acid Red 18 and methyl orange dyes were recorded against their respective blank solutions in order to fix the analytical wavelength of each dye. The spectra are shown in Figure 3-1

Acid Red 18 gives a strong visible band with a maximum at 506.5 nm.The visible maximum arises from the π→π* transition of the azo–naphthalene chromophore, which is delocalised over the whole of the conjugated system, while the ultraviolet band belongs to the naphthalene rings themselves [109]. A wavelength of 506.5 nm was adopted for all quantitative measurements of this dye.

The ultraviolet–visible absorption spectrum of methyl orange is characterized by two principal absorption bands: a prominent visible band at 485.5 nm arising from n→π* and charge transfer transitions in the azo chromophore, and a secondary UV band at 270–272 nm associated with aromatic ring absorption. The spectral properties of methyl orange are highly sensitive to environmental factors. pH changes induce dramatic spectral shifts, with protonation below pH 5 causing a bathochromic shift to 510 nm and the appearance of an isosbestic point at 480 nm.



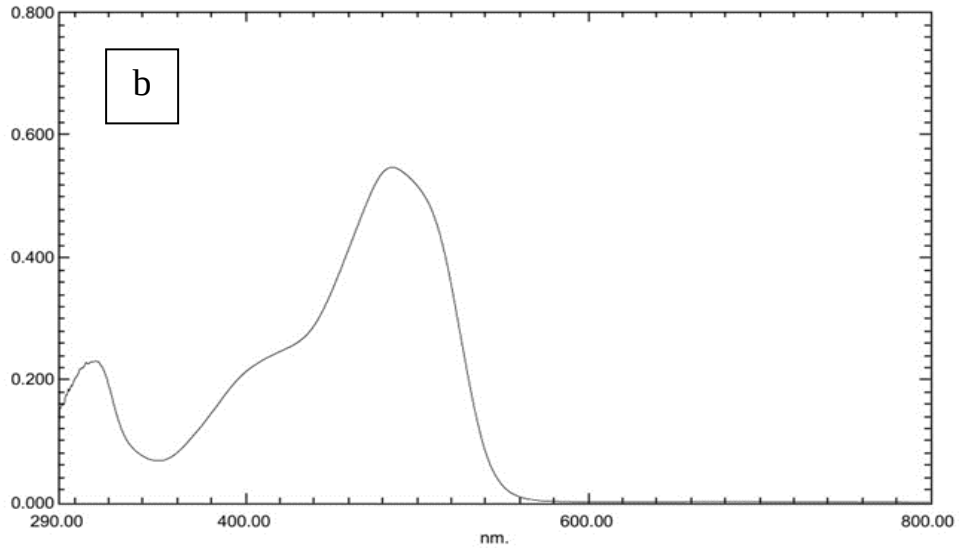


Figure 3-1: Ultraviolet–visible absorption spectra of the two dyes. (a) Acid Red 18, (b) Methyl orange

3.2 Characterization of the Prepared Magnetic Nanomaterial

The sorbent is a polyaniline layer carried on magnetite. It was designed to combine two properties: the magnetic separability of the oxide, and the anion-exchange capacity of the protonated polymer. Five techniques were used to confirm that the material has both.

3.2.1 X-ray diffraction

The X-ray diffraction (XRD) patterns presented below provide clear and direct evidence that the surface of magnetite (Fe_3O_4) was successfully coated with polyaniline (PANI). Two patterns were recorded using Cu Kα radiation (2θ range: 10°–80°). The XRD pattern of pure magnetite (Figure 3-2 a) displays sharp, well-defined diffraction peaks characteristic of the inverse spinel structure of Fe_3O_4. The dominant peaks appear at approximately 2θ ≈ 30.1° (220), 35.5° (311), 43.1° (400), 57.0° (511), and 62.6° (440),

The XRD pattern of the Fe_3O_4/polyaniline composite (Figure 3-2 b) exhibits several distinctive changes compared to pure magnetite, each constituting direct proof of the polyaniline coating.

A significantly raised, broad is visible at low scattering angles in (Figure 3-2 b) that is completely absent in (Figure 3-2a). This broad amorphous scattering envelope is the hallmark of the semi-crystalline polyaniline polymer matrix surrounding the magnetite nanoparticles, confirming the presence of an amorphous organic coating.

Also (Figure 3-2 b) shows additional diffraction peaks in the 20–25° region that are not present in the pure magnetite pattern. These peaks are characteristic of the periodic repeat distances of the polyaniline chain structure (emeraldine form), typically attributed to the periodicity along the polymer backbone and interchain spacing.The characteristic magnetite peaks at 35.5° and 43.1° are still identifiable in (Figure b) but exhibit reduced relative intensities and increased peak widths. This attenuation is consistent with the magnetite nanoparticle core being encapsulated within a polyaniline shell, which scatters X-rays diffusely and partially screens the crystalline Fe_3O_4 domains.A prominent sharp peak near $2\theta \approx 20°$ appears in (Figure b). This reflection is absent in pure magnetite and is attributed to the organized packing of polyaniline chains at the magnetite surface, indicating a well-formed coating layer rather than merely mixed phases.

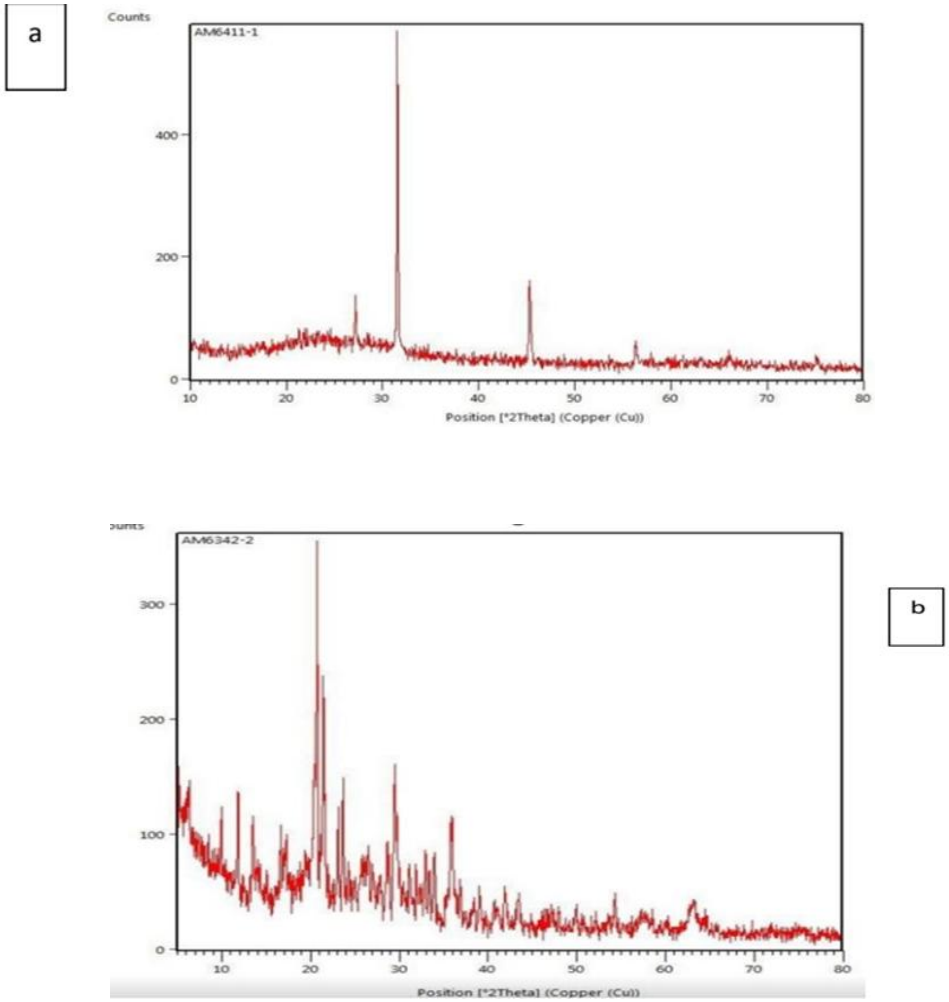


Figure 3-2: X-ray diffraction patterns of the a) pure Fe_3O_4 (magnetite) b) Fe_3O_4/polyaniline composite

3.2.2 Infrared spectroscopy

The Fourier-transform infrared (FTIR) spectroscopic analysis of magnetite (Fe_3O_4) nanoparticles and Fe_3O_4/polyaniline (PANI) composite materials studies. Figure 3-3 and Table 3-1) .Pure Fe_3O_4 exhibits characteristic Fe–O stretching band at 590 cm^{-1} that serve as diagnostic fingerprints of the inverse spinel structure. Fe_3O_4/PANI composites display both magnetite Fe–O bands and polyaniline-specific features including quinoid ring (C=N, ~1490 cm^{-1}), benzenoid ring (C=C, 1570cm^{-1}), C–N stretching (1294cm^{-1}), and N–H vibrations (3322 cm^{-1}). Critically, composite formation induces systematic spectral changes: PANI aromatic bands shift (red- or blue-shifts depending on synthesis), Fe–O band intensity decreases and position shifts, and overall

band broadening occurs. These changes provide direct FTIR evidence for interfacial interaction between PANI and Fe_3O_4 through hyd rogen bonding and coordination mechanisms [111-114].

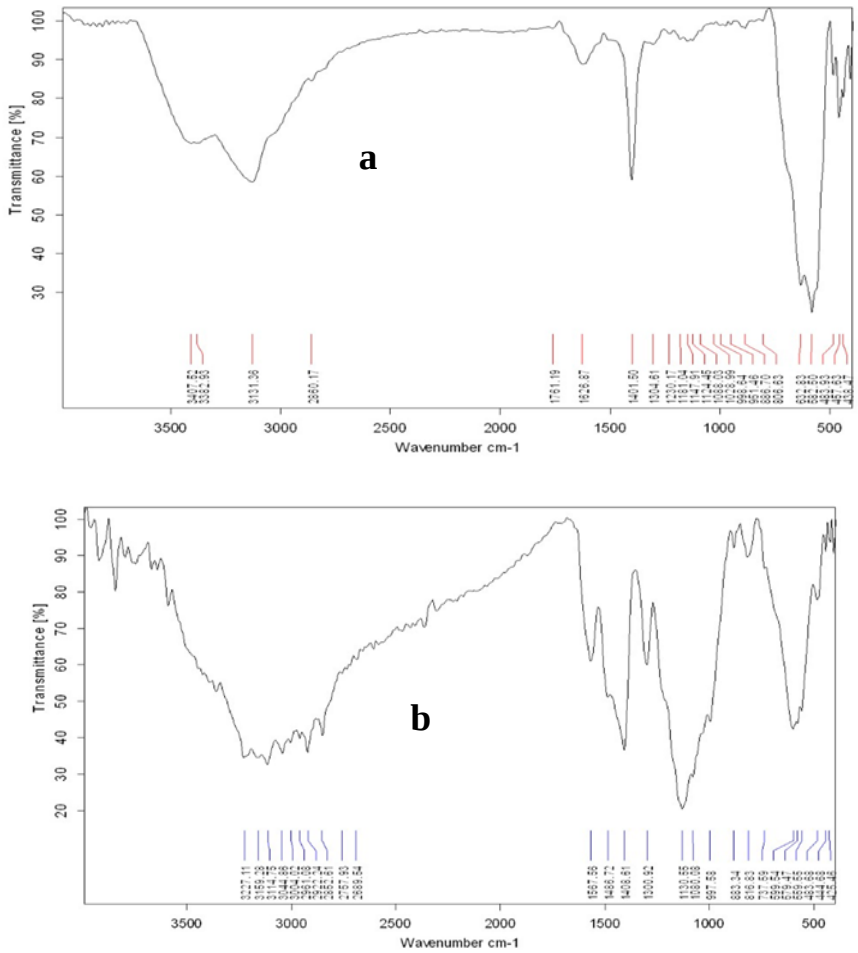


Figure 3-3: Infrared spectra recorded as potassium bromide discs. (a) pure Fe_3O_4 (magnetite) (b) Fe_3O_4/polyaniline composite.

Table 3-1: The principal infrared bands and their assignment.

Band(s) (cm^{-1})	Specimen	Assignment
3407.5	Fe_3O_4 nanoparticles	O–H stretch of water
590	Fe_3O_4 nanoparticles	Fe–O stretch of the spinel
1490	composite	ring stretch of the quinoid unit of polyaniline
1570	composite	ring stretch of the benzenoid unit of polyaniline
1294	composite	C–N stretch of the secondary aromatic amine

Band(s) (cm^{-1})	Specimen	Assignment
3322	composite	N–H vibrations
559.6	composite	Fe–O stretch of the spinel, retained after coating

3.2.3 Electron microscopy

Scanning electron microscopy (SEM) is a powerful surface characterization technique that provides high-resolution images of material morphology. Scanning electron microscopy shows a clear change in surface texture (Figure 3-4). the smooth, granular texture of pure magnetite (a, b) is replaced by a characteristic fibrous, sheet-like polyaniline network uniformly covering the magnetite particles (c, d). This morphological change the appearance of a continuous polymer coating with fibrous PANI structures directly confirms the formation of the PANI/Fe_3O_4 composite and demonstrates that the magnetite surface has been coated with polyaniline

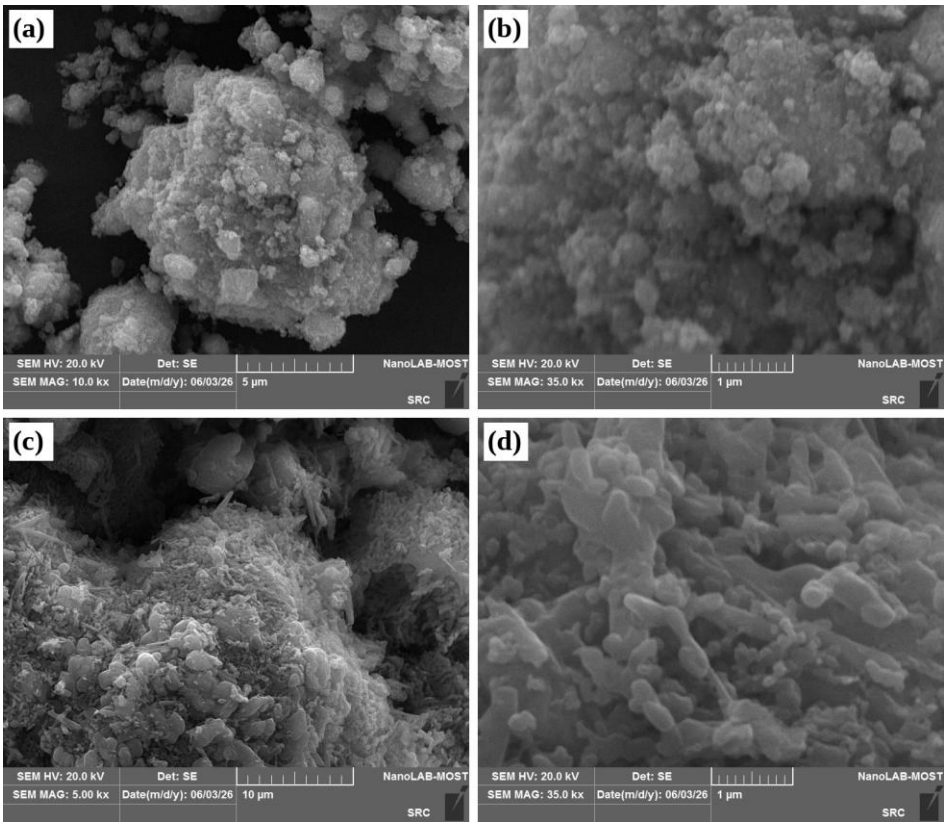


Figure 3-4: Scanning electron micrographs of pure Fe_3O_4 (magnetite) (a, b) and of Fe_3O_4/polyaniline composite (c, d), recorded at 20.0 kV with a secondary-electron detector.

TEM analysis provides direct visual and quantitative evidence of the successful synthesis and coating of Fe_3O_4 nanoparticles with polyaniline (PANI). Fe_3O_4 nanoparticles (Figure 3-5a) are quasi-spherical with a narrow size distribution centered at 11.7 ± 4.3 nm, and show strong magnetic aggregation typical of uncoated iron oxide nanomaterials. PANI/Fe_3O_4 composite particles (Figure 3-5 b) display a well-defined core–shell morphology, with a visible low-contrast PANI matrix surrounding the Fe_3O_4 cores. The mean particle size increases to 21.0 ± 8.0 nm, indicating a PANI shell thickness of approximately 4–5 nm. The broader size distribution and right-skewed histogram of the composite reflect the inherent variability of polymer coating processes.These TEM results confirm that the PANI coating is homogeneous, conformal, and successfully encapsulates the magnetic nanoparticle cores, producing a nanocomposite with potential applications in electromagnetic shielding, supercapacitors, and biomedical sensing.

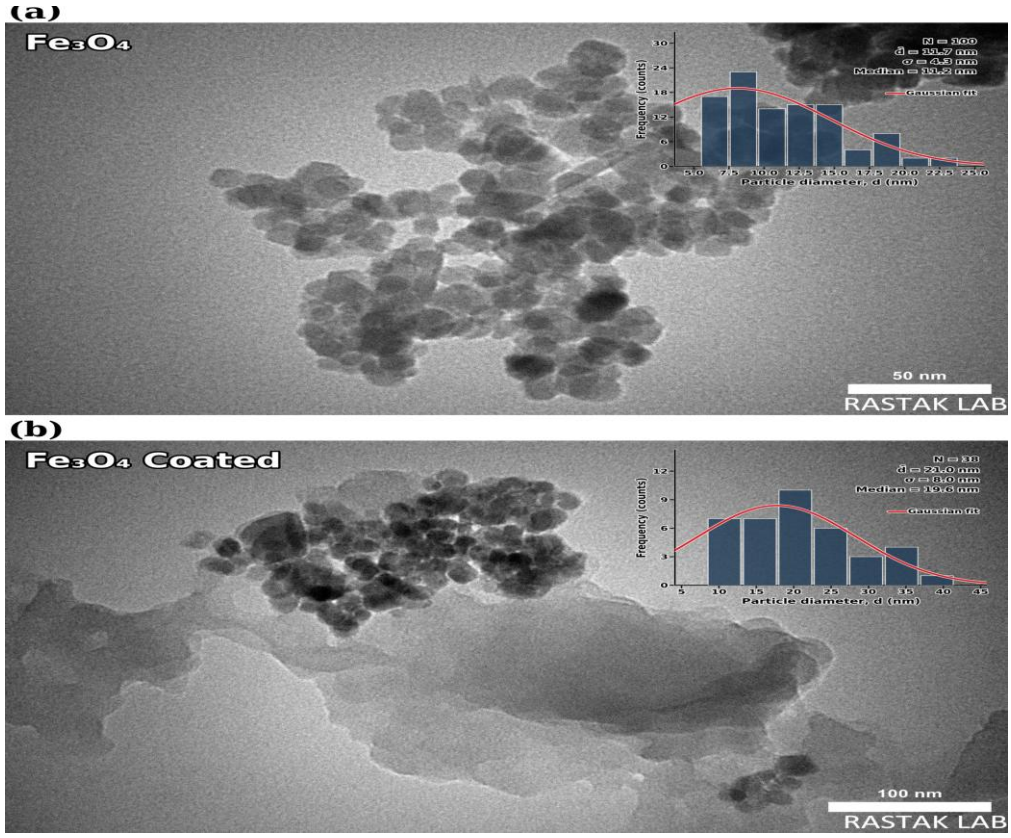


Figure 3-5: Transmission electron micrographs of (a) pure Fe_3O_4 (magnetite) and (b) Fe_3O_4/polyaniline composite.

3.2.4 Magnetic properties

A magnetic hysteresis loop of the composite material, as shown in Figure (3-6) was recorded at room temperature. In comparison with the preformed Fe3O4 nanoparticles, the saturation magnetisation falls from 11.42 emu g^{-1} for the bare oxide to 4.68 emu g^{-1} for the composite. Magnetisation is measured per gram of powder, so adding a non-magnetic polymer lowers it simply by adding mass that carries no moment. The ratio of the two values, 0.406, says that one gram of the composite contains 40.6 wt % of the starting powder, close to the intended 50:50 proportion. A Langevin analysis of the same curves returns a magnetic core diameter of 8.3 nm before coating and 8.2 nm after it, so the coating adds mass without damaging the magnetic core [115, 116].

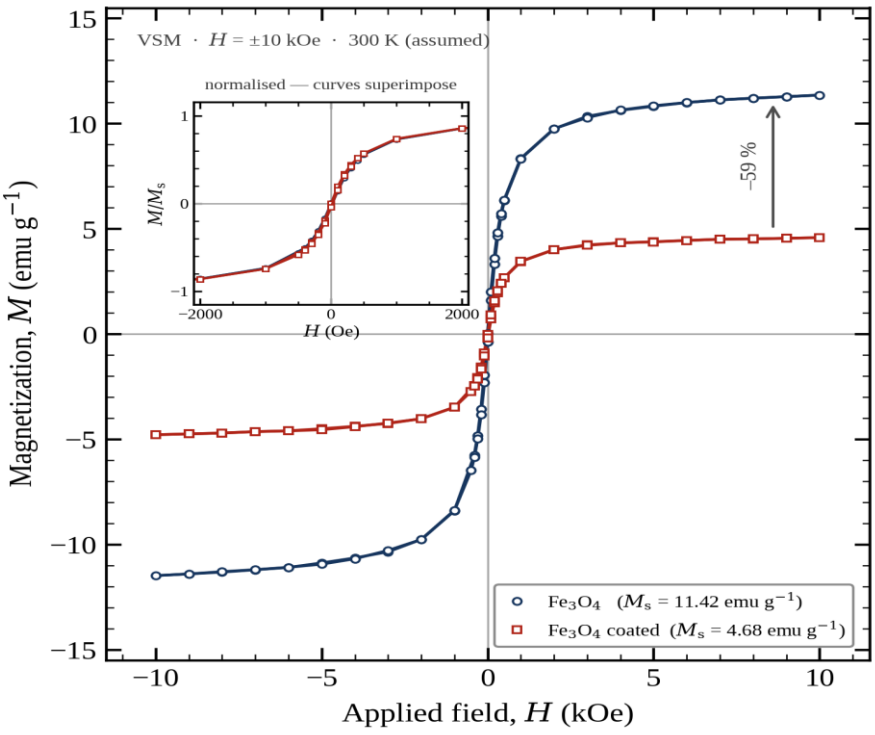


Figure 3-6: Magnetisation curves of the pure Fe_3O_4 (magnetite) and Fe_3O_4/polyaniline composite measured between ± 10 kOe.

3.2.5 Surface area and porosity

Nitrogen physisorption at 77 K gives the results shown in Figure 3-7. The BET surface area (SBET) of magnetite (Fe_3O_4) is 33.61 $m^2\ g^{-1}$, while the polyaniline-coated composite (PANI/Fe_3O_4) shows a dramatically reduced surface area of only 9.08 $m^2\ g^{-1}$ a reduction of approximately 73%. This substantial decrease in accessible surface area is the primary indicator that the polyaniline polymer chains have been deposited onto the magnetite particle surfaces, effectively covering and blocking the surface sites that would otherwise be available for nitrogen adsorption. The BET regression quality confirms these values are reliable: Fe_3O_4 yielded R = 0.99996 and PANI/Fe_3O_4 yielded R = 0.99958. The BET C constant reflects the energy of interaction between the adsorbate (nitrogen) and the adsorbent surface. For Fe_3O_4, C = 73, while for PANI/Fe_3O_4, C = 25.

This drop in C value indicates a change in surface chemistry: the high-energy Fe–O surface sites of magnetite are replaced by the lower-energy organic surface of polyaniline. This is consistent with a polymer coating that fundamentally alters the adsorption energy landscape of the material.The pore-size distribution analysis reveals that Fe_3O_4 exhibits a dominant pore radius peak at r_p = 3.53 nm, whereas the PANI/Fe_3O_4 composite shows a shifted peak at r_p = 6.95 nm. This shift to a larger average pore radius is explained by the PANI coating selectively filling or blocking the smaller mesopores (narrower channels) of the magnetite framework, while the larger pores remain partially accessible. The result is a biased distribution toward larger apparent pore sizes. This pore-blocking effect is a well-established signature of polymer encapsulation in core–shell nanomaterials. The cumulative pore volume (V_p) of Fe_3O_4 reaches approximately 0.150 $cm^3\ g^{-1}$, whereas the PANI/Fe_3O_4 composite reaches only approximately 0.050 $cm^3\ g^{-1}$ a reduction of nearly 67%.

The three-fold decrease in total pore volume is direct physical proof that the pore space of the magnetite has been substantially occupied by the polyaniline layer. Pore volume is a measure of the total void space within the material accessible to nitrogen; a reduction of this magnitude cannot be attributed to measurement artifact and unambiguously indicates that a new solid phase (PANI) has been deposited inside and around the magnetite pore network.

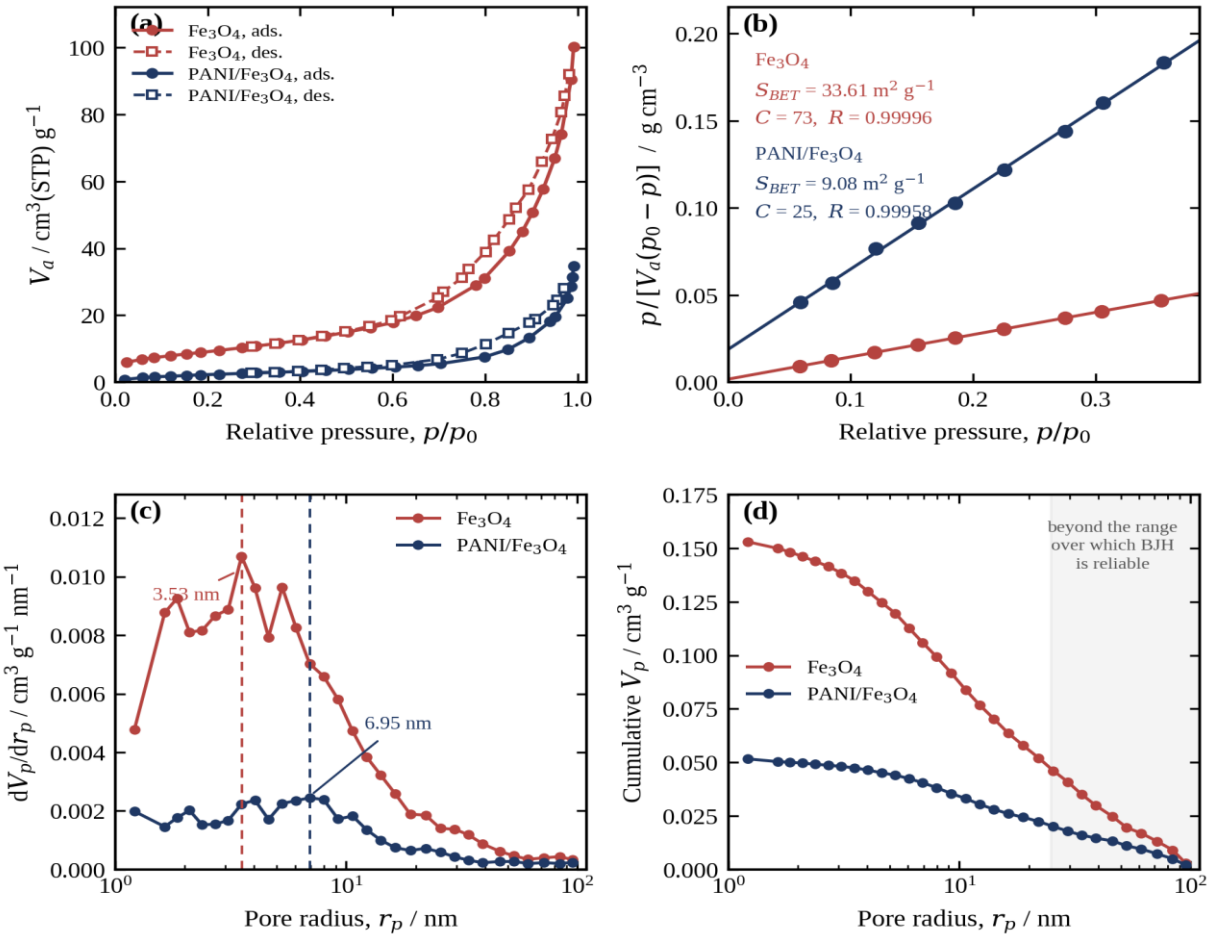


Figure 3-7: Nitrogen physisorption at 77 K for the pure Fe_3O_4 (magnetite) and the Fe_3O_4/polyaniline composite: (a) adsorption–desorption isotherms, (b) BET plots, (c) pore-size distributions and (d) cumulative pore volume.

3.3 Factors Affecting the Extraction of Acid Red 18 by the SHS-LLME Method

Eight factors were examined one at a time. Each was varied while the others were held at the value already found to be best. They were the pH of the aqueous phase, the type of switchable extraction solvent, the volume of the switchable solvent, the volumes of hydrochloric acid and sodium hydroxide, the temperature, the extraction time, and the type and concentration of added electrolyte. The two reagent volumes govern the two halves of the switching cycle, which rests on the reversible protonation of a tertiary amine. Hydrochloric acid converts N,N-dimethylcyclohexylamine into its water-miscible ammonium salt, so that solvent and sample mix as one phase. Sodium hydroxide then regenerates the free amine, which separates again as an organic layer carrying the extracted dye [32–34]. The results are shown in Figures 3-8 to 3-15 and summarised in Table 3-10.

3.3.1 Effect of the pH of the aqueous phase

The acidity of the aqueous phase was varied between pH 1 and pH 9. As shown in Figure (3-8) and Table (3-2), the absorbance rises at pH 1 to a maximum at pH 3 then falls steadily, Acid Red 18 is a trisulfonated azo dye and carries three negative charges over essentially the whole of this range, so it can pass into a neutral amine solvent only if that charge is neutralised. At pH 3 the amine is protonated and forms an ion pair with the sulfonate groups, and the neutral pair partitions into the organic phase

As the pH rises the amine is progressively deprotonated, the ion pair no longer forms and the dye remains in the aqueous phase. The maximum does not lie at the lowest pH tested. At pH 1 and 2 the large excess of acid competes for the amine and raises the ionic strength of the aqueous phase, and both effects work against the transfer. A pH of 3 is therefore the best

compromise between complete protonation of the extractant and a moderate ionic strength, and it was adopted for all subsequent experiments. [36, 95].

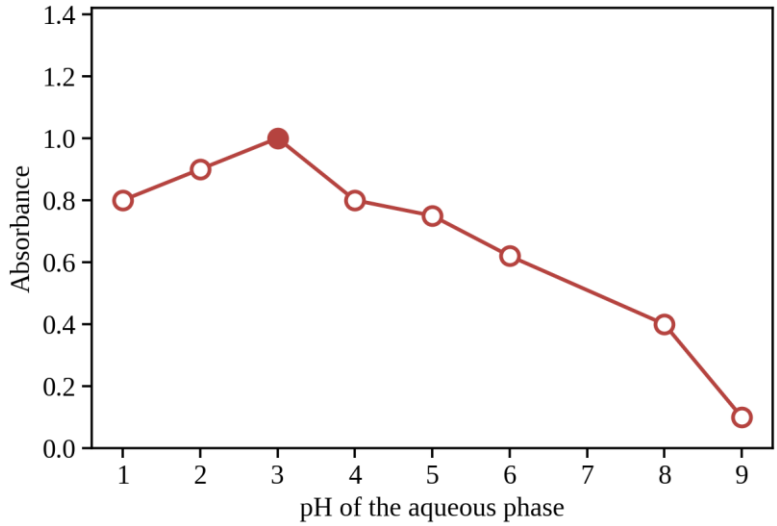


Figure 3-8: Effect of the pH of the aqueous phase on the extraction of Acid Red 18 by the SHS-LLME method.

Table 3-2: Effect of the pH of the aqueous phase on the extraction percentage, (%E) of Acid Red 18 by the SHS-LLME method.

pH	**1**	**2**	**3**	**4**	**5**	**6**	**7**	**8**	**9**
%E	**71**	**74**	**82**	**68**	**65**	**61**	**58**	**46**	**29**

3.3.2 Effect of the extraction solvent type

Three switchable-hydrophilicity solvents were compared under otherwise identical conditions: N,N-dimethylcyclohexylamine (DMCHA), DPA and triethylamine (TEA). the order is DMCHA > DPA > TEA (Figure 3-9) and Table (3-3). DMCHA gives the largest response and was adopted for all the work that follows.

The choice of amine matters because three of its properties act together. Its basicity decides how completely it switches between the water-miscible ammonium salt and the free base. Its partition coefficient decides how much of it separates again as an organic layer. The bulk of the groups around the

nitrogen decides how closely it can approach the sulfonate groups of the dye [32–34]. DMCHA is the best compromise of the three. Triethylamine is the poorest, and the simplest reason is that it is the most water-soluble of the three amines, so less of it is recovered as a separate phase and the extract that is recovered is more dilute.

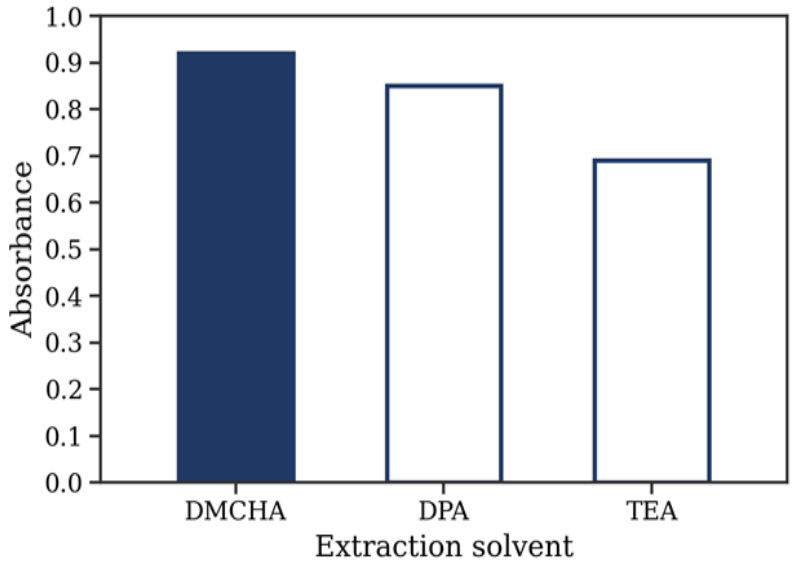


Figure 3-9: Effect of the extraction solvent type on the extraction of Acid Red 18 by the SHS-LLME method.

Table 3-3: Effect of the extraction solvent type on the extraction percentage, (%E) of Acid Red 18 by the SHS-LLME method.

Extraction Solvent type	DMCHA	DPA	TEA
%E	79	69	56

3.3.3 Effect of the volume of the switchable solvent

The influence of the extraction solvent volume on the recovery of Acid Red 18 was evaluated using the SHS-LLME method. Various volumes of DMCHA, ranging from 1.0 to 3.0 mL, were tested. As illustrated in Figure (3-10) and Table (3-4) the extraction efficiency increased with increasing solvent volume, reaching its maximum at 2.5 mL. Beyond this point, further volume decrease the efficiency by a dilution effect.

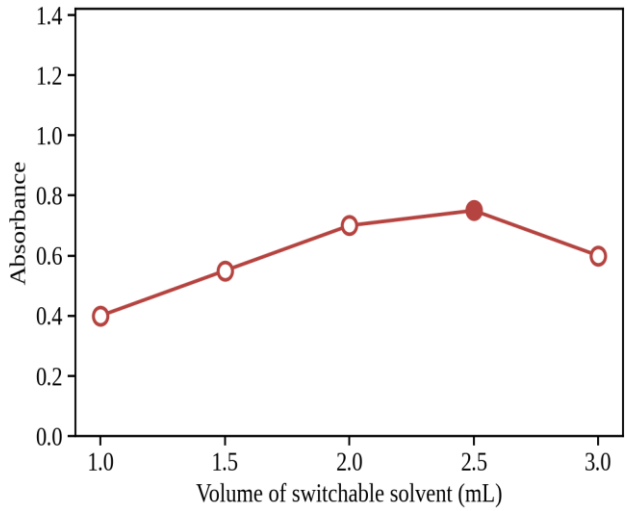


Figure 3-10: Effect of the volume of the switchable solvent on the extraction of Acid Red 18 by the SHS-LLME method**.**

Table 3-4: Effect of the extraction solvent volume on the extraction percentage, (%E) of Acid Red 18 by the SHS-LLME method

solvent volume(mL)	1.0	1.5	2.0	2.5	3.0
%E	49	59	68	74	61

3.3.4 Effect of the volume of hydrochloric acid

In the SHS-LLME procedure, DMCHA served as a switchable solvent, and hydrochloric acid (HCl) was used to protonate DMCHA. Protonation converted DMCHA from hydrophobic to hydrophilic, enabling efficient Acid Red 18 extraction. To determine the optimal phase-switching volume, 6 mol L^{-1} HCl was tested in volumes from 100 to 1000 µL. Figure (3-11) and table(3-5) shows that 400 µL of HCl yielded the highest extraction efficiency. This amount fully protonated DMCHA, promoting its transition to the hydrophilic phase and facilitating Acid Red 18 migration from the aqueous to the organic phase. Increasing the HCl volume beyond 400 µL did not further improve extraction, likely due to saturation of the phase-switching process. Thus, 400 µL was selected as the optimal HCl volume for subsequent experiments.

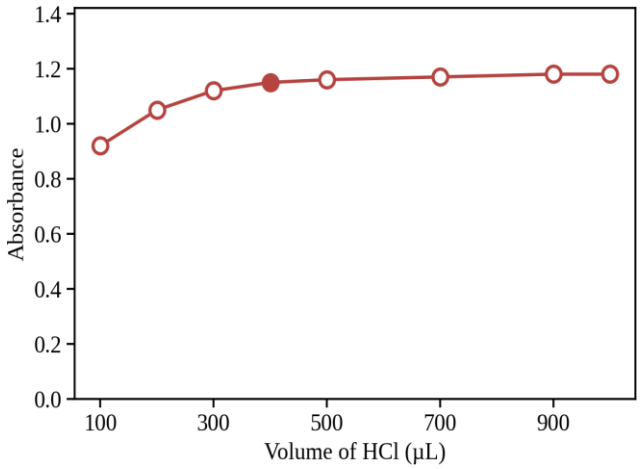


Figure 3-11: Effect of the volume of hydrochloric acid on the extraction of Acid Red 18 by the SHS-LLME method.

Table 3-5: Effect of the volume of hydrochloric acid on the extraction percentage, (%E) of Acid Red 18 by the SHS-LLME method

hydrochloric acid volume(µL)	100	200	300	400	500	700	900	1000

%E	75	79	80	84	84	84	84	84

3.3.5 Effect of the volume of sodium hydroxide

The effect of NaOH volume on the phase reversion behavior of DMCHA during Acid Red 18 extraction was evaluated using 10 M NaOH in volumes ranging from 100 to 1000 µL. According to the data presented in Figure (3-12) and Table (3-6) a volume of 400 µL achieved the optimal basicity required to completely deprotonate DMCHA and regenerate the hydrophobic form. This transformation enabled efficient partitioning of Acid Red 18 into the organic phase. Increasing the NaOH volume beyond 400 µL did not enhance extraction efficiency, indicating that saturation conditions were established under the applied experimental parameters.

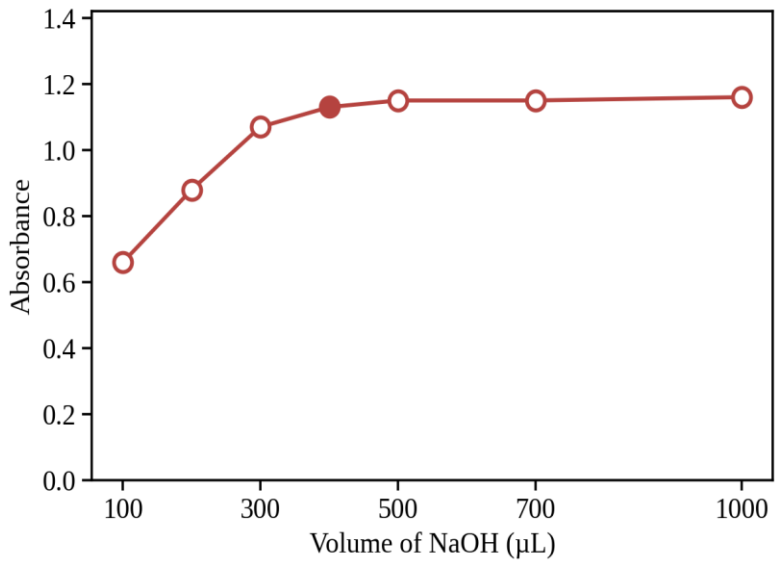


Figure 3-12: Effect of the volume of sodium hydroxide on the extraction of Acid Red 18 by the SHS-LLME method.

Table 3-6: Effect of the volume of sodium hydroxide on the extraction percentage, (%E) of Acid Red 18 by the SHS-LLME method

volume of sodium hydroxide(µL)	100	200	300	400	500	700	1000

%E	59	71	80	83	83	83	83

3.3.6 Effect of temperature

The study evaluated the impact of temperature on Acid Red 18 extraction. As illustrated in Figure (3-13) and Table (3-7) the highest extraction efficiency was achieved at 40 °C. This increase in efficiency can be attributed to enhanced molecular mobility and reduced solvent viscosity, which facilitate better mass transfer. However, at temperatures above 40 °C, extraction efficiency decreased due to solvent evaporation and potential degradation of the analyte. Consequently, 40 °C was determined to be the optimum extraction temperature for subsequent experiments.

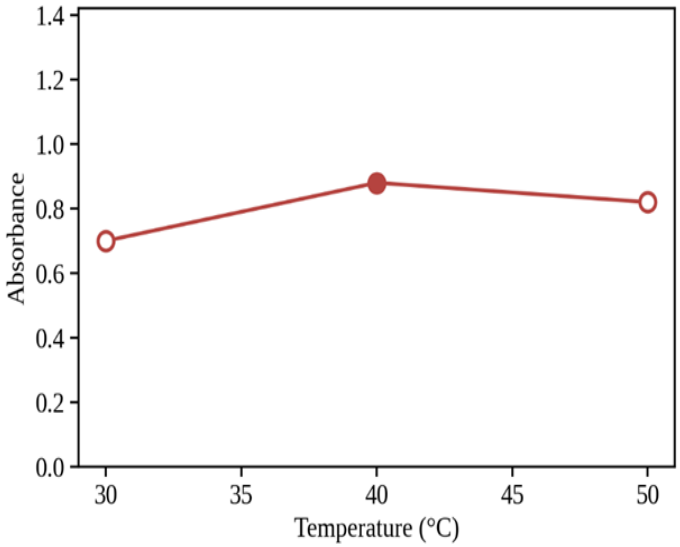


Figure 3-13: Effect of temperature on the extraction of Acid Red 18 by the SHS-LLME method.

Table 3-7: Effect of temperature on the extraction percentage, (%E) of Acid Red 18 by the SHS-LLME method

temperature (°C)	30	40	50
%E	**69**	**79**	**72**

3.3.7 Effect of extraction time

The extraction time is a crucial parameter that significantly influences the efficiency of SHS-LLME process. To evaluate its effect on the extraction of Acid Red 18 dye , a series of experiments were conducted with contact times ranging from (1 -10)s, while keeping all other experimental conditions constant. As shown in (Figure 3-14) and table (3-8) the extraction efficiency increased progressively with time, reaching a maximum at 10 s. This enhancement is attributed to the gradual establishment of equilibrium between the two phases. [36]..

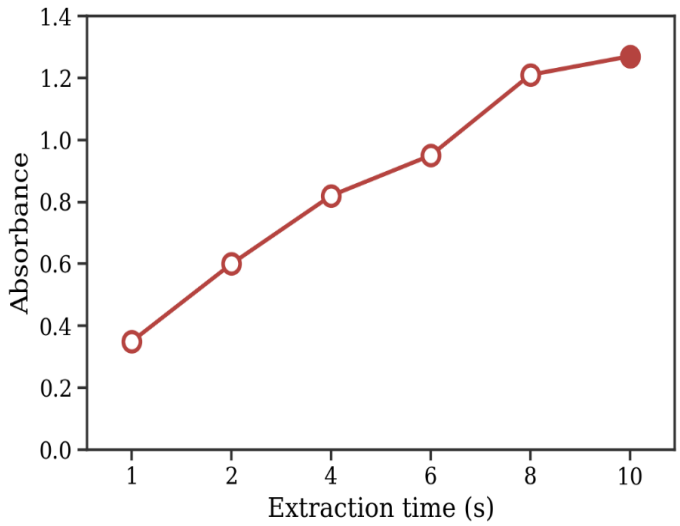


Figure 3-14: Effect of extraction time on the extraction of Acid Red 18 by the SHS-LLME method.

Table 3-8: Effect of extraction time on the extraction percentage, (%E) of Acid Red 18 by the SHS-LLME method

extraction time (s)	1	2	4	6	8	10
%E	**36**	**59**	**72**	**78**	**81**	**85**

3.3.8 Effect of the type and concentration of added electrolyte

The effect of adding an electrolyte was examined with sodium chloride, potassium chloride and calcium chloride over the range 1–10 % (w/v)..the ordering is $CaCl_2$ > KCl ≈ NaCl (Figure 3-15) and table(3-9) . The result follows the salting-out expectation: raising the ionic strength lowers the activity of the anionic dye in the aqueous phase and drives the ion pair into the organic phase. The divalent cation is the more effective at a given mass concentration because it contributes more ionic strength per gram and because it can bridge two sulfonate groups of the same dye molecule [36, 42]. Calcium chloride at 10 % (w/v) gives the largest response of any condition tested in this section.

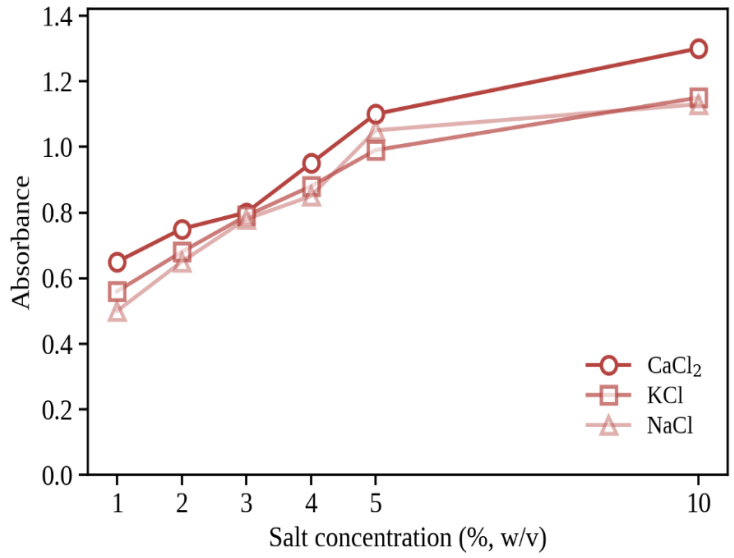


Figure 3-15: Effect of the type and concentration of added electrolyte on the extraction of Acid Red 18 by the SHS-LLME method.

Table 3-9: Effect of the type and concentration of added electrolyte on the extraction percentage, (%E) of Acid Red 18 by the SHS-LLME method

electrolyte	**NaCl**						**KCl**						**$CaCl_2$**					
concentration (%)	1	2	3	4	5	10	1	2	3	4	5	10	1	2	3	4	5	10

%E	52	56	71	77	78	82	53	57	71	75	78	83	57	59	71	78	83	85

Table 3-10: Univariate optimisation of the switchable-solvent microextraction of Acid Red 18.

Factor	Range studied	Value adopted
pH of the aqueous phase	1 – 9	3
Extraction solvent	DMCHA, DPA, TEA	DMCHA
Volume of solvent (mL)	1.0 – 3.0	2.5
Volume of HCl (µL)	100 – 1000	400
Volume of NaOH (µL)	100 – 1000	400
Temperature (°C)	30 – 50	40
Extraction time (s)	1 – 10	10
Electrolyte, 10 % (w/v)	NaCl, KCl, $CaCl_2$	$CaCl_2$

3.4 Factors Affecting the Extraction of Methyl Orange by the SHS-LLME Method

Eight factors were examined for methyl orange under the same univariate scheme. They were the pH of the aqueous phase, the type of extraction solvent, the volume of the switchable solvent, the volumes of hydrochloric acid and sodium hydroxide, the temperature, the type and concentration of added electrolyte, and the extraction time.. The results are shown in Figures 3-16 to 3-23 and summarized in Table 3-19.

3.4.1 Effect of the pH of the aqueous phase

The acidity of the aqueous phase was varied between pH 2 and pH 9. As shown in (Figure 3-16) and Table (3-11), the absorbance rises at pH 2 to a maximum at pH 3 then falls steadily, Methyl orange is a monosulfonated azo dye that also carries a dimethylamino group, so it exists as a zwitterion in acid and as a simple anion above about pH 4.4 [95, 110]. The maximum at pH 3 corresponds to the region in which the sulfonate charge can be paired with the protonated amine solvent while the dimethylamino group is itself protonated, which lowers the overall charge on the molecule. Above pH 4 the dye is a plain anion, the ion pair is progressively lost and it stays in the aqueous phase. A pH of 3 was adopted.

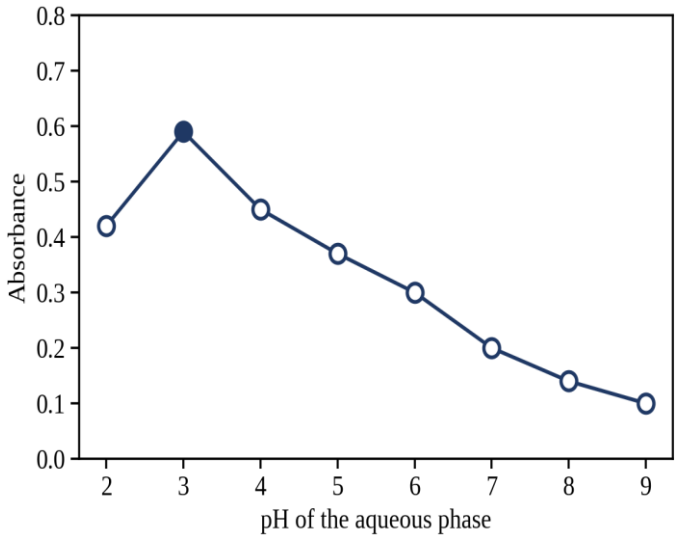


Figure 3-16: Effect of the pH of the aqueous phase on the extraction of methyl orange by the SHS-LLME method.

Table 3-11: Effect of the pH of the aqueous phase on the extraction percentage, (%E) of methyl orange by the SHS-LLME method

pH	**2**	**3**	**4**	**5**	**6**	**7**	**8**	**9**
%E	53	72	53	41	38	29	22	20

3.4.2 Effect of the extraction solvent type

The same three solvents were compared for methyl orange under otherwise identical conditions. The order is that already found for Acid Red 18, DMCHA > DPA > TEA, and DMCHA was adopted (Figure 3-17) and Table (3-12).

That the two dyes rank the three amines in the same order is worth noting. The ranking is a property of the solvents rather than of the dye, and it follows the basicity and the water solubility of the amine rather than anything specific to the azo group [32–34]. The gap between the best solvent and the worst is the same in the two systems.

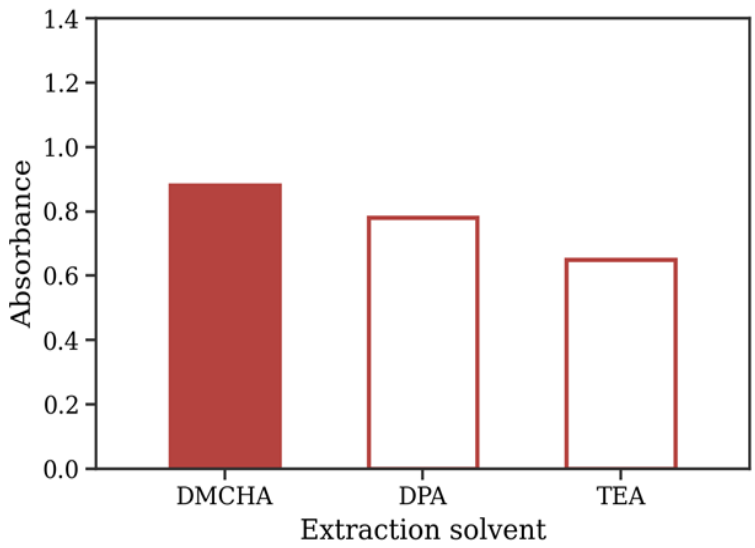


Figure 3-17: Effect of the extraction solvent type on the extraction of methyl orange by the SHS-LLME method.

Table 3-12: Effect of the extraction solvent type on the extraction percentage, (%E) of methyl orange by the SHS-LLME method.

extraction solvent type	DMCHA	DPA	TEA
%E	88	78	72

3.4.3 Effect of the volume of the switchable solvent

The impact of the extraction solvent volume on the recovery of methyl orange was evaluated using the SHS-LLME method. Various volumes of DMCHA, ranging from 1.0 to 3.0 mL, were tested. As illustrated in Figure (3-18) and Table (3-13) the extraction efficiency increased with increasing solvent volume, reaching its maximum at 2.0 mL. Beyond this point, further volume decreases the efficiency by a dilution effect.

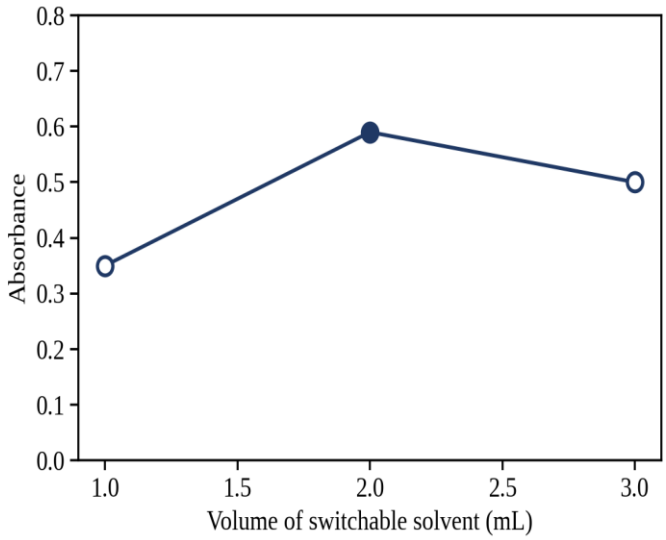


Figure 3-18: Effect of the volume of the switchable solvent on the extraction of methyl orange by the SHS-LLME method.

Table 3-13: Effect of the volume of the switchable solvent on the extraction percentage, (%E) of methyl orange by the SHS-LLME method.

solvent volume(mL)	1.0	2.0	3.0
%E	45	72	56

3.4.4 Effect of the volume of hydrochloric acid

To determine the optimal phase-switching volume, 6 mol L^{-1} HCl was tested in volumes from 100 to 1000 µL. Figure (3-19) and Table (3-14) shows that 300 µL of HCl yielded the highest extraction efficiency. This amount fully protonated DMCHA, promoting its transition to the hydrophilic phase and facilitating methyl orange migration from the aqueous to the organic phase. Increasing the HCl volume beyond 300 µL decrease the extraction efficiency, likely due to saturation of the phase-switching process. Thus, 300 µL was selected as the optimal HCl volume for subsequent experiments.

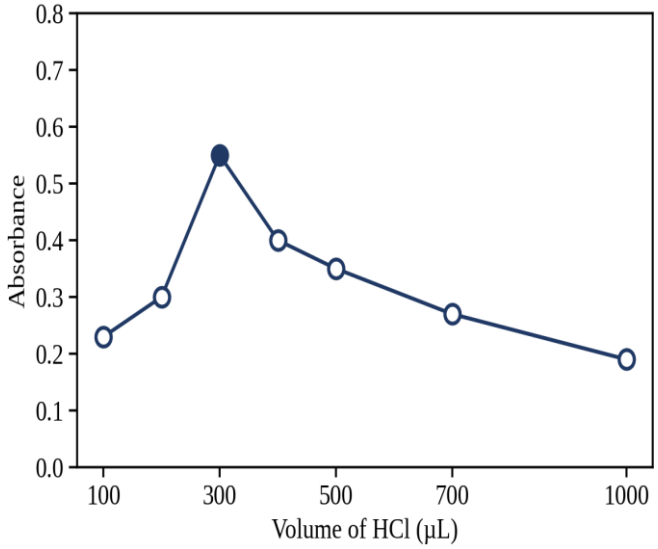


Figure 3-19: Effect of the volume of hydrochloric acid on the extraction of methyl orange by the SHS-LLME method.

Table 3-14: Effect of the volume of hydrochloric acid on the extraction percentage, (%E) of methyl orange by the SHS-LLME method

hydrochloric acid volume(µL)	100	200	300	400	500	700	1000
%E	35	40	71	56	44	40	23

3.4.5 Effect of the volume of sodium hydroxide

The effect of NaOH volume on the phase reversion behavior of DMCHA during methyl orange extraction was evaluated using 10 M NaOH in volumes ranging from 100 to 1000 µL. According to the data presented in Figure (3-20) and Table (3-15), a volume of 100 µL achieved the optimal basicity required to completely deprotonate DMCHA and regenerate the hydrophobic form. This transformation enabled efficient partitioning of methyl orange into the organic phase. Increasing the NaOH volume beyond 100 µL did not enhance extraction efficiency, indicating that saturation conditions were established under the applied experimental parameters [72].

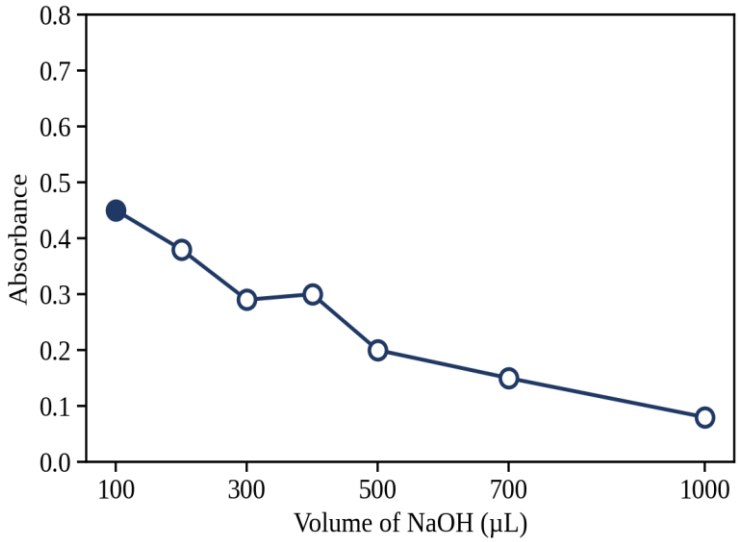


Figure 3-20: Effect of the volume of sodium hydroxide on the extraction of methyl orange by the SHS-LLME method.

Table 3-15: Effect of the volume of sodium hydroxide on the extraction percentage, (%E) of methyl orange by the SHS-LLME method

volume of sodium hydroxide(µL)	100	200	300	400	500	700	1000
%E	59	46	40	40	37	34	25

3.4.6 Effect of temperature

The study evaluated the impact of temperature on methyl orange extraction. As illustrated in (Figure 3-21) and **(**Table 3-16) the highest extraction efficiency was achieved at 40 °C. This increase in efficiency can be attributed to enhanced molecular mobility and reduced solvent viscosity, which facilitate better mass transfer. However, at temperatures above 40 °C, extraction efficiency decreased due to solvent evaporation and potential degradation of the analyte. Consequently, 40 °C was determined to be the optimum extraction temperature for subsequent experiments

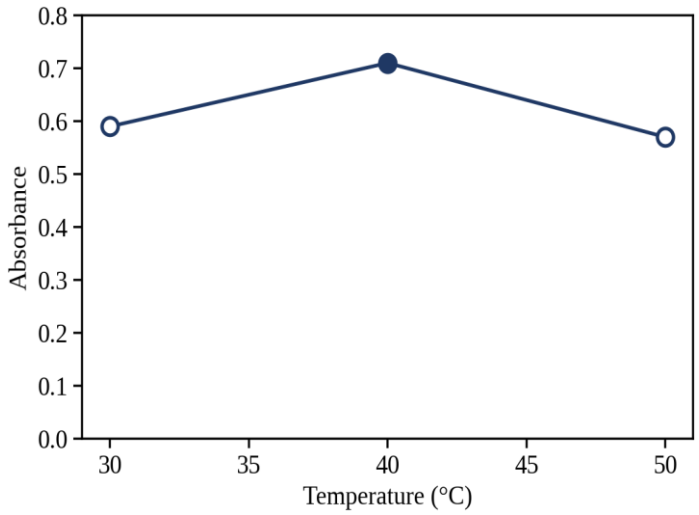


Figure 3-21: Effect of temperature on the extraction of methyl orange by the SHS-LLME method.

Table 3-16: Effect of temperature on the extraction percentage, (%E) of methyl orange by the SHS-LLME method

Temperature (°C)	30	40	50
%E	**72**	**79**	**70**

3.4.7 Effect of the type and concentration of added electrolyte

The three electrolytes were tested over 1–10 % (w/v). Each raises the absorbance up to 5 % and then falls back at 10 %, so all three describe an

interior maximum, and the ordering at every concentration is $CaCl_2$ > NaCl > KCl (Figure 3-16) and (Table 3-17). The best condition is 5 % (w/v) calcium chloride, The fall beyond 5 % is the point at which methyl orange differs from Acid Red 18, whose response was still rising at 10 %. At high ionic strength two effects begin to outweigh the reduction in dye activity: the aqueous phase becomes more viscous, and the added anions compete for the protonated amine. A weakly bound ion pair feels that competition first.

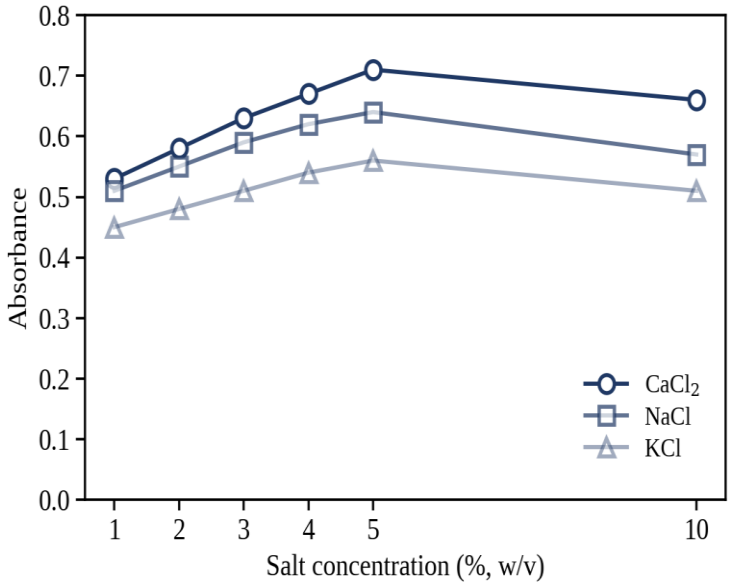


Figure 3-22: Effect of the type and concentration of added electrolyte on the extraction of methyl orange by the SHS-LLME method.

Table 3-17: Effect of the type and concentration of added electrolyte on the extraction percentage, (%E) of methyl orange by the SHS-LLME method

electrolyte	**NaCl**						**KCl**						**$CaCl_2$**					
concentration (%)	1	2	3	4	5	10	1	2	3	4	5	10	1	2	3	4	5	10
%E	61	63	65	66	79	77	50	51	56	60	62	56	64	66	71	74	78	73

3.4.8 Effect of extraction time

The last factor examined was the time for which the sample and the solvent were kept in contact. Six times were tested over 1–10 s (Figure 3-23) and **(**Table 3-18). The absorbance rises steadily at 8 s, and then falls back at 10 s. A time of 8 s was adopted.

The rise is easy to explain. The dye needs a moment to cross from the water into the solvent, so a longer contact transfers more of it. The fall after 8 s is the more interesting half of the curve. Methyl orange forms a weak ion pair with the amine.

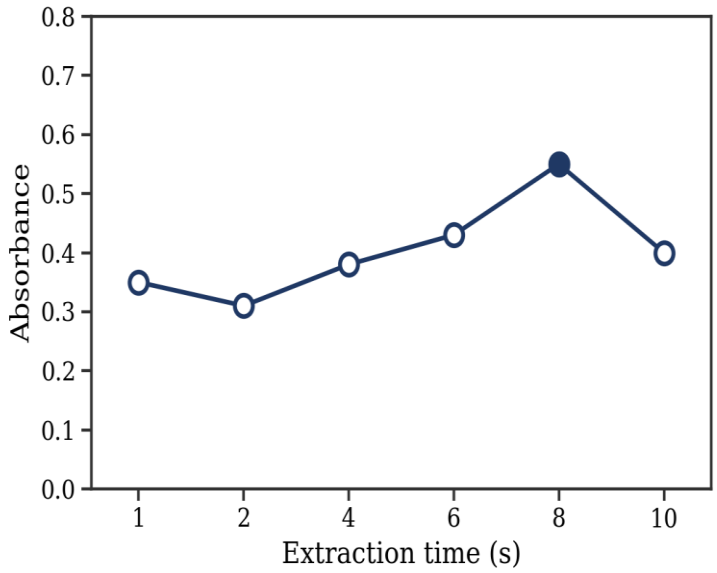


Figure 3-23: Effect of extraction time on the extraction of methyl orange by the SHS-LLME method.

Table 3-18: Effect of extraction time on the extraction percentage, (%E) of methyl orange by the SHS-LLME method

extraction time (s)	1	2	4	6	8	10
%E	**55**	**51**	**60**	**66**	**70**	**60**

Table 3-19: Univariate optimization of the switchable-solvent microextraction of methyl orange.

Factor	Range studied	Value adopted
pH of the aqueous phase	2 – 9	3
Extraction solvent	DMCHA, DPA, TEA	DMCHA
Volume of solvent (mL)	1.0 – 3.0	2.0
Volume of HCl (µL)	100 – 1000	300
Volume of NaOH (µL)	100 – 1000	100
Temperature (°C)	30 – 50	40
Extraction time (s)	1 – 10	8
Electrolyte (%, w/v)	1 – 10	$CaCl_2$, 5 %

3.5 Chemometric Optimization by Central Composite Design

In Sections 3.3 and 3.4 each variable was studied on its own. That is simple, but it cannot show whether two variables act together [77, 78]. The response surface methodology using central composite design (CCD) presents a statistical alternative that minimizes the total number of experiments, identifies both individual and interaction effects among several factors and determines the optimum operating point. For k factors, $N=2^k+2k+n_0$ (factorial + axial + centre points) runs are needed to construct a rotatable CCD; for k=4, N=16 factorial points +8 axial points +7 centre points=31 runs The four most important variables pH, solvent volume, HCl volume and NaOH volume were therefore studied together in a central composite design, run separately for each dye. The response was the absorbance of the recovered phase.

3.5.1 Design of the experiments

Experimental designis applicable for simultaneous optimization of the effects of variables to improve characteristic performance and minimize the errors . A central composite design has three parts: factorial runs that measure the

main effects and the interactions, axial runs that measure curvature, and centre runs that measure the experimental error [78, 85]. Thirty-one runs were made for each dye. Table 3-20 gives the factors and the levels used and Table 3-21 gives Central composite design matrix with the experimental and model-predicted absorbance of Acid red-18 dye.

Table 3-20: Structure of the two central composite designs, as executed.

Feature	Acid Red 18	Methyl Orange
Factorial levels, pH (−1 / +1)	2.0 / 9.0	2.0 / 9.0
Factorial levels, solvent volume (mL)	1 / 3	1 / 3
Factorial levels, HCl volume (µL)	100 / 1000	100 / 1000
Factorial levels, NaOH volume (µL)	100 / 1000	100 / 1000
Centre point (pH, mL, µL, µL)	5.5, 2, 550, 550	5.5, 2, 550, 550

Table 3-21: Central composite design matrix with the experimental and model-predicted absorbance of Acid Red 18.

Run	pH	Solvent (mL)	HCl (µL)	NaOH (µL)	Abs (exp.)	Abs (pred.)
1	2.0	1	1000	100	0.265	0.294
2	2.0	1	1000	1000	0.291	0.301
3	2.0	1	100	100	0.139	0.124
4	5.5	2	550	350	0.213	0.190
5	2.0	1	100	1000	0.200	0.196
6	2.0	3	100	1000	0.339	0.347
7	9.0	3	1000	1000	0.295	0.311
8	5.5	2	550	550	0.200	0.194
9	9.0	3	1000	100	0.321	0.325
10	5.5	2	550	550	0.210	0.194
11	9.0	1	100	1000	0.083	0.105

12	2.0	3	1000	1000	0.560	0.540
13	5.5	2	550	550	0.192	0.194
14	9.0	1	1000	1000	0.153	0.146
15	5.5	2	550	550	0.195	0.194
16	2.0	3	1000	100	0.580	0.559
17	5.5	2	550	550	0.182	0.194
18	9.0	1	1000	100	0.142	0.134
19	5.5	2	550	550	0.182	0.194
20	9.0	1	100	100	0.008	0.028
21	5.5	0	550	550	0.100	0.076
22	9.0	3	100	1000	0.212	0.183
23	5.5	2	550	550	0.192	0.194
24	9.0	3	100	100	0.140	0.131
25	5.5	1	550	550	0.182	0.194
26	9.0	2	550	550	0.147	0.138
27	5.5	2	1000	550	0.278	0.276
28	2.0	2	550	550	0.293	0.300
29	5.5	2	550	1450	0.269	0.270
30	5.5	2	550	550	0.295	0.218
31	2.0	3	100	100	0.294	0.301

3.5.2 Acid Red 18

3.5.2.1 Model fitting and analysis of variance

The thirty-one responses were fitted to a full quadratic model with four linear, four quadratic and six interaction terms. The ANOVA results in Table 3-22 confirmed that the quadratic model was highly significant ($F = 6.13$, $P < 0.001$). The lack-of-fit was not significant ($P = 0.640$), demonstrating that the proposed model adequately described the experimental data.

Based on the results of the performed experiments the second- order poly nomial equation was obtained as shown in the following equation:

$$Abs = 0.25421 - 0.063849\,pH + 0.13054\,V - 6.0989\times10^{-4}\,V(HCl) + 9.1486\times10^{-6}\,V(NaOH) + 0.013258\,pH^2 + 8.9934\times10^{-3}\,V^2 + 5.2556\times10^{-7}\,V(HCl)^2 + 1.5105\times10^{-8}\,V(NaOH)^2 - 0.034821\,pH\cdot V - 5.4365\times10^{-5}\,pH\cdot V(HCl) - 1.9444\times10^{-5}\,pH\cdot V(NaOH) + 1.6528\times10^{-4}\,V\cdot V(HCl) + 9.7222\times10^{-6}\,V\cdot V(NaOH) + 2.0062\times10^{-7}\,V(HCl)\cdot V(NaOH)$$

where V is the solvent volume in millilitres and the reagent volumes are in microlitres. This equation reproduces the printed one to every figure given.

Table 3-22: Analysis of variance for the quadratic model fitted to the Acid Red 18 response.

Source	DF	Adj SS	Adj MS	F-value	P-value
Model	14	1.338230	0.095588	6.13	0.000
Linear	4	0.346955	0.086739	5.57	0.005
pH	1	0.176022	0.176022	11.30	0.004
Solvent volume	1	0.121838	0.121838	7.82	0.013
HCl volume	1	0.040558	0.040558	2.60	0.126
NaOH volume	1	0.007862	0.007862	0.50	0.488
Square	4	0.516662	0.129165	8.29	0.001
pH²	1	0.068262	0.068262	4.38	0.053
Solvent volume²	1	0.002277	0.002277	0.15	0.707
HCl volume²	1	0.027513	0.027513	1.77	0.203
NaOH volume²	1	0.000120	0.000120	0.01	0.931
Two-way interaction	6	0.485187	0.080865	5.19	0.004
pH × solvent volume	1	0.237656	0.237656	15.25	0.001
pH × HCl volume	1	0.117306	0.117306	7.53	0.014
pH × NaOH volume	1	0.015006	0.015006	0.96	0.341
Solvent × HCl volume	1	0.088506	0.088506	5.68	0.030
Solvent × NaOH volume	1	0.000306	0.000306	0.02	0.890
HCl × NaOH volume	1	0.026406	0.026406	1.69	0.211
Error	16	0.249338	0.015584		
Lack of fit	9	0.249338	0.027704	-	0.64
Pure error	7	0.000000	0.000000		
Total	30	1.587568			

3.5.2.2 Main effects and interactions

The Pareto chart of effects is a useful field to identify the most important factors. (Figure 3-24) ranks the terms by their t values and draws the significance line at t = 2.12, the critical value for sixteen degrees of freedom at the 0.05 level. Five terms cross it: pH × solvent (3.91), pH (3.36), solvent

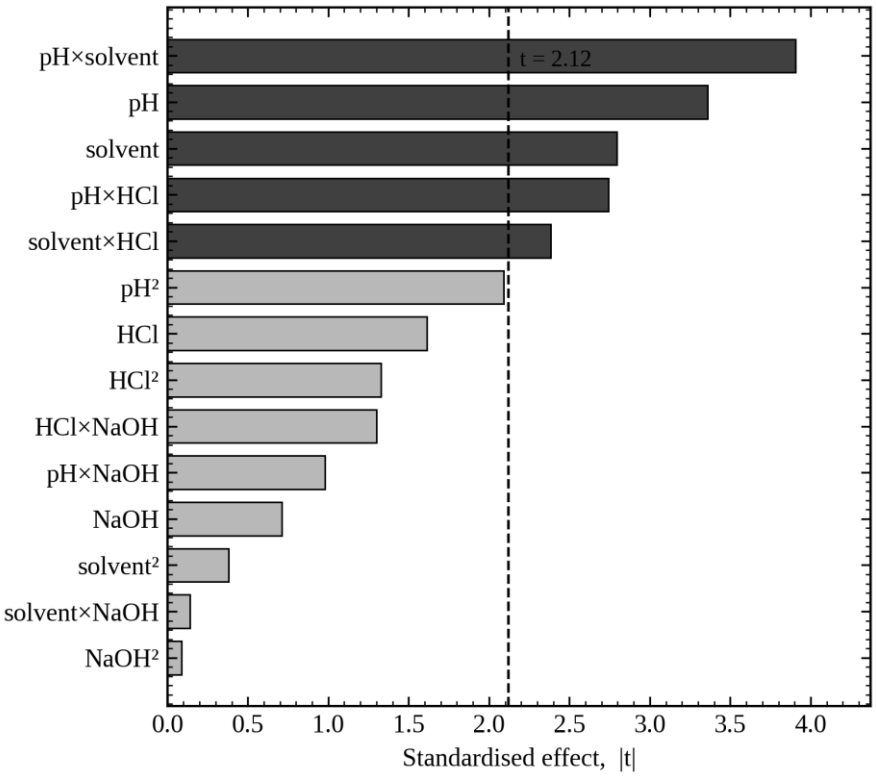


Figure 3-24: Pareto chart of the standardised effects on the absorbance of the extracted Acid Red 18.

A main-effects plot shows how changing a single factor affects the response (absorbance) while all other factors are fixed. The shape of each curve directly indicates the mathematical relationship between that factor and the response.The main-effects plots (Figure 3-25) show each factor with the other three at the centre. Absorbance falls as pH rises, for the reason that the more acidic the medium, the more of the amine stays protonated and able to pair with the dye anion. Absorbance rises with solvent volume. The two reagent curves are almost flat.

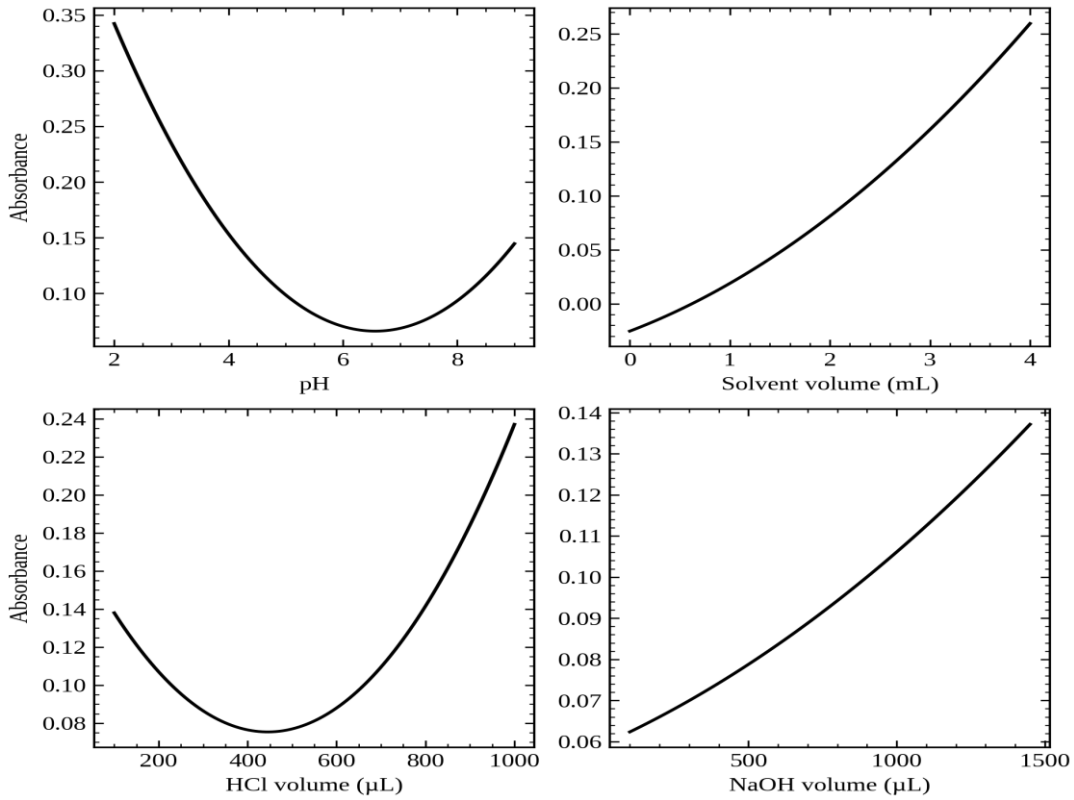


Figure 3-25: Main-effects plots for the Acid Red 18 model: fitted absorbance against each factor with the other three held at the centre of the design (pH 5.5, 2 mL of solvent, 550 µL of HCl and 550 µL of NaOH).

An interaction plot shows how the effect of one factor on absorbance changes depending on the level of a second factor. Two lines are drawn one at a low level and one at a high level of the second factor. The key diagnostic is the relationship between the two lines:

-Parallel lines signal no interaction: each factor acts independently.

-Non-parallel (diverging) lines signal an ordinal interaction: one factor consistently outperforms the other, but the size of the gap changes.

-Crossing lines signal a disordinal interaction: the factor that gives higher absorbance actually reverses depending on the level of the second factor. This is the strongest form of interaction.

(Figure 3-26) show why the main effects cannot stand alone. Solvent volume has a large effect at pH 2 and almost none at pH 9, because at pH 9 there is little protonated amine for the dye to pair with. HCl volume behaves the same way, and its effect is larger at the higher solvent volume. The curves in each panel are far from parallel, and that is what an interaction looks like.

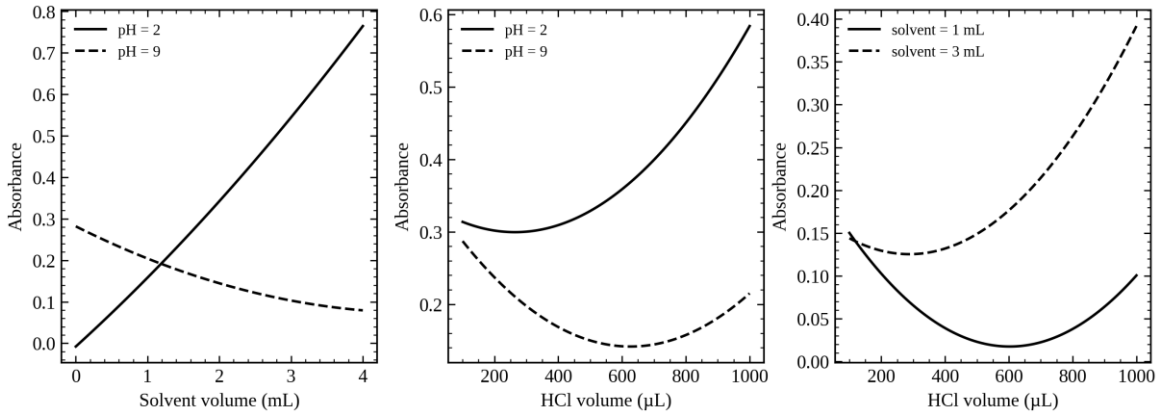


Figure 3-26: Interaction plots for the Acid Red 18 model: (left) solvent volume at two levels of pH, (centre) HCl volume at two levels of pH, and (right) HCl volume at two solvent volumes. The remaining factors are held at the centre of the design.

3.5.2.3 Response surface

The three-dimensional response surfaces and the corresponding contour plots Figures (3-27) and (3-28) provide a visual reading of the model. The surface for absorbance against pH and solvent volume is the most structured: the response rises toward the acidic, high solvent-volume corner and falls away sharply toward higher pH. The surface involving the HCl volume shows a clear upward trend with increasing acid, whereas the NaOH surface is comparatively flat, reflecting its smaller effect. The contour plots locate the most favourable region in the low-pH part of the domain, in agreement with both the univariate study and the analysis of variance.

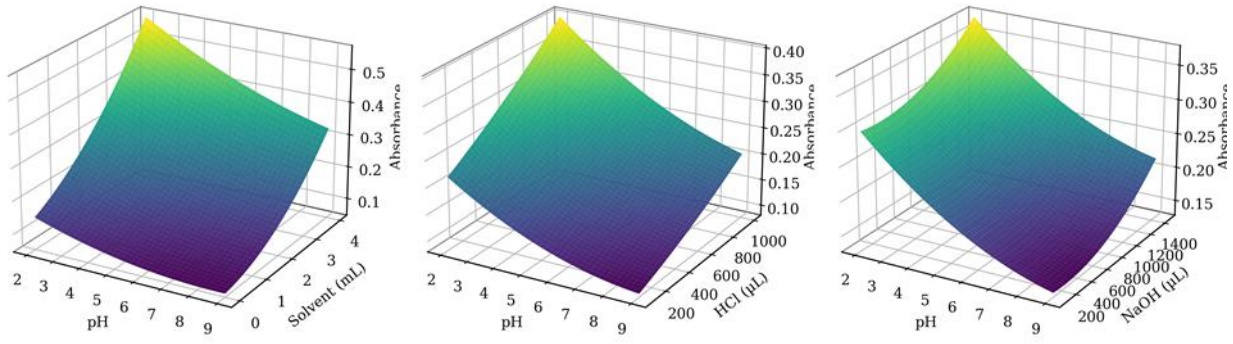


Figure 3-27: Three-dimensional response surfaces for absorbance as a function of (left) pH and solvent volume, (centre) pH and HCl volume, and (right) pH and NaOH volume.

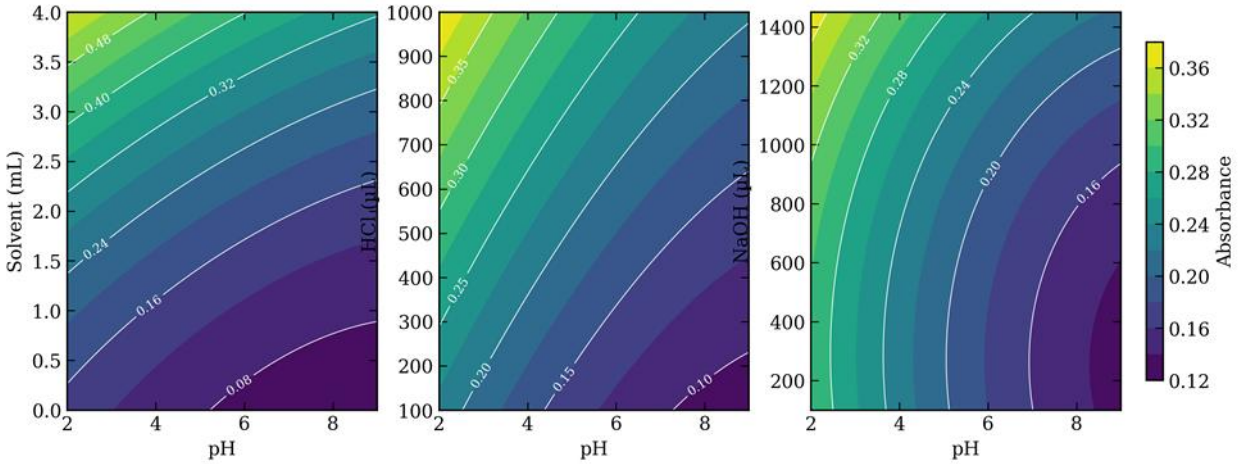


Figure 3-28: Contours of the quadratic model fitted to the Acid Red 18 response: (left) pH–solvent plane, (centre) pH–acid plane and (right) pH-base plane.

Figure 3-29 illustrates a comparison between experimental and predicted absorbance values (Experimental vs. Predicted Absorbance), which is statistically known as a "Parity Plot" to evaluate the accuracy of a reliable predictive or mathematical model. The results confirm that the model used has very high predictive accuracy, as the relative error between what was predicted and what was measured in the laboratory is very small. It has a very strong linear correlation and a high coefficient of agreement (close to 1), which means

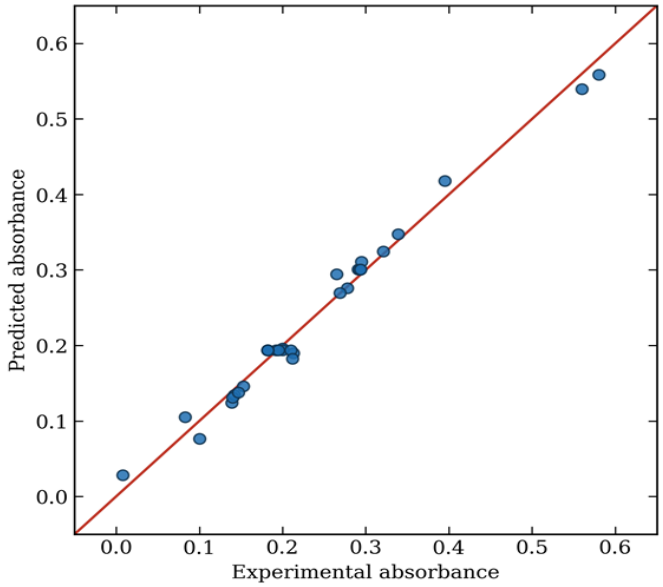


Figure 3-29: Predicted against measured absorbance for the thirty-one runs of the Acid Red 18 design

3.5.2.4 Optimisation and confirmation

The desirability function identified the conditions that gave the highest absorbance within the experimental region [87, 88]. The solution is pH 2, 2.77 mL of solvent, 1000 µL of HCl and 1450 µL of NaOH, with a fitted absorbance of 1.000 and a composite desirability of 1.000 Figure 3-30 (Table 3-23).

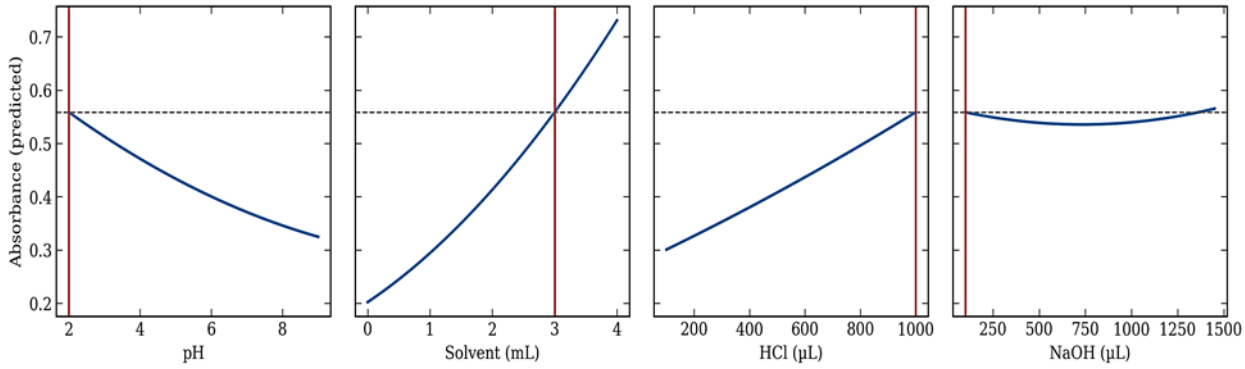


Figure 3-30: Response-optimization (desirability) plot for Acid Red 18

Table 3-23: Optimum predicted for Acid Red 18 by the desirability function.

Quantity	Value
pH	2
Volume of solvent (mL)	2.77
Volume of HCl (µL)	1000
Volume of NaOH (µL)	1450
Composite desirability	1.000
Largest absorbance measured in the design	1.100
Largest value the model reaches inside the region	1.271 (pH 2; 4 mL; 1000 µL; 1450 µL)

3.5.3 Methyl Orange

3.5.3.1 Model fitting and analysis of variance

The thirty-one responses were fitted to a full quadratic model with four linear (Table 3-24), four quadratic, and six interaction terms. The ANOVA results in Table 3-25confirmed that the quadratic model was highly significant (F = 42.70, P <0.001). The lack-of-fit was not significant (P = 0.640), demonstrating that the proposed model adequately described the experimental data.

Table 3-24: Central composite design matrix with the experimental and model-predicted absorbance of Methyl Orange

Run	pH	Solvent (mL)	HCl (µL)	NaOH (µL)	Abs (exp.)	Abs (pred.)
1	2.0	3	100	1000	0.450	0.449347
2	2.0	1	100	1000	0.426	0.446225
3	5.5	2	550	550	0.300	0.278392
4	5.5	2	350	550	0.241	0.281705
5	5.5	2	550	550	0.300	0.278392
6	9.0	1	1000	1000	0.114	0.049571
7	5.5	2	350	550	0.350	0.281705
8	5.5	2	550	350	0.264	0.291252
9	2.0	1	1000	1000	0.392	0.431321
10	2.0	3	100	100	0.512	0.507214

11	2.0	1	1000	100	0.510	0.489188
12	9.0	3	1000	1000	0.040	0.052692
13	5.5	2	550	550	0.230	0.278392
14	2.0	3	1000	1000	0.399	0.434442
15	9.0	3	100	100	0.123	0.125464
16	5.5	2	1450	550	0.250	0.263488
17	9.0	1	100	1000	0.050	0.064475
18	9.0	1	100	100	0.092	0.122343
19	2.0	3	1000	100	0.510	0.492310
20	5.5	4	550	550	0.276	0.281514
21	5.5	2	550	1450	0.225	0.220525
22	9.0	3	100	1000	0.059	0.067597
23	5.5	2	550	550	0.300	0.278392
24	5.5	2	550	550	0.300	0.278392
25	5.5	2	550	550	0.300	0.278392
26	9.0	3	1000	100	0.097	0.110560
27	5.5	2	550	550	0.300	0.278392
28	2.0	1	100	100	0.500	0.504093
29	5.5	2	550	550	0.300	0.278392
30	5.5	2	550	550	0.300	0.278392
31	9.0	1	1000	100	0.070	0.107438

The second-order polynomial equation obtained is

$$Abs = 0.57973 - 0.055893\ pH + 0.041792\ V + 4.2352\times10^{-5}\ V(HCl) - 7.7958\times10^{-5}\ V(NaOH) - 3.4917\times10^{-4}\ pH^2 - 4.4564\times10^{-3}\ V^2 - 3.4703\times10^{-8}\ V(HCl)^2 - 1.0195\times10^{-8}\ V(NaOH)^2 - 8.9286\times10^{-4}\ pH\cdot V + 2.9365\times10^{-6}\ pH\cdot V(HCl) + 9.7619\times10^{-6}\ pH\cdot V(NaOH) - 1.6111\times10^{-5}\ V\cdot V(HCl) - 1.4444\times10^{-5}\ V\cdot V(NaOH) + 0\cdot V(HCl)\cdot V(NaOH)$$

where V is the solvent volume in millilitres and the reagent volumes are in microlitres. This equation reproduces the printed software output exactly, confirming that different methods of centring the factors describe the same response surface.

Table 3-25: Analysis of variance for the quadratic model fitted to the Methyl Orange response.

Source	DF	Adj SS	Adj MS	F-value	P-value
Model	14	0.609118	0.043508	42.70	0.000
Linear	4	0.312714	0.078178	76.73	0.000
pH	1	0.301088	0.301088	295.52	0.000
Solvent volume	1	0.000164	0.000164	0.16	0.694
HCl volume	1	0.001290	0.001290	1.27	0.277
NaOH volume	1	0.010148	0.010148	9.96	0.006

Source	DF	Adj SS	Adj MS	F-value	P-value
Square	4	0.002379	0.000595	0.58	0.679
pH²	1	0.000062	0.000062	0.06	0.809
Solvent volume²	1	0.000238	0.000238	0.23	0.636
HCl volume²	1	0.000585	0.000585	0.57	0.460
NaOH volume²	1	0.000051	0.000051	0.05	0.826
Two-way interaction	6	0.005798	0.000966	0.95	0.489
pH × solvent volume	1	0.000156	0.000156	0.15	0.701
pH × HCl volume	1	0.000342	0.000342	0.34	0.570
pH × NaOH volume	1	0.003782	0.003782	3.71	0.072
Solvent × HCl volume	1	0.000841	0.000841	0.83	0.377
Solvent × NaOH volume	1	0.000676	0.000676	0.66	0.427
HCl × NaOH volume	1	0.000000	0.000000	0.00	1.000
Error	16	0.016302	0.001019		
Lack of fit	7	0.006006	0.000858	0.75	0.640
Pure error	9	0.010296	0.001144		
Total	30	0.625419			

3.5.3.2 Main effects and interactions

The Pareto chart (Figure 3-31) ranks the terms by their absolute t-values and draws the significance line at t = 2.12, the critical value for sixteen degrees of freedom at the 0.05 level. Only two terms cross it: pH, which extends far beyond all other bars, and NaOH volume. Every other term solvent volume, HCl volume, all four quadratic terms, and all six two-way interactions falls short of the threshold. This picture is markedly simpler than the one for Acid Red 18, where five terms were significant and the pH × solvent and pH × HCl interactions were among the most prominent. For Methyl Orange, the response is driven almost entirely by pH, with NaOH volume as a secondary influence and the remaining factors contributing noise rather than signal

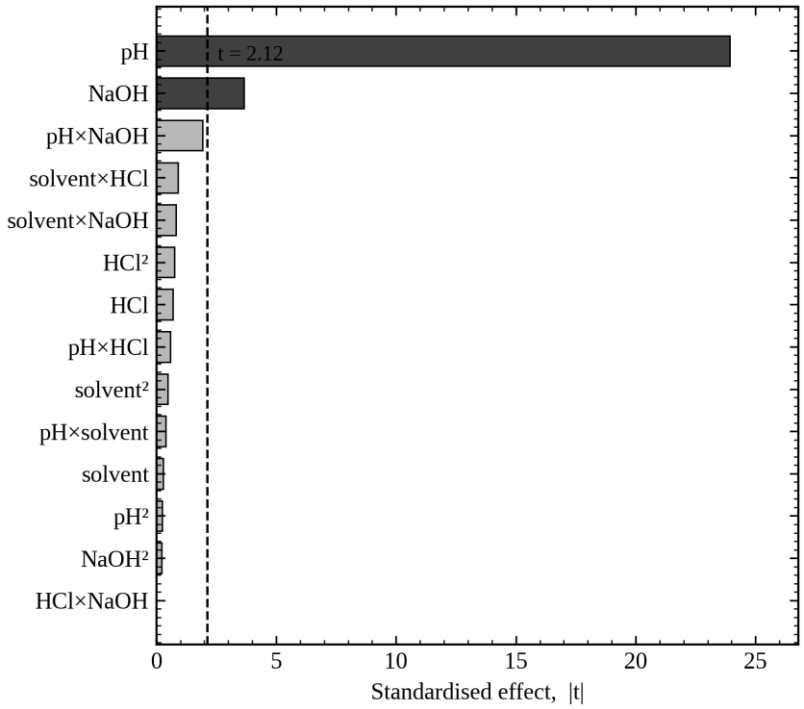


Figure 3-31: Pareto chart of the standardised effects on the absorbance of the extracted Methyl Orange.

A main-effects plot shows how changing a single factor affects the response (absorbance) while all other factors are fixed at the centre of the design. The shape of each curve directly indicates the mathematical relationship between that factor and the response.

The main-effects plots (Figure 3-32) show each factor with the other three held at the centre. Absorbance falls steeply and almost linearly as pH rises from 2 to 9, for the same chemical reason that governs Acid Red 18: the more acidic the medium, the more of the amine stays protonated and available to pair with the dye anion. The slope is steep enough that pH alone carries 93% of the total model variation. Solvent volume shows only a shallow curve with a slight peak near 2.2 mL, and HCl volume is essentially flat up to roughly 500 µL before a gentle decline at higher volumes. NaOH volume decreases gently from approximately 0.32 to 0.22 over its entire range, consistent with its borderline significance. Unlike Acid Red 18, whose reagent curves were nearly flat, the

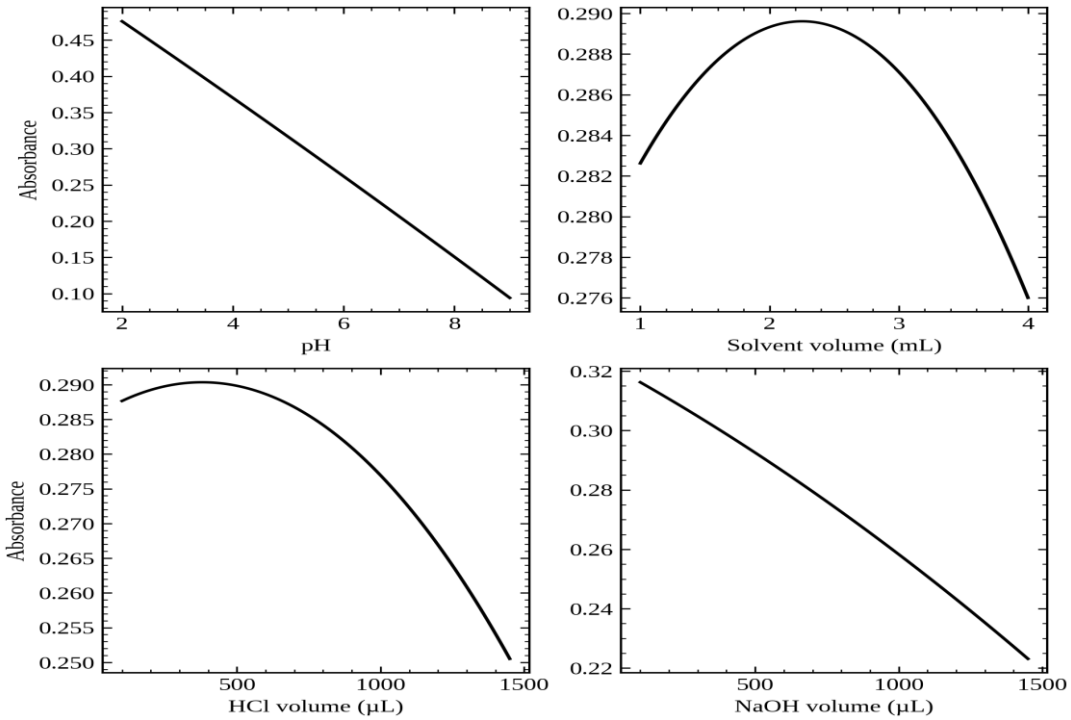


Figure 3-32: Main-effects plots for the Methyl Orange model.

fitted absorbance against each factor with the other three held at the centre of the design.

The interaction plots (Figure 3-33) show near-parallel curves in every panel. Parallel curves mean that one factor does not change the effect of the other, that is, no interaction, and that is what the analysis of variance reports. The gap between the two curves in each panel is the pH effect, and it is the only large feature in the figure.

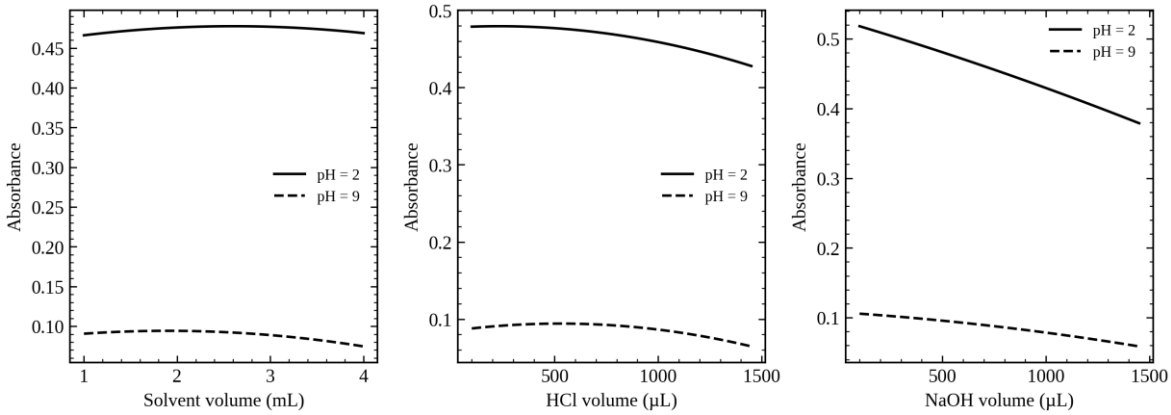


Figure 3-33: Interaction plots for the Methyl Orange model: (left) solvent volume, (centre) HCl volume and (right) NaOH volume.

3.5.3.3 Response surface and diagnostics

The three-dimensional response surfaces and the corresponding contour plots (Figures 3-34 and 3-35) provide a visual reading of the model. All three surfaces absorbance against pH and solvent volume, absorbance against pH and HCl volume, and absorbance against pH and NaOH volume share the same character: the surface rises steadily and monotonically toward the low-pH corner and has no maximum anywhere inside the experimental region.

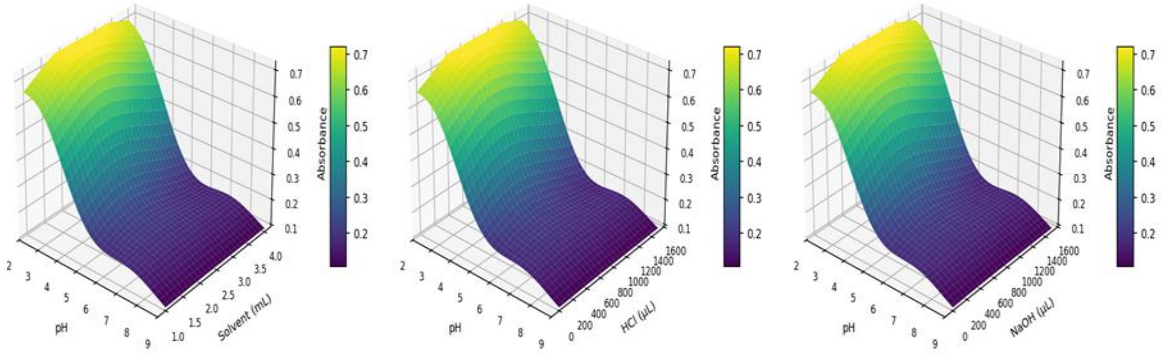


Figure 3-34: Three-dimensional response surfaces for Methyl Orange absorbance as a function of (left) pH and solvent volume, (centre) pH and HCl volume, and (right) pH and NaOH volume

The contour plots (Figure 3-35) reinforce this reading. The iso-absorbance lines run almost vertically nearly parallel to the reagent axes confirming that pH drives the response and the other variables contribute comparatively little curvature or interaction. The highest-absorbance region is concentrated in the acidic corner of each panel, in agreement with both the univariate study and the ANOVA

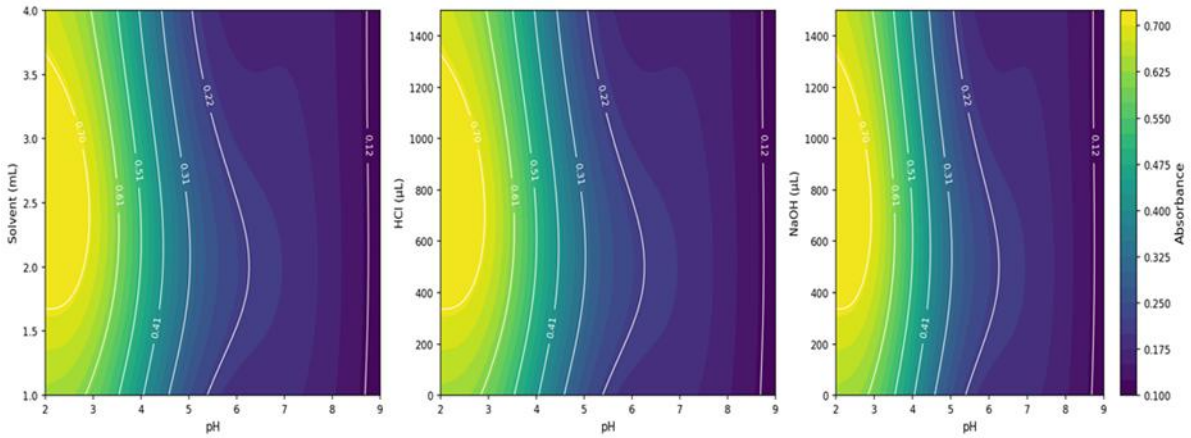


Figure 3-35: Contours of the quadratic model fitted to the Methyl Orange response. (left) pH–solvent plane, (centre) pH–acid plane and (right) pH-base plane.

Figure 3-36 illustrates a comparison between measured and predicted absorbance values for all thirty-one runs what is statistically known as a parity plot, used to evaluate the accuracy of a predictive model. The thirty-one points lie close to the 1:1 reference line, and no standardised residual exceeds ±2; the largest is +1.96. The first-order and full quadratic models give virtually identical predictions for every run, which is consistent with the ANOVA finding that the quadratic and interaction blocks together add very little beyond the linear block. The high R^2 (97.39%), the non-significant lack of fit (P = 0.640), and the absence of large residuals together confirm that the model is reliable and that it can be used with confidence to predict absorbance values within the studied region

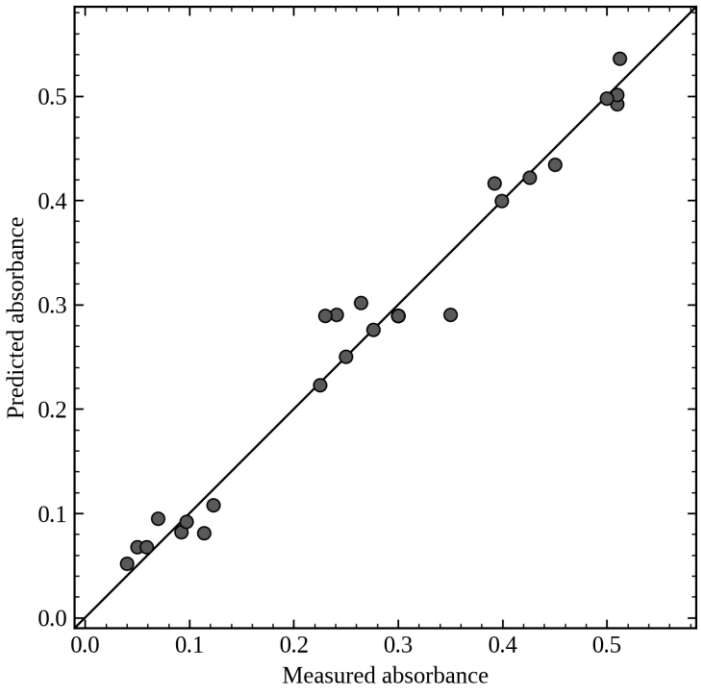


Figure 3-36: Predicted against measured absorbance for the thirty-one runs of the Methyl Orange design

3.5.3.4 Optimisation and confirmation

The surface rises steadily towards low pH and small reagent volumes and has no maximum inside the region. Searching the whole region pH 2 to 9, solvent 1 to 4 mL and both reagents 100 to 1450 µL the highest value the model reaches is 0.734, at pH 2, 4 mL of solvent, 100 µL of HCl and 100 µL of NaOH Figure 3-37 and (Table 3-26).

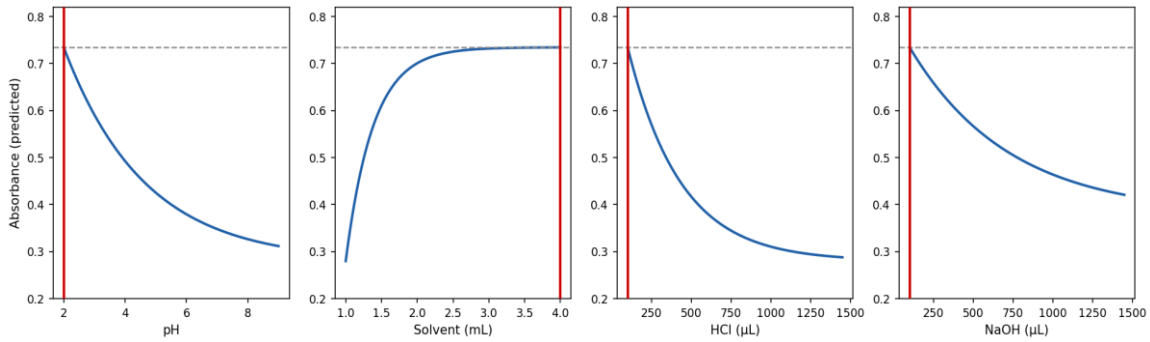


Figure 3-37: Response-optimization (desirability) plot for Methyl Orange

Table 3-26: Optimum predicted for Methyl Orange from the fitted model.

Quantity	Value
pH	2 (lower limit of the design)
Volume of solvent (mL)	4 (upper limit, one run only)
Volume of HCl (µL)	100 (lower limit)
Volume of NaOH (µL)	100 (lower limit)
Composite desirability	1.000
Largest absorbance measured in the design	0.734
Largest value the model reaches inside the region	0.763 (pH 2; 4 mL; 100 µL; 100 µL)

3.6 Calibration of the SHS-LLME Method

The dyes was quantified by measuring the absorbance of the recovered organic phase against a reagent blank under the conditions established in Sections 3.3 and 3.4. A calibration set of ten standards covering 10–100 mg L^{-1} was prepared and measured, and a further standard at 1000 mg L^{-1} was measured in order to define the upper end of the working range. The calibration line is shown in Figure 3-38 and the figures of merit derived from it are collected in Table 3-27

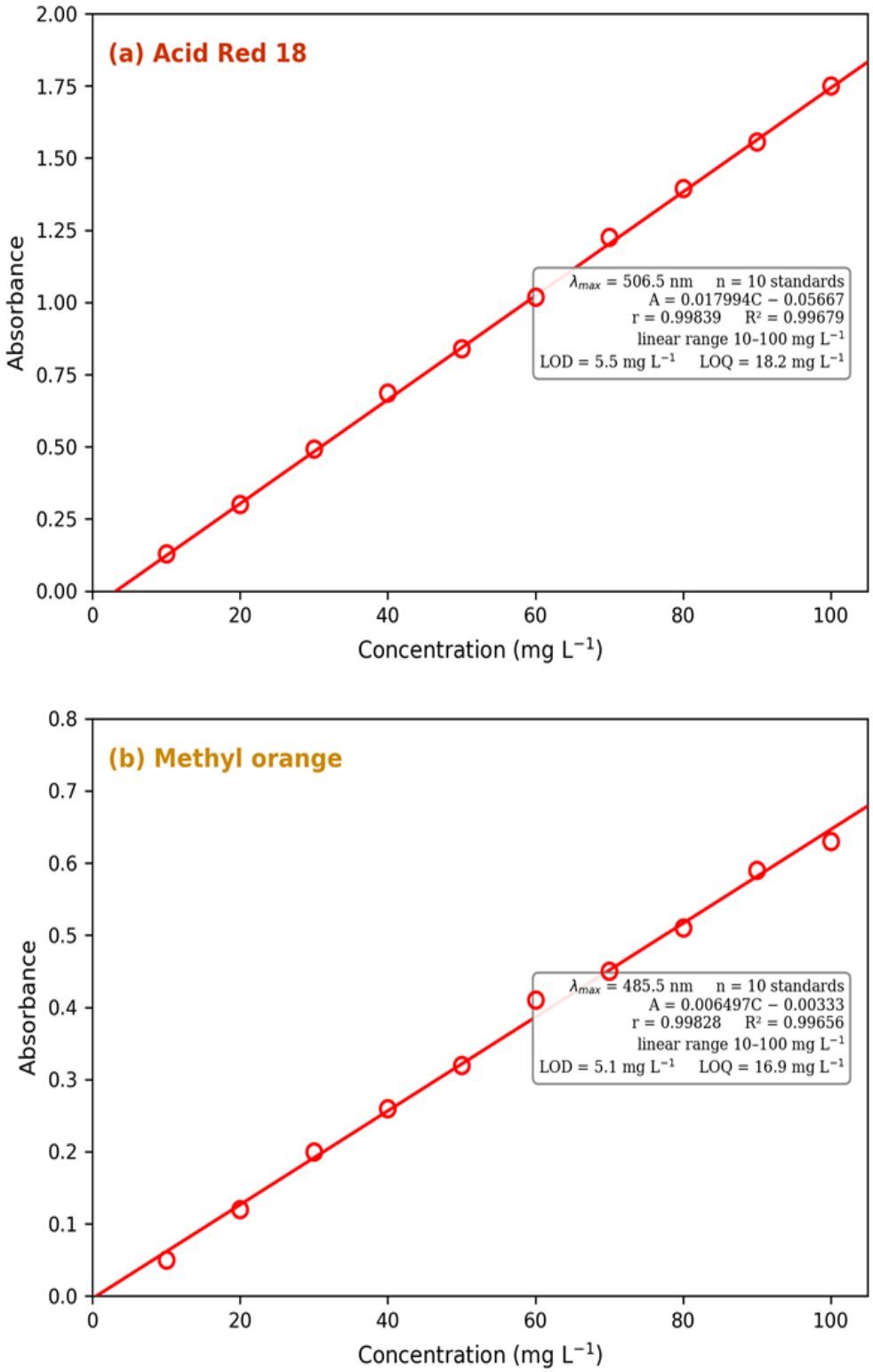


Figure 3-38: Calibration of the spectrophotometric determination. Linear range, 10–100 mg L^{-1}, (a) Acid Red 18, (b) Methyl Orange

Table 3-27: Calibration data and the figures of merit derived from them.

Quantity	Acid Red 18	Methyl Orange
Linear range	10 – 100 mg L^{-1}	10 – 100 mg L^{-1}
Number of standards, n	10	10
Slope, m	0.017994 L mg^{-1}	0.006497 L mg^{-1}
Intercept, b	− 0.05667	-0.00333
Correlation coefficient, r	0.9983	0.9928
Coefficient of determination, R^2	0.9967	0.9965
Residual standard deviation, s(y/x)	0.0328	0.0122
Standard deviation of the intercept, s(b)	0.0224	0.00837
LOD = 3. s(y/x)/m	5.50 mg L^{-1}	5.10 mg L^{-1}
LOQ = 10 s(y/x)/m	18.23 mg L^{-1}	16.90 mg L^{-1}

3.7 Factors Affecting the Extraction of Acid Red 18 by the MSPE Method

The magnetic solid-phase extraction on the polyaniline-coated magnetite was optimised over four factors: the mass of sorbent, the adsorption time, the type of desorption solvent and the desorption time. Retention rests on the electrostatic interaction between the sulfonate groups of the dye and the protonated nitrogen centres of the emeraldine salt [61, 64, 65]. The sorbent is recovered from the suspension with a hand-held magnet at each stage. The results are shown in Figures 3-39 to 3-42 and summarised in Table 3-32.

3.7.1 Effect of the mass of the magnetic sorbent

The effect of varying amounts of Fe_3O_4/polyaniline magnetic sorbent on the extraction efficiency of Acid Red 18 was systematically investigated. Different sorbent masses, ranging from 0.1 g to 0.5 g, were tested under consistent experimental conditions. As illustrated in Figure (3-39) and Table (3-28), the highest extraction efficiency was achieved with a sorbent mass of 0.5 g. Increasing the sorbent mass beyond this level did not result in further

improvements and, in some cases, even slightly decreased efficiency. This phenomenon can be attributed to the saturation of active sites on the sorbent's surface. Once all analyte molecules are effectively adsorbed, adding more sorbent does not provide additional benefits. Furthermore, larger quantities of Fe_3O_4/polyaniline composite can increase the viscosity of the suspension, potentially hindering the diffusion of analyte molecules and reducing mass transfer between the aqueous phase and the sorbent surface. Consequently, 0.5 g was selected as the optimal sorbent mass for subsequent extractions, ensuring maximum efficiency while minimizing material usage sorbent.

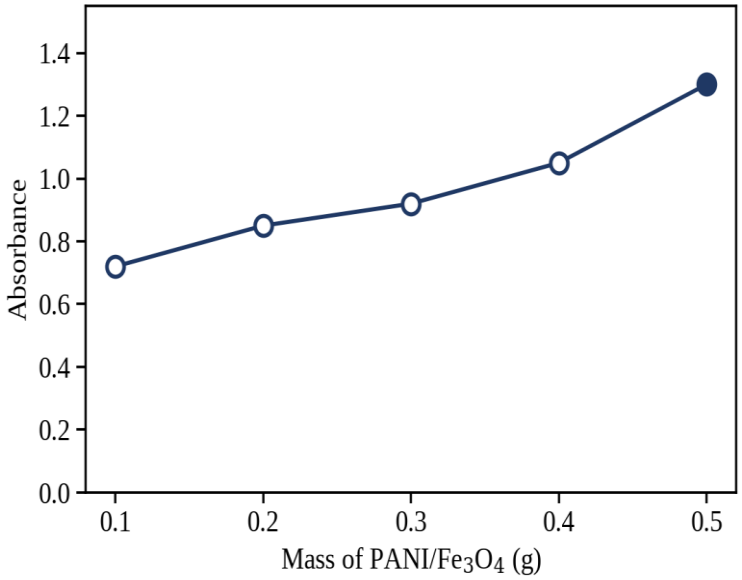


Figure 3-39: Effect of the mass of the magnetic sorbent on the extraction of Acid Red 18 by the MSPE method

Table 3-28: Effect of the mass of the magnetic sorbent on the extraction percentage, (%E) of Acid Red 18 by the MSPE method

Mass of PANI/Fe_3O_4 (g)	0.1	0.2	0.3	0.4	0.5

%E	68	74	79	86	94

3.7.2 Effect of the adsorption time

Adsorption time is a critical parameter that significantly influences the efficiency of the magnetic solid-phase extraction (MSPE) process. To evaluate its effect on the extraction of Acid Red 18 dye, a series of experiments were conducted with contact times ranging from 5 to 30 minutes, while keeping all other experimental conditions.

Constant. As shown in Figure (3-40), and Table (3-29**)** the extraction efficiency increased progressively with time, reaching a maximum at 30 minutes. This enrichment is attributed to the gradual establishment of adsorption equilibrium between Acid Red 18 molecules in the aqueous phase and the active sites on the surface of Fe_3O_4/polyaniline magnetic sorbent nanoparticles.

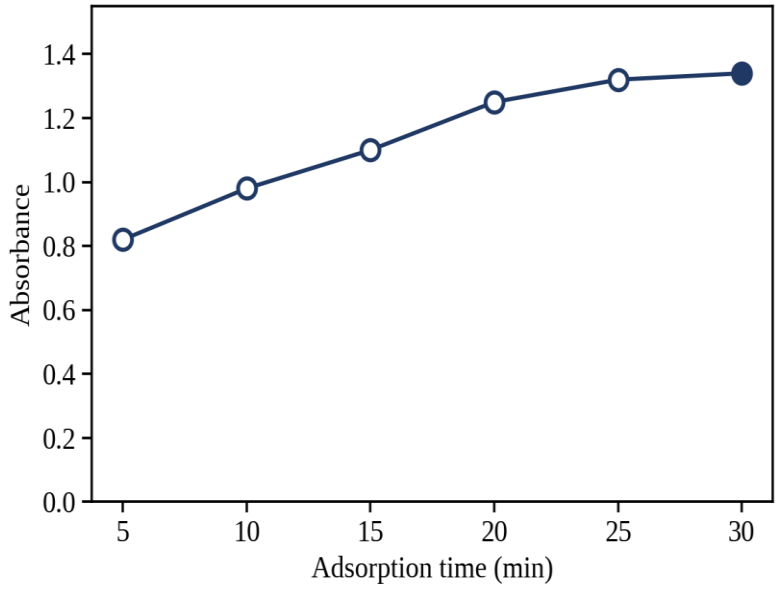


Figure 3-40: Effect of the adsorption time on the extraction of Acid Red 18 by the MSPE method.

Table 3-29: Effect of the adsorption time on the extraction percentage, (%E) of Acid Red 18 by the MSPE method

Adsorption time (min)	5	10	15	20	25	30
%E	**78**	**82**	**87**	**90**	**92**	**94**

3.7.3 Effect of the type of desorption solvent

Desorption is the process by which adsorbed molecules are released from the surface of an adsorbent, essentially reversing the process of adsorption. In this study, four organic solvents methanol, ethanol, acetonitrile and, acetone was evaluated to identify the most effective desorbing agent for Acid Red 18. As shown in Figure (3-41) and Table (3-30**)**, methanol exhibited the highest desorption efficiency This effectiveness is attributed to its high polarity and small molecular size, which enhances its ability to disrupt the interactions between Acid Red 18 molecules and the nanoparticle surface.

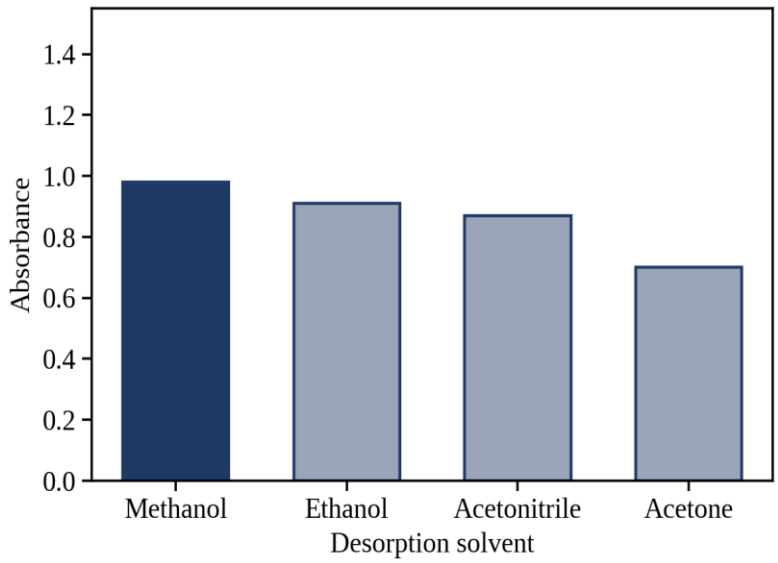


Figure 3-41: Effect of the type of desorption solvent on the extraction of Acid Red 18 by the MSPE method

Table 3-30: Effect of the type of desorption solvent on the extraction percentage, (%E) of Acid Red 18 by the MSPE method

extraction time (s)	Methanol	Ethanol	Acetonitrile	Acetone
%E	**85**	**82**	**80**	**75**

3.7.4 Effect of the desorption time

Desorption time is crucial for the efficiency of analyte recovery in magnetic solid-phase extraction. In this study, we evaluated desorption durations ranging from 5 to 30 minutes to determine the release of Acid Red 18 from Fe_3O_4/polyaniline nanoparticles. As shown in Figure (3-42) and Table (3-31**)**, the highest recovery rate was achieved at 20 minutes. Beyond this duration, no significant improvement in recovery was observed, indicating that equilibrium between the analyte and the elution solvent had been reached, allowing for complete desorption. Therefore, 20 minutes was selected as the optimal desorption time

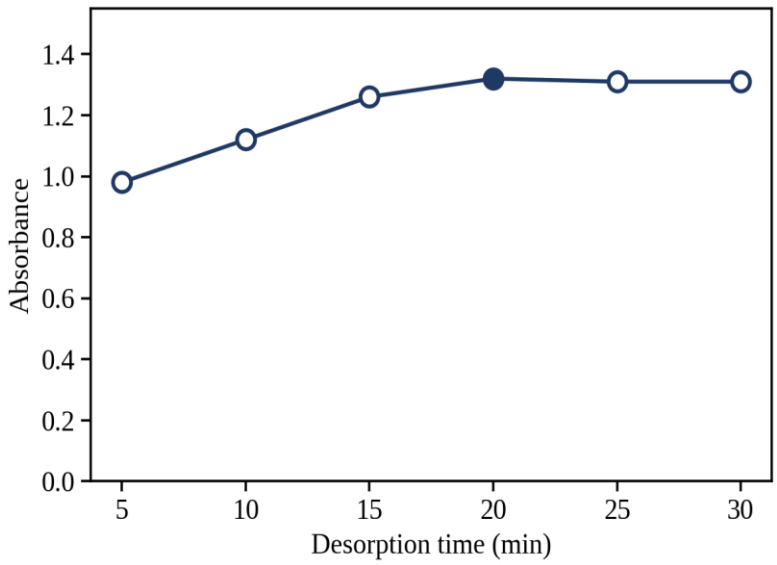


Figure 3-42: Effect of the desorption time on the extraction of Acid Red 18 by the MSPE method

Table 3-31: Effect of the desorption time on the extraction percentage, (%E) of Acid Red 18 by the MSPE method

desorption time (min)	**5**	**10**	**15**	**20**	**25**	**30**
%E	**83**	**87**	**90**	**93**	**93**	**93**

Table 3-32: Univariate optimisation of the magnetic solid-phase extraction of Acid Red 18

Factor	Range studied	Value adopted
Mass of sorbent (g)	0.1 – 0.5	0.5
Adsorption time (min)	5 – 30	30
Desorption time (min)	5 – 30	20
Desorption solvent	four solvents	methanol

3.8 Factors Affecting the Extraction of Methyl Orange by the MSPE Method

3.8.1 Effect of the mass of the magnetic sorbent

The quantity of magnetic nanoparticles (MNPs) is crucial for the adsorption-based extraction process. Increasing the amount of MNPs enhances the available surface area for the adsorption of Methyl Orange thereby improving extraction efficiency. However, after reaching a certain threshold of 0.4 g, further increases do not result in significant improvements. This plateau may be attributed to surface saturation or particle aggregation, which limit effective adsorption. Consequently, 0.4 g is identified as the optimal amount

for achieving maximum extraction efficiency, as illustrated in Figure (3-43) and Table (3-33**)**.

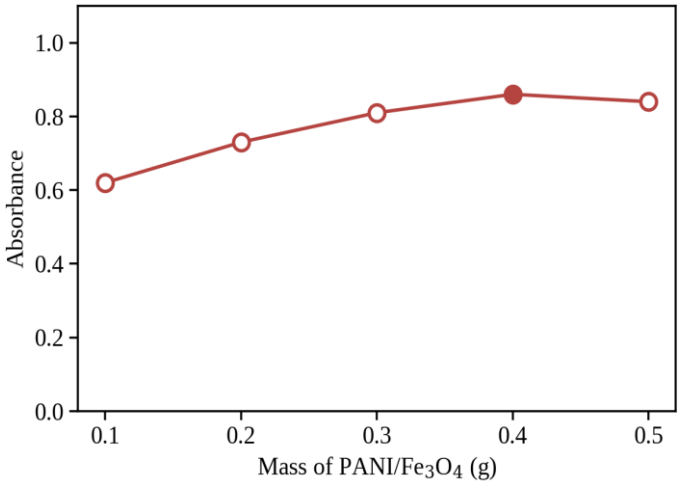


Figure 3-43: Effect of the mass of the magnetic sorbent on the extraction of Methyl Orange by the MSPE method.

Table 3-33: Effect of the mass of the magnetic sorbent on the extraction percentage, (%E) of Methyl Orange by the MSPE method.

3.8.2 Effect of the adsorption time

Mass of Fe_3O_4/polyaniline(g)	**0.1**	**0.2**	**0.3**	**0.4**	**0.5**
%E	**75**	**80**	**85**	**90**	**90**

Contact time is a critical factor that affects the efficiency of Methyl Orange adsorption onto modified Fe_3O_4 nanoparticles. Initially, the many active sites on the nanoparticle surface allow for rapid adsorption. However, as time progresses, these sites become increasingly occupied, causing the adsorption process to slow down until it reaches equilibrium. In this study, the optimal contact time was found to be 20 minutes, during which maximum adsorption efficiency was achieved. After this time frame, no significant improvement in

adsorption was observed, indicating that the surface had become saturated, as shown in Figure (3-44) and Table (3-34**)**.

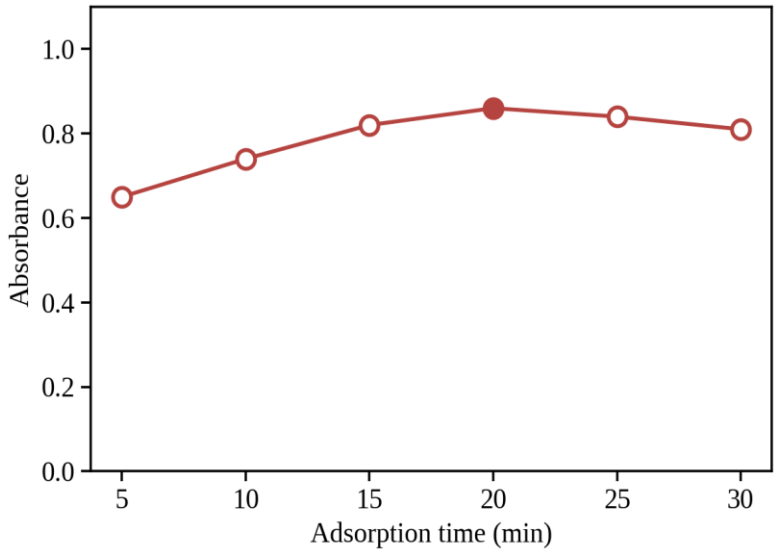


Figure 3-44: Effect of the adsorption time on the extraction of Methyl Orange by the MSPE method

Table 3-34: Effect of the adsorption time on the extraction percentage, (%E) of Methyl Orange by the MSPE method.

adsorption time (min)	**5**	**10**	**15**	**20**	**25**	**30**
%E	**77**	**82**	**87**	**90**	**90**	**87**

3.8.3 Effect of the type of desorption solvent

Four eluents were compared. Methanol is the best of them, giving 0.92 against 0.85 for ethanol, 0.76 for acetonitrile and 0.73 for acetone (Figure 3-45) and Table (3-35). The ordering follows the polarity and the hydrogen-bonding ability of the solvents. That is what is expected when a sulfonated dye has to be displaced from a protonated polyaniline surface. The eluent must solvate the anionic sulfonate groups well enough to break their

interaction with the positively charged nitrogen atoms of the polymer, and the small, strongly hydrogen-bonding methanol molecule does so most effectively [62, 64]. Methanol was therefore adopted

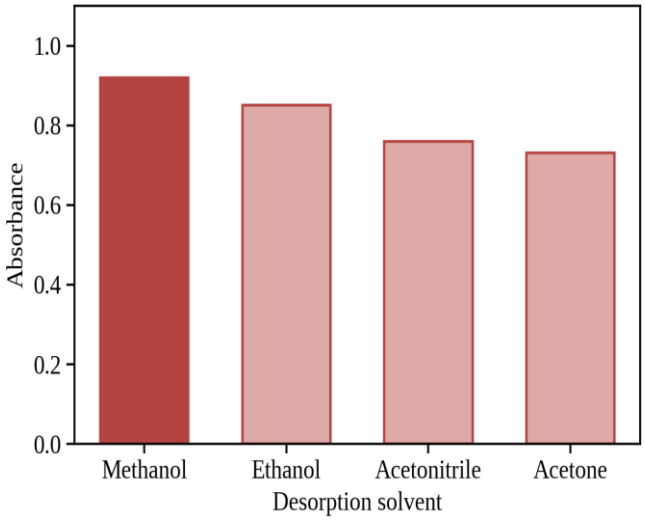


Figure 3-45: Effect of the type of desorption solvent on the extraction of Methyl Orange by the MSPE method

Table 3-35: Effect of the type of desorption solvent on the extraction percentage, (%E) of Methyl Orange by the MSPE method

extraction time (s)	Methanol	Ethanol	Acetonitrile	Acetone
%E	**94**	**92**	**90**	**85**

3.8.4 Effect of the desorption time

The effect of desorption time on the efficiency of Methyl Orange recovery from modified Fe_3O_4 nanoparticles was examined over a range of 5 to 35 minutes. As shown in Figure (3-46) and Table (3-36**)**, the optimal desorption time was found to be 20 minutes, during which the maximum recovery of Methyl Orange was achieved. This result is likely due to sufficient interaction time to disrupt the adsorbate-adsorbent interactions without causing re-

adsorption or subjecting the sample to excessive solvent exposure. Longer desorption times did not result in a significant increase in efficiency, indicating that an equilibrium had been reached. The optimum conditions from Sections 3.8.1–3.8.4 are summarised in Table 3-37.

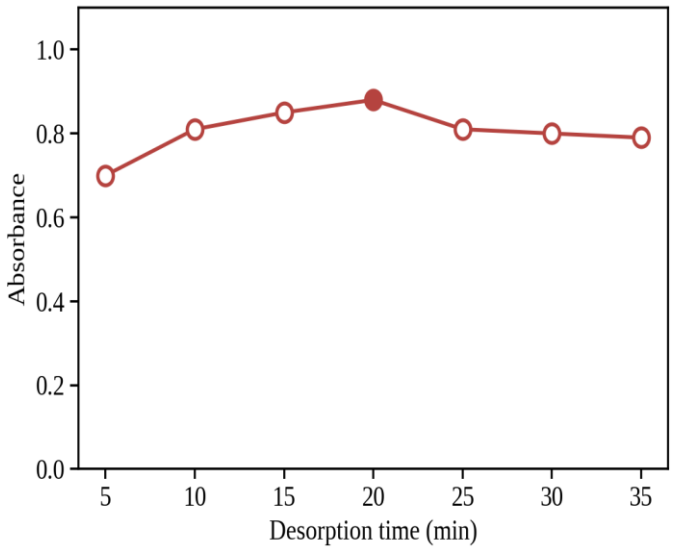


Figure 3-46: Effect of the desorption time on the extraction of Methyl Orange by the MSPE method.

Table 3-36: Effect of the desorption time on the extraction percentage, (%E) of Methyl Orange by the MSPE method

desorption time(min)	**5**	**10**	**15**	**20**	**25**	**30**	**35**
%E	**82**	**88**	**90**	**92**	**89**	**89**	**89**

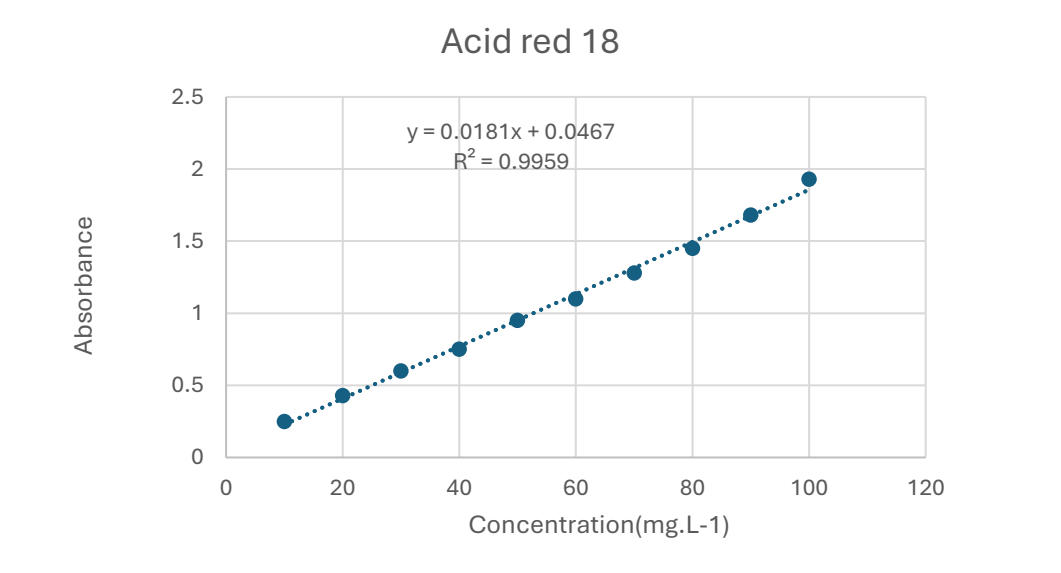
Table 3-37: Univariate optimisation of the magnetic solid-phase extraction of Methyl Orange.

Factor	Range studied	Value adopted
Mass of sorbent (g)	0.1 – 0.5	0.4
Adsorption time (min)	5 – 30	20

Factor	Range studied	Value adopted
Desorption time (min)	5 – 35	20
Desorption solvent	four solvents	methanol

3.9 Calibration Curves of the Dyes Using the SHS-LLME Method Coupled with the MSPE Method

To evaluate the linearity of the analytical method, calibration curves were constructed for Acid Red 18 and methyl orange dyes under the optimized experimental conditions. The calibration covered concentration ranges of 10-100 mg/L for both dyes. The calibration curves are shown in Figure (3-47), and the figures of merit are listed in Table (3-38).



Quantity	Acid Red 18	Methyl Orange

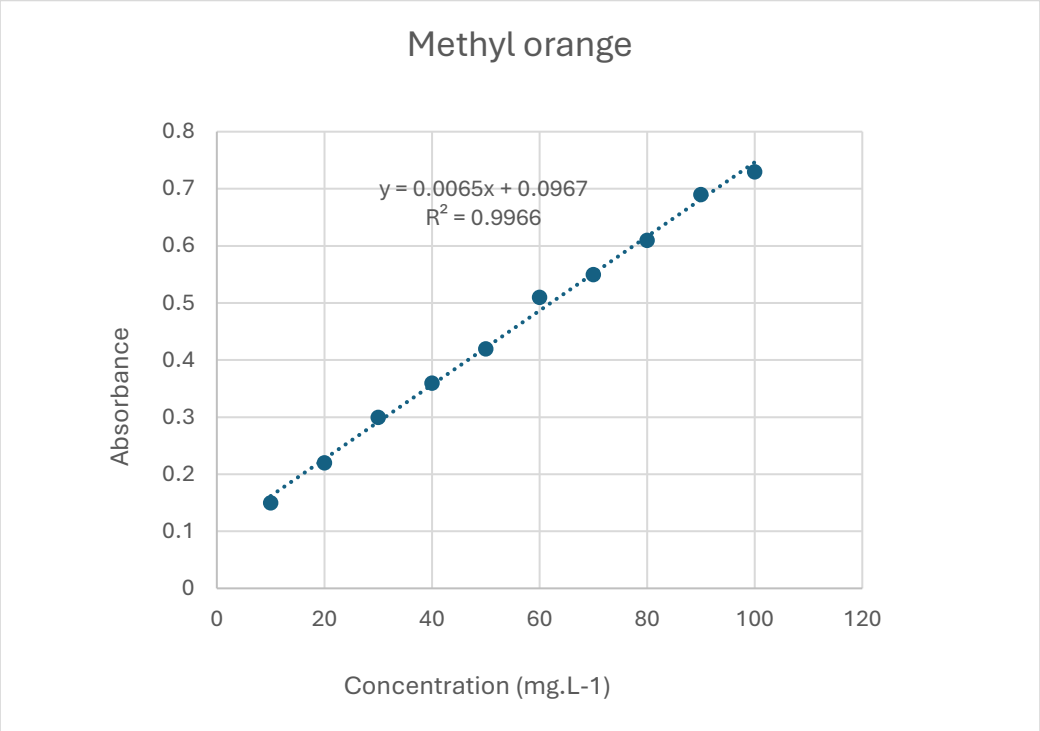


Figure 3-47: Calibration of the spectrophotometric determination of Acid Red 18 and Methyl Orange dyes

Table 3-38: Calibration data and the figures of merit derived from them

Quantity	Acid Red 18	Methyl Orange
Linear range	10 – 100 mg L^{-1}	10 – 100 mg L^{-1}
Number of standards, n	10	10
Slope, m	0.01810 L mg^{-1}	0.0065 L mg^{-1}
Intercept, b	0.0467	0.0967
Correlation coefficient, r	0.9951	0.9936
Coefficient of determination, R^2	0.9959	0.9966
Residual standard deviation, s(y/x)	0.0126	0.0057
Standard deviation of the intercept, s(b)	0.0523	0.0416
LOD = 3 s(y/x)/m	2.088 mg L^{-1}	2.630 mg L^{-1}
LOQ = 10 s(y/x)/m	6.961mg L^{-1}	8.769 mg L^{-1}

3.10 Application to Real Samples

The optimized procedure was applied to tap, river, and wastewater samples. Acid Red 18 was not detected in the unspiked tap and river water samples, whereas 19.76 mg L^{-1} was determined in the wastewater sample. The samples were spiked at concentrations ranging from 20 to 100 mg L^{-1} and analyzed using the optimized procedure. Relative recoveries ranged from 96.0 to 103.0%, with relative standard deviations below 5.0%, indicating that the sample matrices did not significantly affect the analytical performance of the method and demonstrating its applicability to real water samples Table (3-39).

Table 3-39: Determination and recovery of **Acid Red 18** in real water samples using the proposed method

Sample	Added (mg L^{-1})	Found (mg L^{-1})	Recovery (%)	RSD (%)
Tap water	—	ND	—	—
	20	19.67	98.35	3.65
	50	48.73	97.5	4.12
River water	—	ND	----	—
	50.0	50.16	103	3.52
	100.0	96.42	96.42	2.96
Wastewater	—	19.76	—	3.32
	20	38.98	96.1	4.21
	30	48.53	96.0	3.66

3.11 Conclusions

The main conclusions of this study are :

1-SHS-LLME is a green chemistry technique, characterized by its environmental friendliness. This technique relies on the use of switchable solvents, reducing the need for harmful organic solvents and thus minimizing negative environmental impacts.

2- Switchable Solvent Liquid-Liquid Microextraction (SHS-LLME) using (DMCHA) solvent is an effective method for extracting Acid Red 18 and methyl orange dyes from various samples.

3-. Determining the optimal conditions for dyes extraction was crucial in achieving high efficiency by controlling factors.

4-Traditional optimization approaches, which vary one factor at a time while holding others constant, are time-consuming, resource-intensive, and fail to capture interaction effects between variables.

5- Chemometric optimization using central composite design (CCD) offers several critical advantages over one-factor-at-a-time approaches. First, it dramatically reduces the number of experiments required to explore multi-dimensional factor spaces. Second, it quantifies interaction effects that would remain hidden in univariate studies. Third, it provides mathematical models that enable prediction of responses at untested factor combinations. Fourth, it

identifies optimal conditions with statistical confidence through desirability functions and contour analysis

6-The application of central composite design (CCD) to dyes extraction yielded a highly significant quadratic model with non-significant lack-of-fit ,indicating excellent model adequacy .This statistical validation provides confidence that the response surface accurately captures the relationships between factors and response within the experimental region.

7- The combination of Switchable Solvent-Based Liquid Microextraction (SHS-LLME) and Magnetic Solid Phase Extraction (MSPE) techniques has proven to be highly effective in extracting and determining selected dyes from aqueous samples. The results demonstrated excellent analytical accuracy and high recovery rates, along with notable sensitivity compared to conventional methods. Additionally, these techniques significantly reduced solvent

8. The ease of separating dyes using an external magnetic field made the process simpler and more efficient, reducing the complexity of traditional separation methods.consumption and analysis time.

9- The high sensitivity provided by the magnetically coated nanomaterials allowed for the detection of very low concentrations of dyes , making this technique suitable for the analysis of food and beverages

3.12 Recommendations

1-It is recommended to expand the application of the combined Switchable Solvent-based Liquid Microextraction (SHS-LLME) and Magnetic Solid-Phase Extraction (MSPE) technique for extracting various azo dyes from different matrices,.

2-. Further studies should investigate the use of alternative switchable solvents, particularly biodegradable or biocompatible options, to enhance the method's environmental sustainability

3- Additionally, it is advisable to modify the surfaces of magnetic nanoparticles with novel functional materials, such as biopolymers or selective ligands, to improve their specificity for target analytes, particularly in complex mixtures.

4-Apply the method to Methyl Orange in real samples, and to Acid Red 18 in foods and soft drinks.

5-Compare the method with published methods and with HPLC.

6-Study the selectivity of the method and the reuse of the sorbent.

REFERENCES

[1] Dutta, S.; Adhikary, S.; Bhattacharya, S.; Roy, D.; Chatterjee, S.; Chakraborty, A.; Banerjee, D.; Ganguly, A.; Nanda, S.; Rajak, P. Contamination of textile dyes in aquatic environment: Adverse impacts on aquatic ecosystem and human health, and its management using bioremediation. J. Environ. Manage. 2024, 353, 120103. https://doi.org/10.1016/j.jenvman.2024.120103

[2] Al-Tohamy, R.; Ali, S. S.; Li, F.; Okasha, K. M.; Mahmoud, Y. A.-G.; Elsamahy, T.; Jiao, H.; Fu, Y.; Sun, J. A critical review on the treatment of dye-containing wastewater: Ecotoxicological and health concerns of textile dyes and possible remediation approaches for environmental safety. Ecotoxicol. Environ. Saf. 2022, 231, 113160. https://doi.org/10.1016/j.ecoenv.2021.113160

[3] Kishor, R.; Purchase, D.; Saratale, G. D.; Saratale, R. G.; Ferreira, L. F. R.; Bilal, M.; Chandra, R.; Bharagava, R. N. Ecotoxicological and health concerns of persistent coloring pollutants of textile industry wastewater and treatment approaches for environmental safety. J. Environ. Chem. Eng. 2021, 9, 105012. https://doi.org/10.1016/j.jece.2020.105012

[4] Islam, M. M.; Aidid, A. R.; Mohshin, J. N.; Mondal, H.; Ganguli, S.; Chakraborty, A. K. A critical review on textile dye-containing wastewater: Ecotoxicity, health risks, and remediation strategies for environmental safety. Clean. Chem. Eng. 2025, 11, 100165. https://doi.org/10.1016/j.clce.2025.100165

[5] Ngo, A. C. R.; Tischler, D. Microbial Degradation of Azo Dyes: Approaches and Prospects for a Hazard-Free Conversion by Microorganisms. Int. J. Environ. Res. Public Health 2022, 19, 4740. https://doi.org/10.3390/ijerph19084740

[6] Tkaczyk, A.; Mitrowska, K.; Posyniak, A. Synthetic organic dyes as contaminants of the aquatic environment and their implications for ecosystems: A review. Sci. Total Environ. 2020, 717, 137222. https://doi.org/10.1016/j.scitotenv.2020.137222

[7] Benkhaya, S.; M'rabet, S.; El Harfi, A. Classifications, properties, recent synthesis and applications of azo dyes. Heliyon 2020, 6, e03271. https://doi.org/10.1016/j.heliyon.2020.e03271

[8] Barciela, P.; Perez-Vazquez, A.; Prieto, M. A. Azo dyes in the food industry: Features, classification, toxicity, alternatives, and regulation. Food Chem. Toxicol. 2023, 178, 113935. https://doi.org/10.1016/j.fct.2023.113935

[9] Barbosa, J. INDICATORS | Acid–Base. In Encyclopedia of Analytical Science, 2nd ed.; Worsfold, P.; Townshend, A.; Poole, C., Eds.; Elsevier: Oxford, 2005; pp 360-371. https://doi.org/10.1016/b0-12-369397-7/00270-3

[10] Alves, R. T.; Terceiro, P. S.; de Araújo, C. B.; Ribeiro, A. S.; Pereira, M. S. S.; da Cunha, A. R.; de Oliveira, I. N.; Manzoni, V. Solvatochromic effects on anionic and protonated forms of methyl orange dye: An experimental and theoretical study. Spectrochim. Acta, Part A 2025, 343, 126530. https://doi.org/10.1016/j.saa.2025.126530

[11] Abbey, J.; Fields, B.; O'Mullane, M.; Tomaska, L. D. Food Additives: Colorants. In Encyclopedia of Food Safety; Motarjemi, Y.; Moy, G.; Todd, E., Eds.; Academic

REFERENCES

Press: Waltham, MA, 2014; Vol. 2, pp 459-465. https://doi.org/10.1016/b978-0-12-378612-8.00225-0

[12] EFSA Panel on Food Additives and Nutrient Sources added to Food (ANS). Scientific Opinion on the re-evaluation of Ponceau 4R (E 124) as a food additive. EFSA J. 2009, 7, 1328. https://doi.org/10.2903/j.efsa.2009.1328

[13] European Food Safety Authority. Refined exposure assessment for Ponceau 4R (E 124). EFSA J. 2015, 13, 4073. https://doi.org/10.2903/j.efsa.2015.4073

[14] Kara, S. G.; Yuzbasioglu, D.; Avuloglu-Yilmaz, E.; Unal, F. Do the azo food colorings carmoisine and ponceau 4R have a genotoxic potential? Toxicol. Res. 2025, 14, tfaf033. https://doi.org/10.1093/toxres/tfaf033

[15] Yamjala, K.; Subramania Nainar, M.; Varma, S. K.; Ambore, N. Separation, identification and mutagenic assessment of the photodegradation products of Ponceau 4R (E124) in a beverage. Anal. Methods 2016, 8, 5017-5024. https://doi.org/10.1039/c6ay00716c

[16] Leo, L.; Loong, C.; Ho, X. L.; Raman, M. F. B.; Suan, M. Y. T.; Loke, W. M. Occurrence of azo food dyes and their effects on cellular inflammatory responses. Nutrition 2018, 46, 36-40. https://doi.org/10.1016/j.nut.2017.08.010

[17] Taheri, B.; Zakerhamidi, M. S.; Shamkhali, A. N.; Kian, R.; Sadeghan, A. A. Solvent polarity effect on photophysical properties of some aromatic azo dyes with focus on tautomeric and toxicity competition. Sci. Rep. 2025, 15, 15716. https://doi.org/10.1038/s41598-025-00001-w

[18] Haque, M. M.; Haque, M. A.; Mosharaf, M. K.; Marcus, P. K. Decolorization, degradation and detoxification of carcinogenic sulfonated azo dye methyl orange by newly developed biofilm consortia. Saudi J. Biol. Sci. 2021, 28, 793-804. https://doi.org/10.1016/j.sjbs.2020.11.012

[19] Cikcikoglu Yildirim, N.; Yaman, M. The usability of oxidative stress and detoxification biomarkers in Gammarus pulex for ecological risk assessment of textile dye methyl orange. Chem. Ecol. 2019, 35, 319-329. https://doi.org/10.1080/02757540.2019.1579199

[20] Gałuszka, A.; Migaszewski, Z.; Namieśnik, J. The 12 principles of green analytical chemistry and the SIGNIFICANCE mnemonic of green analytical practices. TrAC, Trends Anal. Chem. 2013, 50, 78-84. https://doi.org/10.1016/j.trac.2013.04.010

[21] Pena-Pereira, F.; Wojnowski, W.; Tobiszewski, M. AGREE—Analytical GREEnness Metric Approach and Software. Anal. Chem. 2020, 92, 10076-10082. https://doi.org/10.1021/acs.analchem.0c01887

[22] Rice, N. M.; Irving, H. M. N. H.; Leonard, M. A. Nomenclature for liquid-liquid distribution (solvent extraction) (IUPAC Recommendations 1993). Pure Appl. Chem. 1993, 65, 2373-2396. https://doi.org/10.1351/pac199365112373

[23] Lord, H.; Pawliszyn, J. Microextraction of drugs. J. Chromatogr. A 2000, 902, 17-63. https://doi.org/10.1016/s0021-9673(00)00836-0

REFERENCES

[24] Pawliszyn, J.; Pedersen-Bjergaard, S. Analytical Microextraction: Current Status and Future Trends. J. Chromatogr. Sci. 2006, 44, 291-307. https://doi.org/10.1093/chromsci/44.6.291

[25] Kabir, A.; Locatelli, M.; Ulusoy, H. Recent Trends in Microextraction Techniques Employed in Analytical and Bioanalytical Sample Preparation. Separations 2017, 4, 36. https://doi.org/10.3390/separations4040036

[26] Płotka-Wasylka, J.; Szczepańska, N.; de la Guardia, M.; Namieśnik, J. Miniaturized solid-phase extraction techniques. TrAC, Trends Anal. Chem. 2015, 73, 19-38. https://doi.org/10.1016/j.trac.2015.04.026

[27] Jeannot, M. A.; Cantwell, F. F. Mass Transfer Characteristics of Solvent Extraction into a Single Drop at the Tip of a Syringe Needle. Anal. Chem. 1997, 69, 235-239. https://doi.org/10.1021/ac960814r

[28] Pedersen-Bjergaard, S.; Rasmussen, K. E. Liquid-phase microextraction with porous hollow fibers, a miniaturized and highly flexible format for liquid–liquid extraction. J. Chromatogr. A 2008, 1184, 132-142. https://doi.org/10.1016/j.chroma.2007.08.088

[29] Pedersen-Bjergaard, S.; Rasmussen, K. E. Electrokinetic migration across artificial liquid membranes: New concept for rapid sample preparation of biological fluids. J. Chromatogr. A 2006, 1109, 183-190. https://doi.org/10.1016/j.chroma.2006.01.025

[30] Rezaee, M.; Assadi, Y.; Milani Hosseini, M.-R.; Aghaee, E.; Ahmadi, F.; Berijani, S. Determination of organic compounds in water using dispersive liquid–liquid microextraction. J. Chromatogr. A 2006, 1116, 1-9. https://doi.org/10.1016/j.chroma.2006.03.007

[31] Jessop, P. G.; Heldebrant, D. J.; Li, X.; Eckert, C. A.; Liotta, C. L. Reversible nonpolar-to-polar solvent. Nature 2005, 436, 1102. https://doi.org/10.1038/4361102a

[32] Jessop, P. G.; Phan, L.; Carrier, A.; Robinson, S.; Dürr, C. J.; Harjani, J. R. A solvent having switchable hydrophilicity. Green Chem. 2010, 12, 809-814. https://doi.org/10.1039/b926885e

[33] Jessop, P. G.; Kozycz, L.; Rahami, Z. G.; Schoenmakers, D.; Boyd, A. R.; Wechsler, D.; Holland, A. M. Tertiary amine solvents having switchable hydrophilicity. Green Chem. 2011, 13, 619-623. https://doi.org/10.1039/c0gc00806k

[34] Vanderveen, J. R.; Durelle, J.; Jessop, P. G. Design and evaluation of switchable-hydrophilicity solvents. Green Chem. 2014, 16, 1187-1197. https://doi.org/10.1039/c3gc42164c

[35] Durelle, J.; Vanderveen, J. R.; Quan, Y.; Chalifoux, C. B.; Kostin, J. E.; Jessop, P. G. Extending the range of switchable-hydrophilicity solvents. Phys. Chem. Chem. Phys. 2015, 17, 5308-5313. https://doi.org/10.1039/c4cp05313c

REFERENCES

[36] Alshana, U.; Hassan, M.; Al-Nidawi, M.; Yilmaz, E.; Soylak, M. Switchable-hydrophilicity solvent liquid-liquid microextraction. TrAC, Trends Anal. Chem. 2020, 131, 116025. https://doi.org/10.1016/j.trac.2020.116025

[37] Lasarte-Aragonés, G.; Lucena, R.; Cárdenas, S.; Valcárcel, M. Use of switchable solvents in the microextraction context. Talanta 2015, 131, 645-649. https://doi.org/10.1016/j.talanta.2014.08.031

[38] Pochivalov, A.; Davletbaeva, P.; Cherkashina, K.; Lezov, A.; Vakh, C.; Bulatov, A. Surfactant-mediated microextraction approach using switchable hydrophilicity solvent: HPLC-UV determination of Sudan dyes in solid food samples. J. Mol. Liq. 2018, 271, 807-814. https://doi.org/10.1016/j.molliq.2018.09.072

[39] Al-Nidawi, M.; Uzcan, F.; Alshana, U.; Soylak, M. Switchable-Hydrophilicity Solvent Liquid-Liquid Microextraction Prior to Spectrophotometric Determination of Sudan I Dye in Spices. Anal. Lett. 2024, 57, 202-212. https://doi.org/10.1080/00032719.2023.2202915

[40] Ahmed, H. E. H.; Gumus, Z. P.; Soylak, M. Switchable solvent-based liquid phase microextraction of Sudan dyes in food and water samples with HPLC-DAD. J. Food Compos. Anal. 2025, 139, 107099. https://doi.org/10.1016/j.jfca.2024.107099

[41] Tariq, Z.; Alwan, N. A. Optimization of Switchable Hydrophilicity Solvent-Based Liquid-Liquid Microextraction for Tartrazine Dye Separation and Preconcentration using Central Composite Design and Response Surface Methodology. Methods Objects Chem. Anal. 2024, 19, 200-205. https://doi.org/10.17721/moca.2024.200-205

[42] Hyde, A. M.; Zultanski, S. L.; Waldman, J. H.; Zhong, Y.-L.; Shevlin, M.; Peng, F. General Principles and Strategies for Salting-Out Informed by the Hofmeister Series. Org. Process Res. Dev. 2017, 21, 1355-1370. https://doi.org/10.1021/acs.oprd.7b00197

[43] Stejskal, J. Recent Advances in the Removal of Organic Dyes from Aqueous Media with Conducting Polymers, Polyaniline and Polypyrrole, and Their Composites. Polymers 2022, 14, 4243. https://doi.org/10.3390/polym14194243

[44] Arthur, C. L.; Pawliszyn, J. Solid phase microextraction with thermal desorption using fused silica optical fibers. Anal. Chem. 1990, 62, 2145-2148. https://doi.org/10.1021/ac00218a019

[45] Vas, G.; Vékey, K. Solid-phase microextraction: a powerful sample preparation tool prior to mass spectrometric analysis. J. Mass Spectrom. 2004, 39, 233-254. https://doi.org/10.1002/jms.606

[46] Baltussen, E.; Sandra, P.; David, F.; Cramers, C. Stir bar sorptive extraction (SBSE), a novel extraction technique for aqueous samples: Theory and principles. J. Microcolumn Sep. 1999, 11, 737-747. https://doi.org/10.1002/(sici)1520-667x(1999)11:10<737::aid-mcs7>3.0.co;2-4

[47] Abdel-Rehim, M. New trend in sample preparation: on-line microextraction in packed syringe for liquid and gas chromatography applications. I. Determination of

local anaesthetics in human plasma samples using gas chromatography–mass spectrometry. J. Chromatogr. B 2004, 801, 317-321. https://doi.org/10.1016/j.jchromb.2003.11.042

[48] Šafaříková, M.; Šafařík, I. Magnetic solid-phase extraction. J. Magn. Magn. Mater. 1999, 194, 108-112. https://doi.org/10.1016/s0304-8853(98)00566-6

[49] Ibarra, I. S.; Rodriguez, J. A.; Galán-Vidal, C. A.; Cepeda, A.; Miranda, J. M. Magnetic Solid Phase Extraction Applied to Food Analysis. J. Chem. 2015, 2015, 919414. https://doi.org/10.1155/2015/919414

[50] Abbas, R. F.; Mohammed Hassan, M. J.; Rheima, A. M. Magnetic Solid Phase Extraction for Determination of Dyes in Food and Water Samples. Indones. J. Chem. 2023, 23, 1181-1198. https://doi.org/10.22146/ijc.80885

[51] Andreeva, K. O.; Savrasova, V. I.; Aleksenko, S. S.; Tyunina, Yu. A.; Shalabai, S. A.; Shtykov, S. N. Magnetic Solid-Phase Extraction and Preconcentration of Anionic Azo Dyes: A Review. J. Anal. Chem. 2026, 81, 891-917. https://doi.org/10.1134/s1061934826700383

[52] Ali, A.; Zafar, H.; Zia, M.; ul Haq, I.; Phull, A. R.; Ali, J. S.; Hussain, A. Synthesis, characterization, applications, and challenges of iron oxide nanoparticles. Nanotechnol. Sci. Appl. 2016, 9, 49-67. https://doi.org/10.2147/nsa.s99986

[53] Xu, P.; Zeng, G. M.; Huang, D. L.; Feng, C. L.; Hu, S.; Zhao, M. H.; Lai, C.; Wei, Z.; Huang, C.; Xie, G. X.; Liu, Z. F. Use of iron oxide nanomaterials in wastewater treatment: A review. Sci. Total Environ. 2012, 424, 1-10. https://doi.org/10.1016/j.scitotenv.2012.02.023

[54] Teja, A. S.; Koh, P.-Y. Synthesis, properties, and applications of magnetic iron oxide nanoparticles. Prog. Cryst. Growth Charact. Mater. 2009, 55, 22-45. https://doi.org/10.1016/j.pcrysgrow.2008.08.003

[55] Lu, A.-H.; Salabas, E. L.; Schüth, F. Magnetic Nanoparticles: Synthesis, Protection, Functionalization, and Application. Angew. Chem., Int. Ed. 2007, 46, 1222-1244. https://doi.org/10.1002/anie.200602866

[56] Wu, W.; He, Q.; Jiang, C. Magnetic Iron Oxide Nanoparticles: Synthesis and Surface Functionalization Strategies. Nanoscale Res. Lett. 2008, 3, 397-415. https://doi.org/10.1007/s11671-008-9174-9

[57] Zhu, N.; Ji, H.; Yu, P.; Niu, J.; Farooq, M. U.; Akram, M. W.; Udego, I. O.; Li, H.; Niu, X. Surface Modification of Magnetic Iron Oxide Nanoparticles. Nanomaterials 2018, 8, 810. https://doi.org/10.3390/nano8100810

[58] Wu, W.; Wu, Z.; Yu, T.; Jiang, C.; Kim, W.-S. Recent progress on magnetic iron oxide nanoparticles: synthesis, surface functional strategies and biomedical applications. Sci. Technol. Adv. Mater. 2015, 16, 023501. https://doi.org/10.1088/1468-6996/16/2/023501

[59] Chiang, J.-C.; MacDiarmid, A. G. 'Polyaniline': Protonic acid doping of the emeraldine form to the metallic regime. Synth. Met. 1986, 13, 193-205. https://doi.org/10.1016/0379-6779(86)90070-6

REFERENCES

[60] MacDiarmid, A. G.; Chiang, J. C.; Richter, A. F.; Epstein, A. J. Polyaniline: a new concept in conducting polymers. Synth. Met. 1987, 18, 285-290. https://doi.org/10.1016/0379-6779(87)90893-9

[61] Mahto, T. K.; Chandra, S.; Haldar, C.; Sahu, S. K. Kinetic and thermodynamic study of polyaniline functionalized magnetic mesoporous silica for magnetic field guided dye adsorption. RSC Adv. 2015, 5, 47909-47919. https://doi.org/10.1039/c5ra08284f

[62] Huang, B.; Liu, Y.; Li, B.; Wang, H.; Zeng, G. Adsorption mechanism of polyethyleneimine modified magnetic core–shell Fe_3O_4@SiO_2 nanoparticles for anionic dye removal. RSC Adv. 2019, 9, 32462-32471. https://doi.org/10.1039/c9ra06299h

[63] Samadi, A.; Xie, M.; Li, J.; Shon, H.; Zheng, C.; Zhao, S. Polyaniline-based adsorbents for aqueous pollutants removal: A review. Chem. Eng. J. 2021, 418, 129425. https://doi.org/10.1016/j.cej.2021.129425

[64] Sowa, I.; Wójciak, M.; Tyszczuk-Rotko, K.; Klepka, T.; Dresler, S. Polyaniline and Polyaniline-Based Materials as Sorbents in Solid-Phase Extraction Techniques. Materials 2022, 15, 8881. https://doi.org/10.3390/ma15248881

[65] Stejskal, J. Interaction of conducting polymers, polyaniline and polypyrrole, with organic dyes: polymer morphology control, dye adsorption and photocatalytic decomposition. Chem. Pap. 2020, 74, 1-54. https://doi.org/10.1007/s11696-019-00982-9

[66] Nasar, A.; Mashkoor, F. Application of polyaniline-based adsorbents for dye removal from water and wastewater—a review. Environ. Sci. Pollut. Res. 2019, 26, 5333-5356. https://doi.org/10.1007/s11356-018-3990-y

[67] Zhao, Y.; Chen, H.; Li, J.; Chen, C. Hierarchical MWCNTs/Fe_3O_4/PANI magnetic composite as adsorbent for methyl orange removal. J. Colloid Interface Sci. 2015, 450, 189-195. https://doi.org/10.1016/j.jcis.2015.03.015

[68] Tran, T. T. A.; Duong, H. T. L.; Pham, T. T. P.; Nguyen, T.; Nguyen, T. D.; Tran, B. A. Preparation of Magnetic Composite Polyaniline/Fe_3O_4−Hydrotalcite and Performance in Removal of Methyl Orange. Adsorpt. Sci. Technol. 2021, 2021, 4150073. https://doi.org/10.1155/2021/4150073

[69] Badola, A.; Prajapati, J.; Bhoi, B.; Chandra, V. Efficient Removal of Anionic Dyes From Water Using Fe_3O_4@PANI Magnetic Nanocomposites. ChemistrySelect 2025, 10, e01782. https://doi.org/10.1002/slct.202501782

[70] Li, J.; Shao, Z.; Chen, C.; Wang, X. Hierarchical GOs/Fe_3O_4/PANI magnetic composites as adsorbent for ionic dye pollution treatment. RSC Adv. 2014, 4, 38192-38198. https://doi.org/10.1039/C4RA05800C

[71] Mohammadi, H.; Ghaedi, M.; Fazeli, M.; Sabzehmeidani, M. M. Removal of hexavalent chromium ions and Acid Red 18 by superparamagnetic $CoFe_2O_4$/polyaniline nanocomposites under external ultrasonic fields. Microporous

Mesoporous Mater. 2021, 324, 111275. https://doi.org/10.1016/j.micromeso.2021.111275

[72] Hassan, M.; Uzcan, F.; Alshana, U.; Soylak, M. Switchable-hydrophilicity solvent liquid–liquid microextraction prior to magnetic nanoparticle-based dispersive solid-phase microextraction for spectrophotometric determination of erythrosine in food and other samples. Food Chem. 2021, 348, 129053. https://doi.org/10.1016/j.foodchem.2021.129053

[73] Tariq, Z.; Hassan, R. A. A Green Switchable Hydrophilic Solvent Liquid-Liquid Microextraction Coupled with Magnetic Solid-Phase Extraction for Preconcentration and Spectrophotometric Determination of Sunset Yellow Dye. Methods Objects Chem. Anal. 2024, 19, 167-173. https://doi.org/10.17721/moca.2024.167-173

[74] Chen, H.; Deng, X.; Ding, G.; Qiao, Y. The synthesis, adsorption mechanism and application of polyethyleneimine functionalized magnetic nanoparticles for the analysis of synthetic colorants in candies and beverages. Food Chem. 2019, 293, 340-347. https://doi.org/10.1016/j.foodchem.2019.04.111

[75] Jangju, A.; Farhadi, K.; Hatami, M.; Amani, S.; Esma-ali, F.; Moshkabadi, A.; Hajilari, F. Application of zein-modified magnetite nanoparticles in dispersive magnetic micro-solid-phase extraction of synthetic food dyes in foodstuffs. J. Sep. Sci. 2017, 40, 1343-1352. https://doi.org/10.1002/jssc.201600856

[76] Faraji, M. Determination of some red dyes in food samples using a hydrophobic deep eutectic solvent-based vortex assisted dispersive liquid-liquid microextraction coupled with high performance liquid chromatography. J. Chromatogr. A 2019, 1591, 15-23. https://doi.org/10.1016/j.chroma.2019.01.022

[77] Bezerra, M. A.; Santelli, R. E.; Oliveira, E. P.; Villar, L. S.; Escaleira, L. A. Response surface methodology (RSM) as a tool for optimization in analytical chemistry. Talanta 2008, 76, 965-977. https://doi.org/10.1016/j.talanta.2008.05.019

[78] Leardi, R. Experimental design in chemistry: A tutorial. Anal. Chim. Acta 2009, 652, 161-172. https://doi.org/10.1016/j.aca.2009.06.015

[79] Czitrom, V. One-Factor-at-a-Time versus Designed Experiments. Am. Stat. 1999, 53, 126-131. https://doi.org/10.1080/00031305.1999.10474445

[80] Box, G. E. P.; Hunter, J. S.; Hunter, W. G. Statistics for Experimenters: Design, Innovation, and Discovery, 2nd ed.; Wiley-Interscience: Hoboken, NJ, 2005.

[81] Plackett, R. L.; Burman, J. P. The Design of Optimum Multifactorial Experiments. Biometrika 1946, 33, 305-325. https://doi.org/10.1093/biomet/33.4.305

[82] Box, G. E. P.; Wilson, K. B. On the Experimental Attainment of Optimum Conditions. J. R. Stat. Soc. Ser. B 1951, 13, 1-38. https://doi.org/10.1111/j.2517-6161.1951.tb00067.x

[83] Ferreira, S. L. C.; Bruns, R. E.; Ferreira, H. S.; Matos, G. D.; David, J. M.; Brandão, G. C.; da Silva, E. G. P.; Portugal, L. A.; dos Reis, P. S.; Souza, A. S.; dos Santos, W. N. L. Box-Behnken design: An alternative for the optimization of

analytical methods. Anal. Chim. Acta 2007, 597, 179-186. https://doi.org/10.1016/j.aca.2007.07.011

[84] Box, G. E. P.; Behnken, D. W. Some New Three Level Designs for the Study of Quantitative Variables. Technometrics 1960, 2, 455-475. https://doi.org/10.1080/00401706.1960.10489912

[85] Myers, R. H.; Montgomery, D. C.; Anderson-Cook, C. M. Response Surface Methodology: Process and Product Optimization Using Designed Experiments, 4th ed.; John Wiley & Sons: Hoboken, NJ, 2016.

[86] Montgomery, D. C. Design and Analysis of Experiments, 9th ed.; John Wiley & Sons: Hoboken, NJ, 2017.

[87] Derringer, G.; Suich, R. Simultaneous Optimization of Several Response Variables. J. Qual. Technol. 1980, 12, 214-219. https://doi.org/10.1080/00224065.1980.11980968

[88] Vera Candioti, L.; De Zan, M. M.; Cámara, M. S.; Goicoechea, H. C. Experimental design and multiple response optimization. Using the desirability function in analytical methods development. Talanta 2014, 124, 123-138. https://doi.org/10.1016/j.talanta.2014.01.034

[89] Tariq, Z.; Alwan, A. S.; Jasim, L. S. Application of central composite design and desirability function in the optimization of spectrophotometric method for quantification of fast green FCF using a green microextraction method. Appl. Chem. Eng. 2025, 8, 5603. https://doi.org/10.59429/ace.v8i2.5603

[90] Heidarizadi, E.; Tabaraki, R. Simultaneous spectrophotometric determination of synthetic dyes in food samples after cloud point extraction using multiple response optimizations. Talanta 2016, 148, 237-246. https://doi.org/10.1016/j.talanta.2015.10.075

[91] Kodalak, O.; Bişgin, A. T. Vortex-assisted simultaneous switchable hydrophilicity deep eutectic solvent-based microextraction of E102 and E132 in foodstuffs and pharmaceuticals. Sustain. Chem. Pharm. 2026, 49, 102286. https://doi.org/10.1016/j.scp.2025.102286

[92] Bagheri, H.; Daliri, R.; Roostaie, A. A novel magnetic poly(aniline-naphthylamine)-based nanocomposite for micro solid phase extraction of rhodamine B. Anal. Chim. Acta 2013, 794, 38-46. https://doi.org/10.1016/j.aca.2013.07.066

[93] Shariati-Rad, M.; Irandoust, M.; Amri, S.; Feyzi, M.; Ja'fari, F. Magnetic solid phase adsorption, preconcentration and determination of methyl orange in water samples using silica coated magnetic nanoparticles and central composite design. Int. Nano Lett. 2014, 4, 91-101. https://doi.org/10.1007/s40089-014-0124-5

[94] Xu, B.; Wang, Y.; Jin, R.; Li, X.; Song, D.; Zhang, H.; Sun, Y. Magnetic solid-phase extraction based on Fe_3O_4@polyaniline particles followed by ultrafast liquid chromatography for determination of Sudan dyes in environmental water samples. Anal. Methods 2015, 7, 1606-1614. https://doi.org/10.1039/c4ay02645d

REFERENCES

[95] Ghasemi, E.; Kaykhaii, M. Application of a Novel Micro-Cloud Point Extraction for Preconcentration and Spectrophotometric Determination of Azo Dyes. J. Braz. Chem. Soc. 2016, 27, 1521-1526. https://doi.org/10.5935/0103-5053.20160030

[96] Hashemi, S. H.; Kaykhaii, M.; Jamali Keikha, A.; Mirmoradzehi, E. Box-Behnken design optimization of pipette tip solid phase extraction for methyl orange and acid red determination by spectrophotometry in seawater samples using graphite based magnetic $NiFe_2O_4$ decorated exfoliated as sorbent. Spectrochim. Acta, Part A 2019, 213, 218-227. https://doi.org/10.1016/j.saa.2019.01.049

[97] Hassan, M.; Uzcan, F.; Shah, S. N.; Alshana, U.; Soylak, M. Switchable-hydrophilicity solvent liquid-liquid microextraction for sample cleanup prior to dispersive magnetic solid-phase microextraction for spectrophotometric determination of quercetin in food samples. Sustain. Chem. Pharm. 2021, 22, 100480. https://doi.org/10.1016/j.scp.2021.100480

[98] Miri, Z.; Elhami, S.; Zare-Shahabadi, V.; Jalali Jahromi, H. Fe_3O_4@PDA@PANI core–shell nanocomposites as a new adsorbent for simultaneous preconcentration of Tartrazine and Sunset Yellow by ultrasonic-assisted dispersive micro solid-phase extraction. Spectrochim. Acta, Part A 2021, 262, 120130. https://doi.org/10.1016/j.saa.2021.120130

[99] Guan, S.; Wu, H.; Lin, W.; Chen, Y.; Wang, Z. Facile synthesis of amino-modified magnetic covalent organic framework for the efficient extraction and determination of anionic azo dyes in carbonated beverages. Anal. Sci. 2024, 40, 1301-1310. https://doi.org/10.1007/s44211-024-00561-3

[100] Mohammadi, Z.; Sabzehmeidani, M. M.; Ghaedi, M.; Dashtian, K.; Abbasi-Asl, H. Dispersive micro-solid phase extraction coupled with spectrophotometric using (MgFe CLDH)/GO magnetically separable sorbent for pre-concentration of anionic food dyes in water samples. Emerging Contam. 2024, 10, 100347. https://doi.org/10.1016/j.emcon.2024.100347

[101] Abbas, R. F.; Hassan, M. J. M.; Rheima, A. M. Determination of AY 23 dye using magnetic solid-phase extraction coupled with spectrophotometry: Application of greenness and blueness assessment tools. Green Anal. Chem. 2025, 12, 100179. https://doi.org/10.1016/j.greeac.2024.100179

[102] Didukh-Shadrina, S. L.; Chash-ool, N. N.; Buyko, O. V.; Losev, V. N.; Golubeva, E. O. Solid-phase extraction and spectroscopic determination of synthetic dyes Sunset Yellow (E110) and Ponceau 4R (E124) in foodstuffs using alumina modified with polyhexamethylene guanidine. Anal. Kontrol' 2025, 29, 68-74. https://doi.org/10.15826/analitika.2025.29.1.004

[103] Cullity, B. D.; Graham, C. D. Introduction to Magnetic Materials, 2nd ed.; IEEE Press/John Wiley & Sons: Hoboken, NJ, 2008. https://doi.org/10.1002/9780470386323

[104] Brunauer, S.; Emmett, P. H.; Teller, E. Adsorption of Gases in Multimolecular Layers. J. Am. Chem. Soc. 1938, 60, 309-319. https://doi.org/10.1021/ja01269a023

REFERENCES

[105] Thommes, M.; Kaneko, K.; Neimark, A. V.; Olivier, J. P.; Rodriguez-Reinoso, F.; Rouquerol, J.; Sing, K. S. W. Physisorption of gases, with special reference to the evaluation of surface area and pore size distribution (IUPAC Technical Report). Pure Appl. Chem. 2015, 87, 1051-1069. https://doi.org/10.1515/pac-2014-1117

[106] Barrett, E. P.; Joyner, L. G.; Halenda, P. P. The Determination of Pore Volume and Area Distributions in Porous Substances. I. Computations from Nitrogen Isotherms. J. Am. Chem. Soc. 1951, 73, 373-380. https://doi.org/10.1021/ja01145a126

[107] ISO 5667-3:2024. Water quality — Sampling — Part 3: Preservation and handling of water samples, 6th ed.; International Organization for Standardization: Geneva, 2024.

[108] U.S. Geological Survey. Chapter A5. Processing of water samples. In National Field Manual for the Collection of Water-Quality Data; Techniques of Water-Resources Investigations, Book 9, Chapter A5; U.S. Geological Survey: Reston, VA, 2002. https://doi.org/10.3133/twri09a5

[109] Bevziuk, K.; Chebotarev, A.; Snigur, D.; Bazel, Y.; Fizer, M.; Sidey, V. Spectrophotometric and theoretical studies of the protonation of Allura Red AC and Ponceau 4R. J. Mol. Struct. 2017, 1144, 216-224. https://doi.org/10.1016/j.molstruc.2017.05.001

[110] Shalaby, A. A.; Mohamed, A. A. Determination of acid dissociation constants of Alizarin Red S, Methyl Orange, Bromothymol Blue and Bromophenol Blue using a digital camera. RSC Adv. 2020, 10, 11311-11316. https://doi.org/10.1039/c9ra10568a

[111] Yang, C.; Du, J.; Peng, Q.; Qiao, R.; Chen, W.; Xu, C.; Shuai, Z.; Gao, M. Polyaniline/Fe_3O_4 Nanoparticle Composite: Synthesis and Reaction Mechanism. J. Phys. Chem. B 2009, 113, 5052-5058. https://doi.org/10.1021/jp811125k

[112] Muhammad, A.; Shah, A.-u.-H. A.; Bilal, S.; Rahman, G. Basic Blue Dye Adsorption from Water Using Polyaniline/Magnetite (Fe_3O_4) Composites: Kinetic and Thermodynamic Aspects. Materials 2019, 12, 1764. https://doi.org/10.3390/ma12111764

[113] Teng, X. P.; Bryan, M. Y. K.; Chai, P. V.; Law, J. Y. Preparation of polyaniline iron oxide composite (PANI/Fe_3O_4) for enhanced Congo red removal performance. Mater. Today: Proc. 2021, 46, 1875-1881. https://doi.org/10.1016/j.matpr.2021.01.766

[114] Elashmawi, I. S.; Alhusaiki-Alghamdi, H. M. Fabrication, characterization, spectroscopic, and magnetic properties of polyaniline/magnetite (PANi/Fe_3O_4) nanocomposites. Opt. Quantum Electron. 2024, 56, 1090. https://doi.org/10.1007/s11082-024-06843-4

[115] Chantrell, R.; Popplewell, J.; Charles, S. Measurements of particle size distribution parameters in ferrofluids. IEEE Trans. Magn. 1978, 14, 975-977. https://doi.org/10.1109/tmag.1978.1059918

REFERENCES

[116] Rajan, A.; Sharma, M.; Sahu, N. K. Assessing magnetic and inductive thermal properties of various surfactants functionalised Fe_3O_4 nanoparticles for hyperthermia. Sci. Rep. 2020, 10, 15045. https://doi.org/10.1038/s41598-020-71703-6

الخلاصة

تناولت هذه الدراسة تطوير طريقة بسيطة لاستخلاص صبغة Acid Red 18 وصبغة Methyl Orange من المياه وتقديرهما طيفياً، باستعمال الاستخلاص الدقيق السائل بالمذيب القابل للتحويل (SHS-LLME) المقترن بالاستخلاص بالطور الصلب المغناطيسي (MSPE) على جسيمات بولي أنيلين المغنيتيت (Fe_3O_4/PANI).

الجزء الأول: تحضير الجسيمات النانوية وتشخيصها

حُضّرت الجسيمات النانوية Fe_3O_4/PANI بنسبة 50:50 وزناً بخلط البولي أنيلين والمغنتايت في الأسيتون، وشُخّصت باستعمال مجموعة من التقنيات التحليلية المتقدمة شملت:

- حيود الأشعة السينية (XRD).
- المجهر الإلكتروني الماسح (SEM).
- المجهر الإلكتروني النافذ (TEM).
- مقياس المغناطيسية (VSM).
- مطيافية الأشعة تحت الحمراء بتحويل فورييه (FTIR).

وقد وفّرت هذه التقنيات معلومات تفصيلية عن الخصائص البنيوية والمورفولوجية والمغناطيسية للجسيمات النانوية المحضّرة؛ إذ أكدت تغليف المغنتايت بالبولي أنيلين، فازداد حجم الدقائق من 11.7 إلى 21.0 نانومتر، ونقصت مغنطة التشبع من 11.42 إلى 4.68 emu/g مع بقاء المادة مغناطيسية.

الجزء الثاني: تطبيق تقنية SHS

تم تطوير طريقة استخلاص دقيق قابلة للتبديل باستخدام المذيبات القابلة للتبديل تعتمد على استخدام-N,N ثنائي ميثيل سيكلوهيكسيلامين (DMCHA) لاستخلاص وتقدير صبغات حمض الحمراء 18 والميثيل البرتقالي طيفيا . من خلال سلوك تبديل الحمض/القاعدة للأمين، جمع الإجراء بين كفاءة الاستخلاص المتجانس والفصل البسيط للطور دون الحاجة إلى مذيب مشتت أو طرد مركزي.

دُرست ثمانية عوامل بطريقة العامل الواحد في كل مرة. درجة حموضة المحلول (2–9)، نوع مذيب الاستخلاص ، حجم DMCHA (1–3 مل)، حجم حمض الهيدروكلوريك (100–1000 ميكرولتر)، حجم هيدروكسيد الصوديوم (100–1000 ميكرولتر)، درجة حرارة الحمام (30–50 درجة مئوية)، وقت الاستخلاص (1–10 ثوانٍ) ونوع وتركيز الملح المضاف

($CaCl_2$، NaCl، و KCl، 1–10% وزن/حجم). وكانت الظروف الفضلى لصبغة Acid Red 18 هي pH 3، و2.5 مل من DMCHA، و400 مايكرولتر من كلٍّ من الحامض والقاعدة، و40 °م، و10 ثوانٍ، و10% من $CaCl_2$؛ ولصبغة Methyl Orange هي pH 3، و2.0 مل، و300 و100 مايكرولتر من الحامض والقاعدة، و40 °م، و8 ثوانٍ، و5% من $CaCl_2$.

الجزء الثالث: تطبيق الطرائق الكيمومترية الإحصائية

طُبّقت الطرق الكيمومترية لتحسين ظروف الاستخلاص ودراسة التأثيرات المتبادلة بين المتغيرات التجريبية، بهدف الوصول إلى الظروف المثلى بطريقة منهجية وتقليل عدد التجارب المطلوبة. واستُعمل التصميم المركب المركزي (31 تجربة لكل صبغة) لدراسة الدالة الحامضية وحجوم المذيب والحامض والقاعدة. وأتاحت النمذجة الكيمومترية تحديد العوامل الأكثر تأثيراً في عملية الاستخلاص وتقييم ملاءمة النموذج للبيانات التجريبية؛ فقد كان النموذجان معنويين ($P < 0.001$)، ولم يكن عدم الملاءمة معنوياً ($P = 0.640$) لصبغة Methyl Orange، وكانت الدالة الحامضية أكثر العوامل تأثيراً وقيمتها المثلى pH 2.

الجزء الرابع: الاستخلاص بالطور الصلب المغناطيسي (MSPE)

في هذا الجزء استُعملت الجسيمات النانوية Fe_3O_4/PANI المحضّرة سابقاً مادةً مازّةً مغناطيسية لاستخلاص الصبغات نفسها. وكان الميثانول أفضل مذيب للإزاحة، وكانت الظروف الفضلى 0.5 غم و30 دقيقة للامتزاز و20 دقيقة للإزاحة لصبغة Acid Red 18، و0.4 غم و و20 دقيقة لصبغة Methyl Orange، وبلغت نسبة الاستخلاص 93% و92% على التوالي.

الجزء الخامس: التطبيق على عينات حقيقية

كانت الطريقة المقترنة خطية من 10 إلى 100 ملغم/لتر، وبلغ حد الكشف 2.088 و2.630 ملغم/لتر وحد التقدير الكمي 6.961 و8.769 ملغم/لتر للصبغتين على التوالي. وفي هذا الجزء النهائي طُبّقت الطريقة المطوّرة على عينات حقيقية (ماء الإسالة وماء النهر ومياه الصرف) بهدف تقييم كفاءتها وقابليتها للتطبيق العملي في تحليل الأصباغ المستهدفة في مصفوفات حقيقية؛ فلم تُكشف صبغة Acid Red 18 إلا في مياه الصرف (19.76 ملغم/لتر)، وتراوحت نسب الاسترجاع بين 96.0 و100.3% بانحراف معياري نسبي أقل من 5%.

وبصورة عامة، أظهرت الدراسة إمكانية استعمال تقنية SHS-LLME المقترنة بتقنية MSPE باستعمال Fe_3O_4/PANI طريقةً تحليليةً واعدة لاستخلاص الأصباغ المدروسة وتقديرها، لما تتميز به من سهولة التشغيل وسرعة الفصل المغناطيسي وتقليل استهلاك المذيبات وإمكانية تحسين الكفاءة التحليلية، مما يجعلها مناسبة للتطبيقات التحليلية في العينات البيئية.

جمهورية العراق
وزارة التعليم العالي والبحث العلمي
جامعة القادسية / كلية العلوم
قسم الكيمياء

تطبيق النماذج الكيميائية الإحصائية لاستخلاص وتقدير بعض الأصباغ الحامضية

رسالة مقدمة الى
مجلس كلية العلوم / جامعة القادسية

وهي جزء من متطلبات نيل شهادة الماجستير في علوم الكيمياء

قدمتها الباحثة

رغد عبد الرضا وساف

بكالوريوس علوم الكيمياء 2019-2020

بأشراف

أ. د. زينب طارق إبراهيم

1446 هـ

2026 م